Roll-to-Roll Advanced Materials Manufacturing DOE Laboratory Collaboration - Early Stage R&D

FY 2020 Final Report

ORNL/SPR-2021/1892

April 2021

Funding provided by:

U.S. Department of Energy
Office of Energy Efficiency and Renewable Energy
Advanced Manufacturing Office

ORNL R2R Slot Die Coating of PEMFC Layers

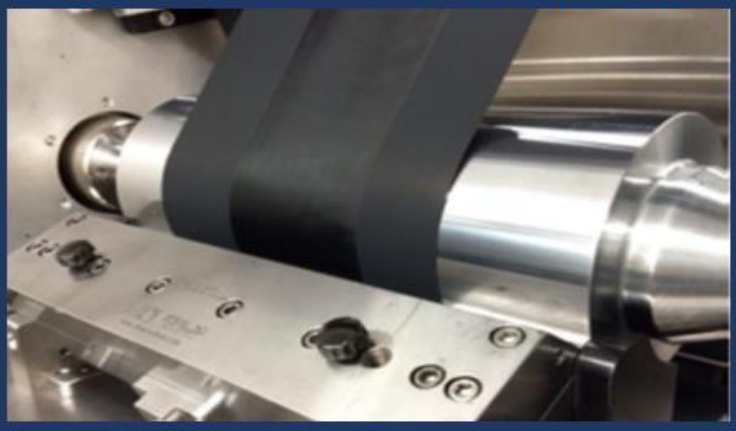

ANL R2R Electrospinning/Annealing System

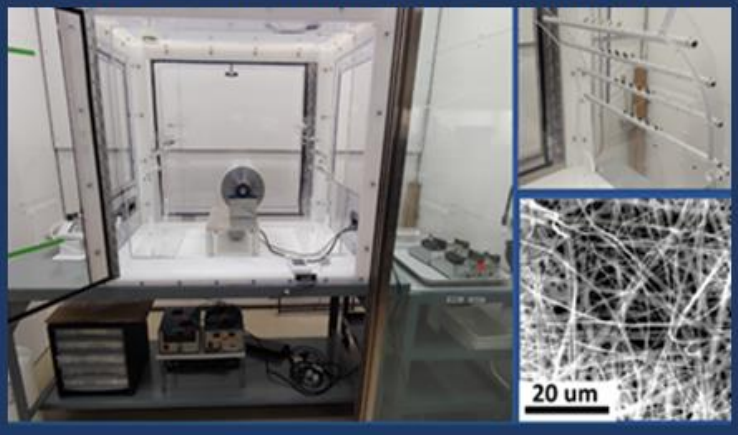

NREL R2R Slide Die Visualization Setup

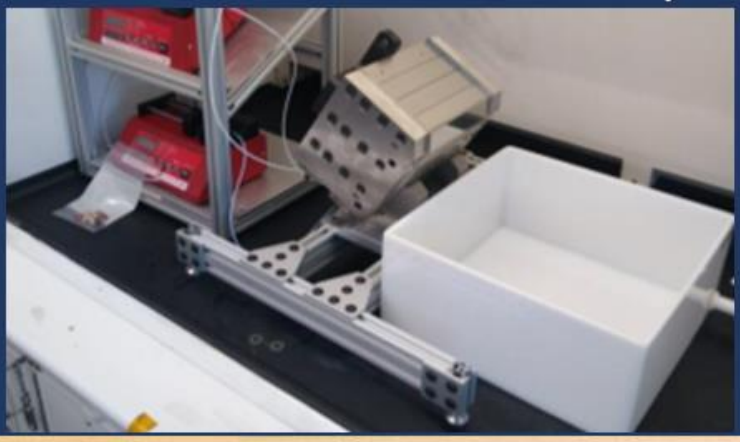

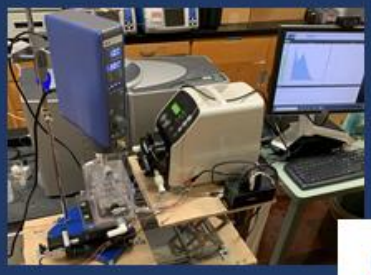

LBNL Experimental Setup for Particle Dispersion Studies

SNL R2R Slide Die Coating Model

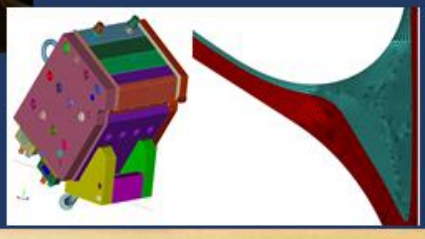

OAK RIDGE National Laboratory
Argonne NATIONAL LABORATORY
NREL NATIONAL RENEWABLE ENERGY LABORATORY
BERKELEY LAB
Sandia National Laboratories

Disclaimer

DOCUMENT AVAILABILITY

Reports produced after January 1, 1996, are generally available free via US Department of Energy (DOE) SciTech Connect.

Website http://www.osti.gov/scitech/

Reports Produced before January 1, 1996, may be purchased by members of the public from the following source:

National Technical Information Service
5285 Port Royal Road
Springfield, VA 22161
Telephone 703-605-6000 (1-800-553-6847
TDD 703-487-4639
Fax 703-605-6900
E-mail info@ntis.gov
Website http://www.ntis.gov/help/ordermethods.aspx

Reports are available to DOE employees, DOE contractors, Energy Technology Data Exchange representatives, and International Nuclear Information System representatives from the following source:

Office of Science and Technical Information
PO Box 62
Oak Ridge, TN 37831
Telephone 865-576-8401
Fax 865-576-5728
Email reports2osti.gov
Website http://www.osti.gov/contact.html

Foreword

Oak Ridge National Laboratory (ORNL), Argonne National Laboratory (ANL), Lawrence Berkeley National Laboratory (LBNL), and the National Renewable Energy Laboratory (NREL) performed as a collaborative Roll-to-Roll Advanced Materials Manufacturing (R2R AMM) Department of Energy (DOE) Laboratory Consortium during Fiscal Year (FY) 2016 through FY 2018 (Phase 1). In June 2018, the Consortium responded to a FY 2019 Advanced Manufacturing Office (AMO) Lab Call, DE-LC-000L059, for Topic 3 titled "Roll-to-Roll Processing" with a proposal "Early-stage advanced national multi-laboratory roll-to-roll research and development collaboration with industrial Cooperative Research and Development Agreement (CRADA) collaboration". Over 50 white papers were solicited from multiple national laboratories, including the four Consortium laboratories, and five were selected for including in the proposal to the Lab Call. One paper from Sandia National Laboratories (SNL), Albuquerque, NM for process modelling was selected, so SNL was added to the multi-laboratory collaboration and rebranded the R2R AMM DOE Laboratory Collaboration (i.e., R2R Collaboration). The proposal was accepted for funding in FY 2019 through FY 2021 (Phase 2) contingent on annual budget authorizations. This report discusses tasks, results, and findings of the second year of Phase 2.

This R2R Collaboration's goal is to advance understanding of R2R processing for high-throughput advanced manufacturing through an early-stage research approach to enable new devices and lower the cost of existing processing routes for competitive U.S. manufacturing. The projects directly address the AMO's Multi-Year Program Plan challenges for the use of multilayer coating technologies applicable to flexible and integrated electronics, separation membranes, photovoltaics (PV), and selective barrier materials. [1] Collaborative research addresses the AMO identified targets of (1) technologies with a 10x production capacity increase and (2) in-line instrumentation tools to evaluate the performance and functionality. Working with industry partners through CRADA projects, the R2R Collaboration is addressing challenges and barriers for continuous R2R processing, registration and alignment, scalability, materials compatibility and defects, macroscopic and continuum drying process model development, stoichiometry control and the availability of materials data for R2R processing. Program goals are the development of technologies that reduce the cost per manufactured throughput of continuous R2R manufacturing processes, and the development of in-line instrumentation tools that will evaluate the quality of single and multilayer materials on process weblines.

The FY 2020 core program continued efforts from the first year of Phase 2 and consisted of a broad range of research task areas focused on colloidal chemistry and slurry formulation, novel R2R deposition systems based on electrospinning (ES) technology, in-line real-time non-destructive evaluation (NDE) and advanced in-situ testing capabilities, physics and methodologies for multilayer coatings, ink formulations and rheology, modeling and simulation of drying and mixing processes, and continuum-scale models for the capillary hydrodynamics of coating deposition. Three CRADA projects continued into FY 2020 with one completing in March 2020 and one completing in September 2020. The primary applications of the research in the CRADA projects include freeze casting studies, advanced separator for flexible solid-state lithium (Li) ion batteries (LIB), diffractive multiplexing laser patterning of flexible organic PV (OPV) modules, and electrodes for low-cost hydrogen production. The Collaboration laboratories have unique assets that complement each other for the research, development, testing and evaluation of these energy-saving technologies. These include the following infrastructure, testing, operations, characterization, and analysis capabilities:

- Precision coating equipment
- Pilot-scale R2R operations
- Device assembly assistance
- Electrochemical and cell performance evaluation
- State-of-the-art microscopy and tomography
- Surface characterization

- X-ray and neutron characterization facilities
- Computational science
- Process modeling and characterization
- World-class data analysis
- In-line quality control (QC)

DOE cost targets for advanced energy storage and conversion applications will not be met without significant and timely advancements in R2R manufacturing. Required R2R advances include adaptation of existing processing methods (gravure, slot die, slide die) and development of novel approaches (simultaneous multilayer coatings and ES) that have the potential to significantly impact U.S. manufacturing sector recovery, environmental applications in clean water, energy security, and sustainable transportation. Economies of scale through increased manufacturing volumes based on traditional assembly and processing methods will not suffice. For example, the current goal for the DOE Vehicle Technologies Office (VTO) is to reduce the cost of electric vehicle batteries from a cost of $197/kWh in 2018 to less than $150/kWh with the ultimate goal of a 2.5x cost reduction to $80/kWh. [2] [3] Commercial lithium ion technology is largely limited to cells with gravimetric energy densities of <250 Wh/kg and volumetric energy densities of <650 Wh/L. Volumetric energy densities are often more important for portable electronics and electric vehicles. There is immense need to push the energy densities to as high as ~500 Wh/kg and 1,000 Wh/L. [4] Novel R2R processing technologies will be required to manufacture lithium ion technologies with these energy densities in high volume.

Current polymer electrolyte membrane (PEM) electrolyzers require 65-75% cost reduction from $1100/kW to $400/kW. The DOE Hydrogen and Fuel Cells Technology Office (HFTO) target that guides fuel cell R&D is to reduce the cost for a fuel cell electric vehicle system from $180/kW at a low-volume production rate to an ultimate target of $30/KW. [5] Water consumption for renewable energy technologies can be as high as a medium value 4,500 gallons/megawatt-hours and more than 44,000 gallons/megawatt-hours for non-renewable energy applications. [6] New technologies are needed to increase the capacity of these systems to meet future needs. Other examples of the Energy Efficiency and Renewable Energy (EERE) Office funded technologies that have a similar cost-target issue are chemical-process industry membranes, window films, PV films, and flexible electronic films. The EERE AMO is poised to assist in reaching the low dollars per unit costs of these various critical energy related applications through addressing R2R manufacturing problems common to each application.

Preface

The following report provides a description of the program structure and technical accomplishments made during FY 2020 to overcome challenges for expanding use of R2R technologies and processes for clean energy applications. Areas of interest encompass colloidal chemistry, surfactant research, slurry processing, and drying and curing; novel R2R deposition using ES; methodologies for ink formulations, multilayer coatings, rheology, and deposition; fabrication and in-situ characterization of prototype components and devices; and in-line real-time NDE. The particle- and continuum-scale modeling and simulations for these layered materials, energy storage technologies, and continuous manufacturing processes that are being developed will allow for improvements and advances in R2R manufacturing applications, particularly for design and scale-up. This report documents the research conducted by five DOE National Laboratories as a collaborative group with participation from industry through formal and informal partnerships. The approach is to develop advanced and novel materials, methods and techniques for multilayer coatings and depositions that can be used for R2R processes that are applicable to enhancing the performance of renewable energy technologies and systems. During the COVID pandemic, the R2R ES technology developed within this program was applied to develop reusable antiviral N95 filter media to address the N95 facepiece respirator shortage. This effort supports building the foundation of technologies, processes and a U.S. manufacturing base that will enable an order of magnitude reduction in process development cycles with the pathway for initial commercialization within months instead of years.

Acknowledgements

First and foremost, the following scientists, investigators and technical support who are working diligently to realize their innovative ideas and technological developments in R2R processing and their desire to deploy them broadly for energy storage applications are acknowledged for their contributions:

ANL: Greg Krumdick, Deborah Myers, Jae Hyung Park, Albert Lipson, Donna Brunner, Yuepeng Zhang, Erik Dahl, Devon Powers, Ashley Simmons

ORNL: David Wood, Jianlin Li, Marissa Wood, Jaswinder Sharma, Georgios Polyzos, Erin Creel, Kelsey (Grady) Livingston, Ritu Sahore, Charl Jafta

NREL: Mike Ulsh, Peter Rupnowski, Brian Green, Scott Mauger, KC Neyerlin, Sunil Khandavalli, Jason Pfeilsticker, Min Wang, Janghoon Park, Nisha Sharma, Reilly Seban, Maikel van Hest, Bertrand Tremolet deVillers

LBNL: Vince Battaglia, Kenny Higa, Zhi Huang, Bei Fan, Buyi Zhang, Ravi Prasher

SNL/University of New Mexico: Randy Schunk, Kristianto Tjiptowidjojo, Nelson Bell, Chris Wall, Ben Wall, Robert Malakhov

DOE EERE AMO: Brian Valentine (Technical Project Management)

DOE EERE HFTO: Nancy Garland (Technical Project Management)

We would also like to acknowledge the principal investigators and project managers at Navitas Systems, LLC; SolarWindow Technologies, Inc.; General Motors, Nel Hydrogen, Giner, Plug Power, Eastman Kodak, and Saint-Gobain for their coordination and collaboration on the R2R projects.

Finally, we would also like to acknowledge the contributions of Fred Crowson, Energetics, for his project management assistance and involvement in preparing and publishing this report.

The research at

- Oak Ridge National Laboratory, managed by UT Battelle, LLC for the U.S. Department of Energy, under contract DE-AC05-00OR22725
- Argonne National Laboratory, managed by University of Chicago Argonne, LLC for the U.S. Department of Energy, under contract DE-AC02-06CH11357
- Lawrence Berkeley National Laboratory, managed by University of California for the U.S. Department of Energy, under contract DE-AC02-05CH11231
- National Renewable Energy Laboratory, managed by Alliance for Sustainable Energy, LLC for the U.S. Department of Energy, under contract DE-AC36-08GO28308
- Sandia National Laboratories managed and operated by National Technology and Engineering Solutions of Sandia, LLC., a wholly owned subsidiary of Honeywell International, Inc., for the U.S. Department of Energy's National Nuclear Security Administration under contract DE-NA-0003525.

was sponsored by EERE AMO, Valri Lightner and Brian Valentine.

Acronyms and Abbreviations

λ	wavelength
µm or µ	micrometers or microns
Ω	ohm
2D	two dimensional
3D	three dimensional
Al	chemical symbol for aluminum
Al-LLZO	aluminum-doped LLZO
AMM	Advanced Materials Manufacturing
AMO	Advanced Manufacturing Office
ANL	Argonne National Laboratory
APS	Advanced Photon Source
ATR-FTIR	Attenuated Total Reflectance - Fourier Transform Infrared
BASF	Badische Anilin und Soda Fabrik (German for Baden Aniline and Soda Factory)
°C	degrees Centigrade
C	chemical symbol for carbon
CA	California
C_e	entanglement concentration
c-LLZO	cubic phase lithium lanthanum zirconium oxide
cm^2	centimeter squared
CO	Colorado
CO_2	carbon dioxide
C-rate	charge rate
CRADA	Cooperative Research and Development Agreement
Cu	copper
DC	District of Columbia
DEHS	di-ethyl-hexyl-sebacate
DMF	dimethylformamide
DLIT	dark lock-in thermography
DOE	U.S. Department of Energy
EDS or EDX	energy dispersive X-ray spectroscopy
EERE	Energy Efficiency and Renewable Energy
e.g.	abbreviation meaning “for example”; a Latin phrase, “exempli gratia” meaning “for the sake of example”
EIS	electrochemical impedance spectroscopy
ES	electrospinning
etc.	abbreviation for the Latin phrase “et cetera” which means “and so forth”
EW	equivalent weight
fpm or ft/min	feet per minute
ft^2/min	square feet per minute
FY	fiscal year
g	gram or grams
GDE	gas diffusion electrode
GDL	gas diffusion layer
h or hr	hour
H_2	diatomic hydrogen
H_2O	water
He	chemical symbol for helium

HFTO	Hydrogen and Fuel Cell Technologies Office
HSC	high surface carbon
I/C_{at}	ionomer-to-catalyst ratio
IL	Illinois
IPA	isopropyl alcohol
IR	infrared
IrO_2	iridium oxide
kg	kilogram
kV	kilovolt
kW	kilowatt
kWh	kilowatt hour
La	chemical symbol for lanthanum
$La_2Zr_2O_7$	lanthanum zirconate
LBNL	Lawrence Berkeley National Laboratory
Li	chemical symbol for lithium
LIB	lithium ion battery
LiPF6	lithium hexafluorophosphate
LLC	limited liability company
LLZO	lithium lanthanum zirconium oxide, $Li_7La_3Zr_2O_{12}$
M	molar
MA	mass activity
MEA	membrane electrode assembly
mg/cm^2	milligram per square centimeter
mg_{Pt}/cm^2	milligrams of platinum per square centimeter
min(s)	minute(s)
ml or mL	milliliter
ML	multilayer
mL/hr	milliliters per hour
mm	millimeters
mm^2/min	square millimeter per minute
m/min	meters per minute
mmol	millimole
MPL	microporous layer
mS/cm	milli-Siemens per centimeter
NaCl	sodium chloride (salt)
NDE	non-destructive evaluation
nm	nanometer
NM	New Mexico
NMC	nickel-manganese-cobalt
NP	nanoparticles
nPA	normal propyl alcohol (or normal propanol)
NREL	National Renewable Energy Laboratory
O_2	diatomic oxygen
OPV	organic photovoltaic
ORNL	Oak Ridge National Laboratory
Pa	Pascal
Pa.s	Pascal seconds
PAA	polyacrylic acid
PAN	polyacrylonitrile

PEM	polymer electrolyte membrane
PEMFC	polymer electrolyte membrane fuel cell
PEO	polyethylene oxide
PFSA	perfluoro sulfonic acid
pH	the negative logarithm of the effective hydrogen-ion concentration or hydrogen-ion activity in gram equivalents per liter of the solution
PMA	poly(methyl acrylate)
Pt	chemical symbol for platinum
Pt/C	platinum to carbon ratio
PV	photovoltaic
PVDF	polyvinylidene fluoride
PVP	polyvinylpyrrolidone
QC	quality control
R&D	research and development
R2R	roll-to-roll
RO	reverse osmosis
rpm	revolutions per minute
s	second(s)
S/cm	Siemens per centimeter
SANS	small angle neutron scattering
SARS-CoV-2	severe acute respiratory syndrome coronavirus 2
SAXS	small-angle X-ray scattering
SEM	scanning electron microscope (or microscopy)
SiO_x	silicon oxide
SNL	Sandia National Laboratories
SSB	solid state battery
SWT	SolarWindow Technologies, Inc.
TEM	transmission electron microscopy (or microscope)
TN	Tennessee
UNM	University of New Mexico
U.S.	United States
USAXS	ultra-small angle X-ray scattering
UT	Utah
UV	ultraviolet
V_{oc}	open circuit voltage
vol%	volume percent
vs.	versus
VTO	Vehicle Technologies Office
WAXS	wide-angle X-ray scattering
Wh/kg	watt-hour per kilogram
Wh/L	watt-hour per liter
wt.%	percent by weight
XPS	X-ray photoelectron spectroscopy
XRD	X-ray diffraction
XRF	X-ray fluorescence spectroscopy
ZnO	zinc oxide
ZnO/ITO/PET	zinc oxide / indium tin oxide / polyethylene terephthalate
Zr	chemical symbol for zirconium

Table of Contents

List of Figures

List of Tables

Executive Summary

R2R processing is used to manufacture a wide range of products for various applications which span many industrial business sectors. The overall R2R methodology has been in use for decades and this continuous technique traditionally involves deposition of material(s) onto moving webs, carriers or other continuous belt-fed or conveyor-based processes that enable successive steps to build a final version which serves to support the deposited materials. Established methods that typify R2R processing include tape casting, silk-screen printing, reel-to-reel vacuum deposition/coating, and R2R lithography. Products supported by R2R manufacturing include micro-electronics, electro-chromic window films, PVs, fuel cells for energy conversion, battery electrodes and electrolytes for energy storage, and barrier and membrane materials for air and water filtration. Due to innovation in materials and process equipment, high-quality yet very low-cost multilayer technologies have the potential to be manufactured on a very cost-competitive basis. To move energy-related products from high-cost niche applications to the commercial sector, the means must be available to enable manufacture of these products in a cost-competitive manner. Fortunately, products such as fuel cells, thin- and mid-film PVs, batteries, electrochromic and piezoelectric films, water separation membranes, and other energy saving technologies readily lend themselves to manufacture using R2R approaches. However, more early-stage research is needed to solve the challenge of linking the materials (particles, polymers, solvents, additives) used in ink and slurry formulations and the coating and drying processes to the ultimate performance of the final R2R product, especially for a process that uses multiple layers of deposition to achieve the end product.

To solve the problems associated with these challenges, the R2R Collaboration is executing a research program with outcomes that will ultimately link modeling, processing, metrology and defect detection tools, thereby directly relating the properties of constituent particles and processing conditions to the performance of final devices. The Collaboration team and their research efforts with industry involvement are illustrated schematically in Figure 1. This collaborative approach was designed to foster identification and development of materials and processes related to R2R manufacturing for clean-energy materials development. Using computational and experimental capabilities by acknowledged subject matter experts within the supported National Laboratory system, this project leverages the capabilities and expertise at each of five National Laboratories to further the development of multilayer technologies that will enable high-volume, cost-competitive platforms.

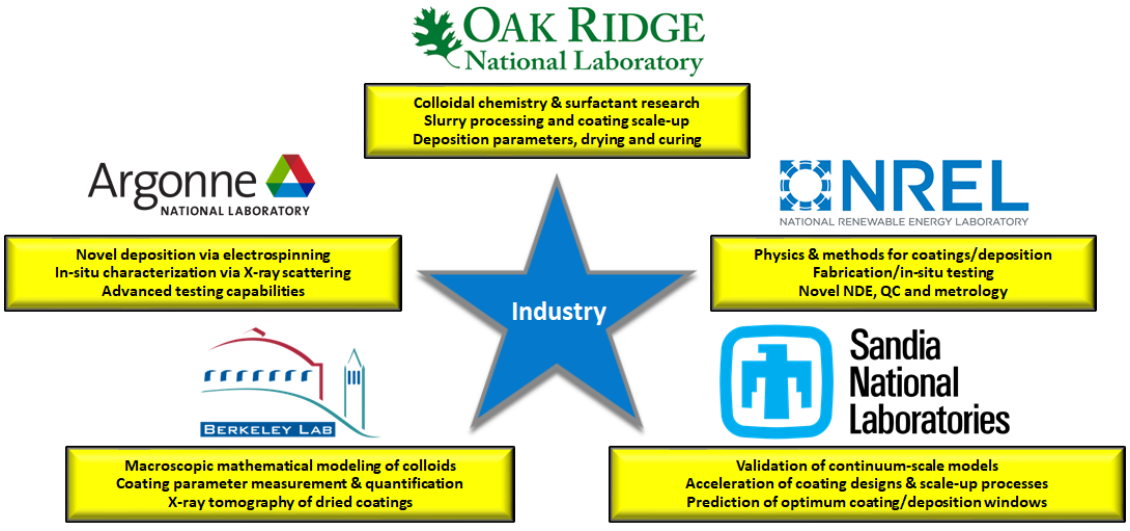

Figure 1. The R2R AMM DOE Laboratory Collaboration team and major research efforts. Source: ORNL

A typical R2R process has three steps: (1) mixing of particles and various constituents in a slurry, (2) coating of the ink/slurry mixture on a substrate, and (3) drying/curing and processing of the coating. Final performance of devices made via R2R processes is dependent on the active materials (e.g., electrochemical particles in battery or fuel cell electrodes) and the device structure that stems from the governing component interactions within the various steps. However, a fundamental understanding of the underlying mechanisms and phenomena is still lacking, which is why industrial-scale R2R process development and manufacturing is still largely empirical in nature.

The FY 2019 through FY 2021 program addresses aspects of the following two targets from the AMO Multi-Year Program Plan:

- Target 8.1 Develop technologies to reduce the cost per manufactured throughput of continuous R2R manufacturing processes.
    - Increasing throughput of R2R processes by 5 times for batteries (to 50 square feet per minute (50 ft^2/min)) and capacitors and 10 times for printed electronics and the manufacture of other substrates and membranes used in support of these products.
    - Developing resolution capabilities to enable registration and alignment that will detect, align, and co-deposit multiple layers of coatings and print < 1 micron (1 μm) features using continuous process scalable for commercial production.
    - Developing scalable and reliable R2R processes for solution deposition of ultra-thin (<10 nm) films for active and passive materials.
    - Develop in-line multilayer (<1 μm) coating technology on thin films (5 – 10 μm) with yields greater than 95%.

- Target 8.2 Develop in-line instrumentation tools that will evaluate the quality of single and multilayer materials in-process.
    - Developing in-line quality control technologies and methodologies for real-time identification of defects and expected product properties "in-use/application" during continuous processing at all size-scales with a focus on the "micro" and "nano" scale traces, lines, and devices, i.e., <1 μm at 300 ft./min for R2R processing in air and <10 nm at 20 ft./min for vacuum processing.
    - Developing technologies to increase the measurement frequency of surface rheology without significant cost increases with a goal of a 10-nanometer in-line profilometry at a production rate of 100,000 square millimeters per minute (100,000 mm^2/min).

The category of electrochemical conversion devices that apply to fuel cells was selected in FY 2019 and continued through FY 2020; however, research was kept general enough that other applications could include solid-state batteries (SSBs), low-temperature water electrolysis, carbon dioxide (CO_2) separation/reduction and water filtration/purification. ES was a specific technology of interest to integrate and adopt as a R2R processing method across a wide range of applications and industrial domains because of its ability to fabricate advanced nanofiber-based materials. This process offers a high surface-to-volume ratio which makes nanofibers the ideal candidate for various applications where high porosity and high surface areas are desirable. Development of a R2R synthesis of nanofiber non-woven structures and membranes continued in FY 2020 for a variety of value-added energy generation, conversion, and storage components and devices.

The R2R Collaboration laboratories successfully completed all tasks toward development of materials and an ES method using R2R manufacturing processes. Additionally, efforts continued for macro-scale and continuum-scale modeling, simulation, processing, manufacturing techniques, and metrology that demonstrated the feasibility and potential for scale-up. The primary tasks for Phase 2 will continue through FY

2021 to develop materials, methods and processes that will transition DOE-supported innovative technologies and practices into U.S. manufacturing capabilities.

Significant high-impact accomplishments that were considered to advance the science and understanding of the R2R processes from an industrial perspective are as follows for each laboratory:

ANL

- Developed scalable nanofiber membrane synthesis recipes and processes for a number of high-profile material systems and applications enabling R2R production, including solid-state battery electrolytes, fuel cell electrodes, ion-exchange membranes, and N95 filter media, which demonstrated ~150x increase in production rate as compared to lab-scale ES.

- Established a low temperature fabrication pathway to synthesize large-quantity, high-purity, undoped cubic phase lithium lanthanum zirconium oxide, $Li_7La_3Zr_2O_{12}$ (LLZO) nanofibers at a temperature that is 500 °C lower than sintered LLZO. This development demonstrated the benefit of continuous R2R membrane synthesis in solid-state lithium battery electrolyte applications.

- Designed and built a scaled co-electrospinning tool that enabled continuous, scalable synthesis of composite and hybrid nano- and micro-fiber membranes with significantly increased material and structure versatility. Dual-fiber ion-exchange membranes were fabricated using co-ES technology, which showed more uniform distribution of functionalities. The application of the continuous synthesis process made it possible to scale-up the membrane for water purification, biofuel treatment, and CO_2 capture applications.

- Converted the R2R ES platform to fabricate reusable N95 facepiece respirator filter media development during the COVID pandemic, in support of the DOE Office of Basic Energy Sciences National Virtual Biotechnology Laboratory consortium. ANL's electrospun filter media showed >95% filtration efficiency and no efficiency degradation after autoclaving disinfection. This filter media also incorporated antiviral function and showed acute virus kill effects with 15 minutes of exposure time, which enabled extended facemask use time and reduced biological waste. This R2R synthesis of reusable N95 filters attracted commercial interest, leading to initiation of a technology transfer process.

- Applied in-situ small-angle X-ray scattering (SAXS) study of the ES process and simultaneous SAXS, wide-angle X-ray scattering (WAXS), and CO_2 detection of in-situ electrospun fiber annealing at Argonne Advanced Photon Source (APS), which revealed material-process-property relationships during ES and phase transformation kinetics during polymer-ceramic fiber conversion. This knowledge enabled further advancement of continuous R2R processing of nanofiber and membrane products.

ORNL

- Simultaneously coated a catalyst ink and an ionomer overlayer onto the gas diffusion layer (GDL) using a dual slot die. This may be the first dual slot-die coating of this kind.

- Conducted annealing studies on LLZO fiber morphology with results that LLZO fibers must be annealed in argon to remove the carbonates and to increase their conductivity.

- Determined that larger variabilities occurred for the thickness and platinum (Pt) loading of a coating prepared from a concentrated slurry for a slot-die coating. Data was provided for SNL modeling to identify improvements to the coating process parameters by adjusting the catalyst slurry formulation. Changes to the operability window achieved a catalyst layer loading of the targeted 0.1 mg_{Pt}/cm^2

across multiple gas diffusion electrodes (GDEs) with 8 wt.% Pt/C slurries processed with a R2R slot-die.

- Performed coating trials with coating gaps smaller and larger than the wet coating thickness resulting in larger gaps having smaller Pt loading variations (4-7%) than the smaller gaps (Pt loading variation 10-40%). Wetting experiments at ORNL using 1-propanol and ethanol solutions with water showed that a lower alcohol content (higher water content) results in higher contact angles because of the hydrophobic microporous layer (MPL) surface. This knowledge allowed improvements that optimized the solvent selection and process conditions for slot-die coating.

- Achieved deposition of an ionomer overlayer on a polymer electrolyte membrane fuel cell (PEMFC) cathode at the same time as the cathode electrocatalyst layer and completed experiments that eliminated the need for an overlayer altogether.

- Synthesized composite aluminum-doped LLZO (Al-LLZO) and polyacrylonitrile (PAN) nanofibers with diameters from approximately 800 nm to 1.4 µm that produced uniformly distributed Al- LLZO on carbon fiber structures. Assembled and tested coin cells based on composite cathodes that exhibited more noticeable power law contributions, in the low frequency regime, which is indicative of a more pronounced ion diffusion mechanism. At higher C-rates, a marked improvement in the specific capacity was evident for the coin cells and especially for the cathode filled with porous Al-LLZO fibers.

NREL

- A new multilayer slide die was commissioned into operation that will enable a new processing capability to explore the potential benefits of multilayer R2R coating related to the reduction of manufacturing energy consumption, footprint, and capital expenditures as well as the potential for new device structures with improved performance and lifetime.

- Performed new studies that confirmed the relationship between heterogeneous ink mixing conditions and the macro-scale morphology of the coated layer. These results assist in the optimization of ink and coating processing across a broad range of industrial applications.

- Conducted a study that revealed an understanding of the impact and optimization of carrier polymer content and R2R ES process conditions for nanofiber-based PEMFC electrodes that are known to provide improved performance over sprayed electrodes.

- Developed novel fast spectroscopy techniques capable of in-line implementation that will enable not-currently-available in-line NDE measurements for multilayer structures like filtration membranes and fuel cell membrane electrode assemblies (MEAs).

LBNL

- Designed a coating and drying observation table to simulate the R2R fabrication conditions of materials used by the other laboratories but at a scale that is small enough to be easily combined with analytical tools such as those at the LBNL Advanced Light Source beamlines. The table will be used to observe solidification of coatings at a microscopic level to collect data for the development and refinement of macroscopic drying models.

- Constructed an automated mixing experimental setup comprised of custom electronics and computer-controlled components, and a flow-through particle size analyzer than can operate up to a 5 Hz sampling rate. This setup will be used to study how agglomerates, inks, and slurries in dilute to

concentrated solutions are structured in 3D and to characterize their properties quantitatively. The information collected will be used to refine mixing/agglomeration models that can improve slurry mixtures and optimize coating material characteristics.

- Performed preliminary experiments with carbon black dispersed in mixtures of 70% alcohol in water and 10% alcohol in water. Results showed significant effects of solvent composition on particle size distribution.

- Transformed the LBNL computer-controlled mixing setup into a portable mixing station allowing reliable recreation of samples in the vicinities of instruments in different locations with minimum variation in samples and increasing the confidence levels of the data.

- Released an update to LBNL's highly flexible open-source simulation package that will be used to implement future models. The open source software is available for download from https://bitbucket.org/berkeleylab/esdr-pygdh.

SNL

- Established models and workflows for single-layer slot-die and slide-die capillary hydrodynamic coating models that can be used to simulate ink deposition from die to substrate and determine the boundaries (in parameter space of web speed, coating die geometry and configuration relative to the web, vacuum pressure, and film thickness) for the R2R process operability window.

- Extended R2R slot-die and slide-coating deposition models to accommodate simultaneous delivery of two layers (slot die and slide die) and even three layers (slide die). The simulation of simultaneous three-layer slide coating flow is the first of its kind to be published in the literature (a technical paper was submitted to the Journal of Coating Research).

- Completed efforts for full accommodation of complex ink rheology in all models using power-law and Carreau constitutive equations for shear-rate-dependent viscosity.

- Validated the single-layer slot-die coating model against coating trials at ORNL with polymer-electrolyte membrane inks with platinum catalyst with carbon support with ionomer in a water-alcohol solvent. The model is predictive of the coating operability windows for lower concentrations of particles. Models will used to guide all future coating trials.

- Developed a user-interface for a slot-die coating simulator that enables wider usage.

- Validated a drying and solidification model with published polymer-solvent drying data.

- Developed an experimental drying capability that enables measurement of solvent loss with time and visualization of particle motion during drying. An extended drying and solidification model that include particles has been constructed.

Technology transfer for technologies applicable to R2R manufacturing was initiated through collaboration with industry partners for the CRADA projects and other associated program areas. Research results from the R2R Collaboration laboratories were presented at conferences, symposia, peer reviews and during direct contact with industry and the commercial sector. Specific research and experimental results were reported in technical journals and through patent applications.

Accomplishments

COVID-19 Statement

Beginning mid-March 2020, all National Laboratories were closed, and no in-house laboratory work was allowed due to COVID-19 restrictions. In accordance with the respective State guidance, the R2R Collaboration teams worked from home and continued with data analysis, literature research, writing manuscripts, performing design activities, and leveraging manufacturers who still had ongoing operations to have parts fabricated. Once restrictions started to relax, a staged reopening of the laboratories was initiated. Some minimum amount of research was conducted in limited blocks of time and on a special case basis and with limitations on the number of people occupying each laboratory at a given time to ensure distancing. This significantly impacted the research tasks and milestone schedules; however, several tasks were able to continue to produce results and accomplishments.

Highlights for the FY 2020 primary tasks at each laboratory are listed below.

Core Program Projects

ANL Novel R2R Deposition System Based on ES Technology and Advanced/In-Situ Characterization and Testing Capabilities

- Developed chemistry and processing conditions for a scalable synthesis of pristine LLZO (non-doped) solid-state electrolyte materials using R2R ES. This included optimum process parameters for electrospun LLZO polymer precursor nanofiber fabrication and a post-spinning annealing process to convert precursor to cubic phase crystalline LLZO. A thermal treatment process was also developed to remove surface lithium carbonate from LLZO nanofibers and improve fiber lithium ion conductivity

- Achieved in-depth understanding of LLZO nanofiber formation and phase transformation from precursors through in-situ simultaneous SAXS, WAXS and CO_2 characterization of electrospun nanofiber annealing at the Argonne APS. The results indicated that the polymer precursor fibers were amorphous at temperatures between room temperature and 500 °C. At 500 °C, the lanthanum zirconate ($La_2Zr_2O_7$) precursor phase formed first, which was accompanied with polymer fiber oxidation. Cubic phase LLZO was formed at 600 °C when polymer oxidation was completed. The cubic phase was stable between 600-800 °C and decomposed at higher temperatures. The same crystallization and phase transformation process was observed for both pristine (non-doped) and Al-LLZO.

- Investigated nanofiber LLZO crystal structure using Large-scale Atomic/Molecular Massively Parallel Simulator partial charge model, which indicated a stable cubic crystal structure for nanocrystalline LLZO. This study explained the reason why nanofiber LLZO had a cubic crystal structure at 600 °C while the bulk or micrometer-scale LLZO powder has a tetragonal structure at this temperature and needed to be sintered above 1100 °C to form the cubic structure. The investigation suggested a unique capability of ES regarding low-temperature manufacturing of cubic LLZO, which is energy efficient. The TEM study of the LLZO nanofibers confirmed the nanocrystalline nature of the LLZO grains and indicated 10-20 nm grain sizes.

- Measured electrochemical impedance spectroscopy of symmetric Li/LLZO/Li cell, which derived 1.3 $x10^{-5}$ S/cm ionic conductivity at 100 °C. The relatively low conductivity was due to the low packing density of the cold-pressed LLZO pellet (60% density).

- Reusable N95 filter media was developed using the R2R ES process. The electrospun media showed filtration efficiency of >95% and no efficiency degradation after ten cycles of disinfection by autoclaving or by a 10% bleach spray. Antibacterial and antiviral functions were also incorporated to the electrospun filter media by introducing antimicrobial ingredients to the electrospun nanofibers. Antibacterial function was demonstrated on E.coli bacteria. Antiviral testing was performed using bacteriophage Phi6 as the severe acute respiratory syndrome coronavirus 2 (SARS-CoV-2) surrogate, which showed effective destruction of the virus after a 15-minute exposure. This development was also supported by the DOE Basic Energy Sciences Office within the National Virtual Biotechnology Laboratory program.

- Developed ES recipe to fabricate cation- and anion-exchange ionomer nanofibers for deionization membrane fabrication. Fiber mats with well-mixed Nafion and Sustainion fibers were demonstrated using a co-electrospinning method. The ionic conductivity of about 0.3 mS/cm was measured for the Nafion, Sustainion, and dual-fiber samples.

- Improved R2R ES processing conditions and demonstrated an increase of fiber production rate by six-fold. This improvement was applicable not only to ANL ES recipes but also to an ORNL ES recipe for Al-LLZO fabrication, showing potential of scalable synthesis of nanofiber-based energy storage materials.

- Collaborated with ORNL and NREL on ES recipe development for battery electrolyte/electrode and fuel cell electrode applications. These recipes were tested on the ANL R2R ES equipment as a scale-up demonstration. Fiber samples were sent to NREL for advanced in-line metrology development. ANL also performed SAXS and ultra-small-angle X-ray scattering (USAXS) analysis of NREL's ES inks at the Argonne APS to understand the influence of ink composition and microstructure on its rheological properties and coating behavior. This development led to two joint publications with NREL.

- Prepared and characterized the rheological properties of high-viscosity copper nanoparticle inks as part of the feasibility study for printed electronics development under the R2R Collaboration program.

ORNL Colloidal Chemistry, Surfactant Research, Slurry Processing, Deposition and Drying and Curing and Curing Methods

- ORNL in collaboration with ANL scaled LLZO and Al-LLZO nanofibers that can be manufactured using the electrospinning technique. Aqueous and non-aqueous precursors were used. The nanofibers were crystalized in the cubic phase. The fabrication conditions were optimized to tailor the diameter of the nanofibers.

- Baseline data for particles sizes from different mixing experiments were provided to LBNL to support modeling efforts. The thickness and Pt loading of a coating prepared from a concentrated slurry was determined to have a larger variability than is typical for slot-die coating.

- A catalyst layer loading of 0.1 mg_{Pt}/cm^2 was achieved across multiple GDEs with 8 wt.% platinum on carbon (Pt/C) slurries processed with a R2R slot-die. X-ray fluorescence (XRF) spectroscopy analysis determined that the Pt loading increases with increasing ink pump speed, as expected.

- Static sessile drop contact angle measurements of 1-propanol and ethanol solutions with water showed that a lower alcohol content (higher water content) results in higher contact angles because of the hydrophobic MPL surface. An 8 wt.% Pt/C catalyst layer ink dispersed in a 28.5 wt.% 1-propanol in

water solution gave a contact angle of 75° on a GDL, higher than expected for the dispersion media composition.

- Catalyst ink rheology measurements showed that the shear viscosity of lower solids-loading 6 wt.% Pt/C ink is lower than that of the higher solids-loading 8 wt.% Pt/C ink. Small angle neutron scattering (SANS) data was collected for 56 ball-milled ink samples with low solids-loading.

- Coatings trials were performed with coating gaps smaller and larger than the wet coating thickness. Larger gaps gave smaller Pt loading variations (4-7%) than the smaller gaps (10-40%). The mean areal Pt loading is too high (0.351 mg_{Pt}/cm^2) with the larger coating gaps because of vacuum and ink pump limitations.

- Dual functionality Al-LLZO/PAN fibers were fabricated using a core-sheath configuration. The fibers can be scaled using coaxial electrospinning. The precursor solutions of the two phases were optimized to obtain uniform fibers. The diameter of the composite Al-LLZO/PAN nanofibers was varied from approximately 800 nm to 1.4 µm. The fibers were carbonized to obtain ionically and electronically conductive nanofibers. Spectroscopic analyses showed that the Al-LLZO was uniformly distributed on the carbon fiber structures

- Slot-die deposition of an ionomer overlayer on a PEMFC cathode at the same time as the cathode electrocatalyst layer was achieved and trials were completed that eliminated the need for it altogether.

- Single and dual slot-die coating parameters were exchanged with SNL to implement into a 2D GOMA model. SNL and ORNL are now having monthly technical conference calls where the model data is guiding the coating parameter selection.

- Electrospun Al-LLZO nanofiber scaffolds were used as cathode additives. Coin cells based on composite cathodes were assembled and tested. The composite cathodes exhibited improved cycling at high C-rates, higher Coulombic efficiency, and higher capacity retention at long-term-cycling.

NREL Physics and Methodologies for Multilayer Coatings/Deposition; Fabrication and In-Situ Testing of Prototype Components and Devices; and Novel NDE, Quality Control and Metrology

- NREL provided SNL a detailed listing of target multilayer coating structures to clearly define priority modeling scenarios as the 2-layer and 3-layer slide die models that are being developed.

- NREL coordinated with ORNL on overall plans for colloids, coating, and drying focus areas and to collaborate on cell fabrication and in-situ testing using the ORNL-coated GDEs. NREL coordinated with ANL on the small-scale ES effort and scaling an initial NREL-developed ES formulation on the ANL R2R ES system.

- The three-layer slide die was received at NREL. Multiple high-resolution cameras were identified for flow imaging, and bracketry was obtained to mount the cameras in different configurations. The slide die was installed in a hood for initial flow testing and the newly machined flow inlets were installed to make the die operational.

- Slurry particle size data was collected during USAXS experiments that confirmed the reduction of agglomerates in the slurry by the addition of poly(acrylic) acid (PAA). XRF measurements were performed to validate catalyst loading.

- NREL fabricated MEAs using R2R slot-die-coated GDEs from ORNL and performed in-situ testing. Electrochemical performance evaluation determined that catalyst layers without ionomer overlayers

(spray or dual slot-die coated) performed better than catalyst layers with ionomer overlayers. None of the overlayer GDEs performed better than the single-layer GDE; however, the two-layer GDE with the least amount (thickness) of overlayer provided the best performance of the two-layer GDEs.

- Electrochemical impedance spectroscopy measurements were performed for two MEAs, and the results were largely consistent with the polarization data. A high level of non-uniformity in the loading as well as the visual appearance of the electrodes was observed.

- Bright and dark field optical microscopy imaging was performed in the reflectance mode for ANL-fabricated LLZO electrospun materials on an aluminum substrate to understand the micro-scale morphology of the nanofiber materials.

- NREL developed spectroscopy methods to be used for heterogeneous particle-polymer inks; one was focused on continuing to improve the Attenuated Total Reflectance - Fourier Transform Infrared (ATR-FTIR) spectroscopy measurement methodology by exploring scattering and index-of-refraction-matching (Christiansen effect) of the spectroscopic behaviors that may be affecting measurements. Indices of refraction data for Nafion were determined to overlap near the previously measured absorption troughs indicating that the Christiansen effect may be prevalent. This finding assists in the proper analysis of the data and correlation to material properties.

- Mid- to far-infrared (IR) measurements of common porous carbon substrates were made to understand the transmission (penetration of dissimilar layers) characteristics of these materials and elucidate possible modes of measurement for observing active layers adjacent to and "through" the porous substrate.

LBNL Macroscopic Mathematical Model of the Drying of a Single Layer Generic Slurry Containing Monodisperse Colloidal Particles, Binder, and Solvent

- A coating and drying observation table was designed to simulate the fabrication conditions for materials being investigated at the other Labs, but at a scale that is small enough to be easily combined with analytical tools such as those at the Advanced Light Source beamlines.

- The base automated mixing experimental setup comprised of custom electronics and computer-controlled disperser, pump and motorized lab jack that is needed for the experiments was constructed. The setup also includes a flow-through particle size analyzer operating up to a 5 Hz sampling rate.

- The chiller for the mixing experimental setup was upgraded with a serial communication port and additional code was added to the equipment control library to control and query the chiller which will improve compatibility with the dispersion preparation techniques used by the other R2R teams.

- Custom temperature bath sample holders were designed that are compatible with the motorized sample stages to load samples consistently and keep them at a controlled temperature.

- A portable custom cart with an adjustable platform was designed to isolate the motorized components of the mixing experiment setup (mixer, stage, pump, and chiller) from vibration-sensitive instruments (particle size analyzer and soon, confocal microscope) and to position the mixer and pump in a consistently reproducible position relative to different instruments.

- The LBNL computer-controlled mixing setup was transformed into a portable mixing station, allowing reliable recreation of samples in the vicinities of instruments in different locations. This station includes a LBNL-designed custom temperature bath along with a heat exchanger and coolant pump that allows the powerful chiller to be used to maintain an open bath.

SNL Validated Continuum-Scale Models to Accelerate Design and Scale-Up of Simultaneous Die Coating Process Technology

- The deposition models of single- and two-layer slot-die coating flow were completed along with a working user interface to improve usability.

- Rheological data for a representative single- and two-layer-slot coating stack were fit with standard constitutive equations and implemented in the models.

- Development continued for the first-of-a-kind, 3-layer slide die model. Configurations were planned for the slide die coating trials. A special slide-only model is being used to help NREL redesign the lip geometry.

- The single-layer model operating space was validated using process inputs from ORNL. SNL models predicted the coating window (11 in H_20 for 60 µm gap and 14 in H_20 for 60 µm vacuum at 3 ft/min coating speed) for ORNL single-layer slot-die coating trials with a complex 8 wt. % Pt/C catalyst ink that guided the experiments aimed at increasing the coating gap (slot-to-web) from 60 µm to 90 µm for better coating quality at a 30 µm coating wet thickness.

- The initial poly(methyl acrylate) (PMA) polymer and toluene solvent single- and two-layer drying model was completed with comparable values found in the literature. Configurations were planned for the slide die coating trials. The multilayer slot-die model was useful in understanding and controlling slot-die coating operability. The single-layer model operating space was validated using process inputs from ORNL.

- A new mesh/solid-model design for the slot-die model was developed to ease in gap-based parameter studies. A significant finding that needs to be experimentally verified is that the models predict that the low-vacuum limit disappears at all web speeds for smaller gaps and concentrated Pt/C inks. Stability analysis on the slide-only multilayer models has revealed potential for interlayer defects.

- With funding from the National Science Foundation, SNL, and University of New Mexico (UNM) continued to advance a machine-learning model to connect coating defects of particulate conductive films (pinholes, striations) to process parameters for gravure coating/printing. Data was captured with high-end optical microscopy coupled with open computer vision image recognition tools.

CRADA Projects

Three CRADA projects that initiated in mid-FY 2018 continued through FY 2019 and into FY 2020.

Navitas Systems, Inc. partnered with ORNL and NREL to demonstrate R2R production of an advanced separator for lithium-ion batteries.

- Gravure printing was demonstrated as a new R2R capability with wide applicability. Two platinum-carbon inks were successfully printed and R2R printing of the pattern was achieved. The pattern was printed at three different relative speeds of the web and cylinder and good matching was achieved with the current webline controls.

- The project was successfully completed in FY 2020.

SolarWindow Technologies, Inc. partnered with NREL and ANL to demonstrate diffractive multiplexing for high-throughput R2R laser patterning of flexible OPV modules.

- Several meters of P1 scribes on zinc oxide / indium tin oxide / polyethylene terephthalate (ZnO/ITO/PET) were scribed on the R2R line. Problems were solved with the ZnO electron transfer layer and PV mini-modules on flexible ITO/PET web substrate using both sheet-to-sheet single-laser and multiplexed diffractive optic laser scriber tools. PV mini modules were made on flexible ITO/PET web substrate.

- Tests were performed that successfully maintained a laser scribe parallel to an existing scribe for a few meters of sample running through the R2R laser scribing tool.

- The organic hole-transport layer that is deposited on top of the absorber was optimized by using a new absorber.

- Dark lock-in thermography was used to investigate the quality of module interconnects with three different ZnO electron transport layers and two different P1 laser scribing settings.

- Surface profile measurements were taken and the ITO sidewalls of the P1 were observed to peel up from the PET. Improvements to the adhesion of the ITO to the PET substate were attempted by thermally evaporating a thin layer of silicon oxide (SiO_x) onto bare PET and then sputtering ITO onto the SiO_x.

- Transforming the laser beam profile from Gaussian to square shaped showed greatly improved scribes, especially at the side walls. A beam expander and "top-hat" beam shaper will be used to improve scribes. Flex modules were built with new P1 scribes. Lower laser repetition rates produced the best scribes, with surface profile measurements showing that new P1 scribes have much reduced side wall heights down to 100-150 nm. Dark lock-in thermography confirmed that the P1 scribe was improved.

- A flexible glass substrate was used as an alternative to the PET. Integration of the flexible glass onto the R2R multiplexed laser scribing tool was achieved. P1 scribes with minimal sidewalls were fabricated by tuning the repetition rate of the laser pulses striking the ITO/glass.

- The R2R multiplexed laser tool was used successfully to scribe P2 lines, and a working PV module comprising 12 individual sub-cells connected in series through the P1/P2/P3 interconnects was fabricated. Working full modules were fabricated on flexible glass using the single line laser scriber, as a comparison to R2R-processed modules. Module performance is similar between the two scribing processes and demonstrates the success of the multiplexed laser scribing on the R2R. The fastest R2R scribing has been 14 simultaneous scribe lines at a rate of 2 ft/min. This speed can be increased by at least 2x.

- This project was successfully completed in FY 2020.

Nel Hydrogen partnered with NREL, ORNL, and ANL to research R2R manufacturing of advanced (low loading and directly coated onto the membrane) electrolysis electrodes for low-cost hydrogen production. The CRADA was initiated in FY 2020 and is scheduled to complete in FY 2021.

- Catalyst inks were prepared with iridium oxide (IrO_2)catalyst and Aquivion ionomer using 1-propanol and ethanol with water in varying ratios of water/alcohol.

- NREL cast catalyst layers on polyimide sheets for USAXS/SAXS and nano X-ray computed tomography at ANL.

- NREL studied the uptake of water/alcohol mixtures by the proton exchange membrane using a force tensiometer with results that pure water and alcohols are absorbed more slowly than mixtures.

- Rheology measurements were performed by NREL to compare the shear viscosity of two common ink compositions with different ionomer-to-catalyst ratios (I/C_{at}). The ink with $I/C_{at} = 1$ has similar viscosity to the fuel cell ink that ORNL successfully slot-die coats onto a GDL.

- NREL prepared R2R gravure coatings to create IrO_2 catalyst layers. Coatings were fabricated with a polytetrafluoroethylene substrate using the baseline catalyst material to tune the loading.

- Two different IrO_2 catalysts were successfully coated on a perfluoro sulfonic acid membrane to make catalyst-coated membranes that achieved the target loading with the baseline material. Overall, the coatings were very uniform. These samples were sent to Nel Hydrogen for in-situ electrochemical testing.

Collaboration and Outreach

The R2R Collaboration team participated in monthly review meetings with DOE AMO and HFTO Technology Managers to ensure information for each project was available on a continuous and regular basis. Team members also presented (virtually) at the Association of International Metallizers, Coaters and Laminators R2R Conference; the symposium of the International Society of Coating Science and Technology; the fall meeting of the Electrochemical Society; the Center for Compact and Efficient Fluid Power Summit; the 2020 DOE Hydrogen and Fuel Cells Program Annual Merit Review, the Vehicle Technologies Office Annual Merit Review; and the 2020 AMO Peer Review. Principal investigators collaborated with the industry partners as a team for the CRADA projects described above. Educational outreach by the R2R Collaboration has supported a total of 19 post docs, graduate and undergraduate students, and interns from 15 separate universities.

Technology Assessment

Because of the nature of the early-stage research tasks, the technologies under development were not matured sufficiently for direct transfer to industry; however, technology transfer for these and other technologies applicable to R2R manufacturing was initiated through collaboration with industry partners and through the continuation of three CRADA projects with industry. Since Phase 2 is a three-year research effort, technologies under development will continue to mature towards commercialization through FY 2021.

Roll-to-Roll Advanced Materials Manufacturing DOE Laboratory Collaboration Project Overview

Collaboration Contacts

Claus Daniel, Collaboration Team Lead (October 2019 through April 2020)

Oak Ridge National Laboratory (ORNL)
National Transportation Research Center
2360 Cherahala Blvd.
Knoxville, TN 37932
Phone: 865-946-1544
Email: danielc@ornl.gov

David L. Wood III, Collaboration Team Lead (May 2020 through September 2020)

Oak Ridge National Laboratory (ORNL)
National Transportation Research Center
2360 Cherahala Blvd.
Knoxville, TN 37932
Phone: 865-574-1157
Email: wooddl@ornl.gov

Georgios Polyzos, ORNL Project Team Lead

Oak Ridge National Laboratory (ORNL)
National Transportation Research Center
2360 Cherahala Blvd.
Knoxville, TN 37932
Phone: 865-576-2348
Email: polyzosg@ornl.gov

Gregory K. Krumdick, ANL Project Team Lead

Argonne National Laboratory (ANL)
9700 S. Cass Avenue
Building 362
Argonne, IL 60439-4844
Phone: 630-252-3952
Email: gkrumdick@anl.gov

Michael Ulsh, NREL Project Team Lead

National Renewable Energy Laboratory (NREL)
15013 Denver West Parkway
Golden, CO 80401
Phone: 303-275-3842
Email: Michael.Ulsh@nrel.gov

Vince Battaglia, LBNL Project Team Lead

Lawrence Berkeley National Laboratory (LBNL)
1 Cyclotron Road
MS 70R 0108B
Berkeley, CA 94720

Phone: 510-495-2679
Email: vsbattaglia@lbl.gov

P. Randall (Randy) Schunk, SNL Project Team Lead

Sandia National Laboratories (SNL)
Advanced Materials Laboratory
1001 University Blvd., SE
Albuquerque, NM 87106
Phone: 505-844-5992
Email: prschun@sandia.gov

Brian Valentine, DOE Roll-to-Roll Technical Project Officer

Department of Energy (DOE)
Energy Efficiency and Renewable Energy (EERE), EE-5A
Advanced Manufacturing Office (AMO)
1000 Independence Ave., S.W., Suite 5F-063
Washington, DC 20585-0121
Phone: 202-586-9741
E-mail: brian.valentine@ee.doe.gov

Technical Contacts:

ORNL: Jianlin, Li, Jaswinder Sharma, Erin Creel, Alexander Kukay
ANL: Deborah Myers, Yuepeng Zhang, Devon Powers
NREL: Scott Mauger, Peter Rupnowski, Bertrand Tremolet deVillers, Kenneth C. Neyerlin
LBNL: Kenny Higa, Zhi Huang, Bei Fan, Buyi Zhang
SNL: Randy Schunk, Nelson Bell
UNM: Kristianto Tjiptowidjojo, Chris Wall, Ben Wall, Robert Malakhov

Industry Partners:

Navitas Systems LLC
SolarWindow Technologies, Inc.
Nel Hydrogen
General Motors
Giner
Plug Power
Saint-Gobain
Eastman Kodak

Annual Operating Plan Title and Corporate Planning System (CPS) Agreement Numbers

Roll-to-Roll Manufacturing Science and Applications: From Ideal Materials to Real-World Devices

ORNL CPS# 97995
ANL CPS #s 29915, 32553 and 32681
NREL CPS #97995
LBNL CPS #31112
SNL CPS #35102

Project Introduction

Modern variants of proven, classical R2R coating technologies, as well as new coating methods, are needed for enabling widespread commercialization of renewable energy storage and conversion technologies. Established coating methods, such as multilayer slot-die, gravure, reverse comma, tape casting, etc. with homogeneity and uniformity superior to spraying methods need to be further adapted for improving performance of various technologies. The shape, size, and morphology of the materials, the chemistry of the formulation, the nature of slurries, their coating rate, the rate of drying etc. all play a role in determining the final coating architecture, quality, and performance. In addition, NDE of the produced coatings for improving in-line QC and identification of defects, prior to down-stream value added steps being performed, is of paramount importance.

More early-stage research is required to solve the challenge of linking particles used in material formulations to the performance of the final R2R product, especially for a process that uses multiple layers of deposition to achieve the end product. This activity brought together expertise from five national laboratories to understand the complex nature of the R2R process and develop methods to improve existing production capabilities.

Objectives

The overall objective of this collaborative effort is to advance technologies applicable to continuous manufacturing to reduce cost, increase precision, and enable in-line QC and defect detection that will result in expanded use of R2R processing to produce clean energy technologies. Modeling and simulation of the materials and processes being developed will be used to understand the fundamental physics and particle interactions of those materials as they relate to the manufacturing process on both a macroscopic scale and a continuum scale.

A specific objective is to develop methodologies for multilayer coatings, including those achieved by a single layer (or single process) construction, with the same performance as structures fabricated in multiple process steps, thus reducing the number of process steps, and reducing manufacturing cost. Another objective is to advance ES and casting technologies to enable functional multilayer coating approaches for a variety of applications. Metrology and analytic tools and methods will be developed to further enable identification of process defects and impacts on a real-time basis. The sum of these efforts that are applicable to flow batteries for grid applications, filtration applications, electrochemical applications, fuel cell and electrolysis membranes, catalysts free of Pt group metals, electrodes for electrochemical CO_2 reduction concepts, water manufacturing, and others will serve to advance the state-of-the-art processing science related to these technologies.

Approach

Core Program

This early stage R&D project on R2R advanced technologies in a national multi-lab collaboration will deliver advances in the fundamental understanding of R2R processing on moving webs, carriers, or other substrates and develop tools, metrology approaches, processes, and new materials to improve yields, overall quality, processing rates and reduce cost. Innovative R&D will overcome the lack of scalability and understanding of fundamental chemistry and materials properties demonstrated on selected key technology applications with cross-cutting impacts. The collaboration will explore and execute new methods to engage with industry and other R2R stakeholders that will enable pre-commercial, low technology readiness level activities.

Technology focus for ORNL, ANL and NREL will be on the process science of multilayered coating deposition and drying and curing, its associated fundamental kinetics, modeling and simulation, and metrology

to understand quality and defects. An advanced mathematical modeling approach will be implemented where LBNL develops particle-scale colloidal and slurry optimization models that enables understanding of particle effects on mixing. This information will be subsequently provided to SNL for developing more accurate rheology constitutive relationships for the continuum-scale coating deposition and drying models. In turn, this latter information will be provided to LBNL for developing models for wet coating consolidation and drying processes. ORNL, ANL, and NREL will support the overall three-phase modeling effort by providing experimental data for materials, components, processing parameters, and devices.

Novel R2R Deposition System Based on ES Technology and Advanced/In-Situ Characterization and Testing (ANL Lead Laboratory)

ANL will perform tasks in coordination with ORNL, LBNL, NREL, and SNL, with a focus on the development of a novel R2R deposition system based on ES technology, as well as advanced and in-situ characterization and testing capabilities. Materials developed through this pathway are applicable to fuel cell/electrolysis, air and water filtration/purification, solid-state battery electrolytes, OPVs, flexible electronics, and CO_2 separation/reduction when integrated with multilayer coating techniques. The development of this highly versatile deposition process will enable significantly improved productivity and device quality (as compared to conventional deposition methods) for a wide range of high performance applications. In addition to toolsets, ANL will also develop recipes and processing parameters that are suitable for high throughput R2R ES processes. Also, under this context, ANL will collaborate with ORNL and NREL to develop three model innovative nanofiber material systems as an effort to demonstrate the benefit of R2R ES manufacturing. In-situ hard X-ray characterization (e.g., SAXS and WAXS) and high-resolution electron microscopy (e.g., high-resolution transmission electron microscopy and scanning transmission electron microscopy) will be applied to accelerate materials development. Finally, ANL will apply knowledge developed around nanomaterials and coatings to ink formulation development for printed electronics applications.

ANL will work closely with ORNL to improve material property and cell performance for LLZO nanofiber-based solid-state electrolyte development. Ionic conductivity and charge-discharge cycle life of the cell will be improved through LLZO fiber quality and electrolyte-electrode interface improvement. ANL will also support NREL's in-situ metrology development by providing electrospun fiber mats of different materials, thicknesses, and fiber morphologies for NREL to perform characterization tool design and testing. In addition, ANL will contribute to modeling and simulation work related to inks and multilayer coatings by providing ink data to SNL and LBNL to enable theoretical studies of correlations between ink compositional properties (e.g., ingredients, solvents, viscosity) and ink flow, deformation, and drying behavior.

Advanced and in-situ testing and characterization of prototype components and devices will be a collaborative effort between ANL, ORNL, and NREL and will focus on fabricating components and devices prevalent within water, fuel cell, and energy storage applications. ANL will provide nanofiber materials, ink solutions, and solvents for distribution to the other laboratory partners for slurry and multilayer composite membrane synthesis and testing. ANL will also develop and optimize coating recipes for new materials and applications using lab-scale coating equipment to deepen scientific understanding of physical mechanisms related to device property and performance as well as property-process relationship. Advanced ink and electrode characterization will focus on obtaining ink and electrode microscopic and tomographic properties using high-resolution synchrotron-based diffraction and imaging techniques, to enable a more in-depth understanding of structure properties of multilayer coatings. ANL will conduct USAXS, SAXS and X-ray computed tomography studies of the ink and electrodes provided by ORNL and NREL.

Colloidal Chemistry, Surfactant Research, Slurry Processing, Deposition and Drying/Curing Methods (ORNL Lead Laboratory)

ORNL will utilize materials provided by ANL and other collaboration partners and provide R2R processed materials to ANL and NREL for characterization. ORNL will also work with SNL on advanced modeling and simulation and processing science for special coating operations such as slot die. ORNL will work with LBNL to provide data for modeling and simulation of the drying behavior with a special focus on interfaces and solvent/curing agent behavior and relevant defect structures. LBNL staff will spend research time at ORNL to understand processing science with hands-on experiments and enable a close integration of modeling and simulation into the results guiding the experiments.

Materials will be received from other project partners and integrated into a fully-controlled and optimized multilayer coating operation. Slurry processing efforts will focus on understanding particle interactions, receiving experimental guidance from the modeling and simulation tasks at LBNL and SNL, measuring zeta-potential of individual slurry constituents, optimizing multi-component mixing and long-term stabilization of slurries. Advanced characterization methods such as transmission electron microscopy (TEM) and X-ray photoelectron spectroscopy (XPS) will be utilized to determine the material properties.

Optimized slurries in single and multi-slurry systems will be deposited in multiple steps and single steps (dry on wet and wet on wet) to create multilayer coatings. During drying and curing operations, phase separations and phase intermixing phenomena will be studied and resulting interfacial behavior and their effects on functional properties will be determined and optimized. This methodology will be conducted in close collaboration with the modeling and simulation tasks at LBNL and SNL. Coated materials will also be distributed to the other laboratory partners to study defect structures and functional device performance.

To support R2R ES platform development by ANL, ORNL will provide lab-scale support of collaboration advancements in the fundamental understanding of R2R processing on moving webs, carriers, and other substrates. ORNL will assist in development of tools, metrology approaches, processes, and new materials such as cubic phase Al-LLZO to improve yields, overall quality, processing rates, while also reducing cost. Benchtop experiments will be performed that are aimed at overcoming the lack of scalability and understanding of fundamental chemistry and materials properties demonstrated on multiple selected key applications with cross-cutting benefits and impacts.

Physics and Methodologies for Multilayer Coatings/Deposition; Fabrication and In-Situ Testing of Prototype Components and Devices; and Novel Non-Destructive Evaluation, Quality Control and Metrology (NREL Lead Laboratory)

The NREL effort for multilayer coatings and deposition will focus on the physics, methodologies, and equipment for multilayer coatings, which are applicable across a vast range of materials, including functionalized membranes and porous media, ion transport media, catalytic membranes, water filtration and purification media, electrochemical active layers, and opto-electronic films. Multilayer structures can be implemented in various forms, including being coated or deposited in simultaneous but discrete layers, or by being coated in a single layer but taking advantage of consolidation physics to stratify individual constituents. A particular focus will be exploration of multilayer coating technologies such as slide dies that generally are not or have not been applied to these applications, but may provide great improvements in throughput, energy consumption, or quality, and could lead to novel structures. In support of a process-focused study, detailed exploration of particle-polymer-solvent interactions in the subject inks and slurries will be undertaken, with advanced characterization, modeling and/or visualization support from other labs. It is expected that close coordination with SNL and LBNL on slurry, coating and drying modeling will be pursued to achieve fundamental understandings of these processes and materials. Small-scale ES fabrication capabilities will be leveraged to pursue basic process understandings for the ES process, including the development of detailed

process windows. NREL will collaborate with ANL to explore scale-up of ES formulations at ANL's R2R ES facility.

Fabrication and in-situ testing of prototype components and devices, representative of potential commercial products, is critical to understand the impact of novel R2R processing techniques on new material technologies. NREL will bring to bear a wide range of application-specific device fabrication and testing capabilities to support the breadth of material technologies within the multi-lab collaboration.

Real-time in-line and in-process measurement techniques for NDE, QC and metrology are a ubiquitous and cross-cutting need for novel R2R materials, as identified in the AMO Multi-Year Program Plan. In close coordination with industry and Collaboration partners, NREL will develop and demonstrate real-time inspection techniques that are broadly applicable. A particular focus of this effort at NREL will be thermal and multispectral imaging techniques to measure material properties or detect defects in multilayer structures. This work will leverage existing thermographic, optical, electro-optical, and fluorescence test-beds, at various scales, and a full-scale industrial web-line, in order to explore excitation physics, impact of material motion, and optimization of sensitivity and resolution, as well as to demonstrate methods on the web-line using sheet or roll materials from industry or fabricated at NREL or partner labs.

Macroscopic Mathematical Model of the Drying of a Single Layer Generic Slurry Containing Monodispersed Colloidal Particles, Binder and Solvent (LBNL Lead Laboratory)

LBNL will prepare an experimental setup to support the mathematical model development of component association and aggregation in mixing and for drying and consolidation of dispersion coatings. As the component interactions and their effects on macroscopic behavior for these concentrated dispersions of interest are poorly understood, LBNL will design and execute novel experiments and build a setup needed to provide the necessary physical insight into these processes. These experiments will include computer-controlled mixing and monitoring of component sizes, as well as computer-controlled drying of cast dispersion films.

The modeling approach for drying of multilayer coatings will consider how component selection and processing affect the arrangement and interaction of dispersion components, how the dispersion formulation and processing affect the dynamics of film drying, and how the component interactions affect the final product quality. Models for the drying of coatings will ultimately address the following factors: (1) the dispersion composition including preparation of components, (2) component mixing order (potentially mixing conditions, mixing times, mixing rates, temperatures, disperser tool geometry, container geometry and positioning or movement of disperser tool in container, etc.), (3) coating conditions (potentially dispersion handling, thickness, deposition mechanism and rate, number of layers, layer composition, and substrate) and (4) drying conditions (potentially atmosphere, heating mechanisms, heating rate, and drying times).

Validated Continuum-Scale Models to Accelerate Design and Scale-up of Simultaneous Die Coating Process Technology (SNL Lead Laboratory)

Continuous liquid film coating process technology is one manufacturing sector that has arguably benefitted the most from continuum scale models of the underpinning capillary hydrodynamics of deposition and subsequent drying/solidification. SNL will focus on building and validating continuum-scale models that support the R2R Collaboration multi-laboratory effort to accelerate design and scale-up of coating process technology underpinning target applications, with a specific focus on simultaneous multilayer coating die/process technology. Model development will also be aimed at drying and solidification of multiple layers, simultaneously, so as to understand the underpinning mechanisms of defect formation and prevention.

SNL will coordinate with ORNL (for processing and characterization), LBNL (for materials/microstructure modeling), and will leverage existing NREL test-beds, platforms, and capabilities in solution processing, R2R processing, and metrology. The aim of the coordinated activities will be model validation (including the sensitivity analysis of the most relevant coating and drying success/failure factors, e.g., rheology, particulate uniformity and microstructure, wettability, and hydrodynamic defect detection at process-envelope boundaries.

The focus will be to develop continuum finite element coating and drying process models of sufficient fidelity to address the range of materials and breadth of processing routes of the collaboration. In these models, material variability manifests in the chosen rheological constitutive relationships, capillary wetting models (static and dynamic), process-model boundary conditions, and composition/microstructural representations during solidification. As such, close collaboration with the other laboratories for ink/solution characterization and metrology will be maintained. Extra focus will be on multilayer coating systems, and model fidelity will be sufficient to capture layer-to-layer stability, process operating window defined by boundaries of hydrodynamic defect formation and drying/solidification defect rate-processes (drying, curing, fluid flow). All these aspects will be examined with varying ink/solution rheology (purely viscous behavior and viscoelastic behavior), process parameters (die-lip/face geometry), wetting/surface energies of die/substrate, and other factors as defined by the collaboration's examples.

To assist in model validation, SNL has reconstructed a drying and solidification setup reproduced from published literature approaches to measure drying extent (solvent weight loss) and particle mobility. The experimental apparatus has been tested with a polymer solvent system, and the drying model has been validated. The next steps will examine model particulate coatings. The measured drying curves will be regressed with the models to help determine thermophysical constants that are difficult to measure.

FY 2021 Plans

Core Projects

The core program tasks that were initiated in FY 2019 as part of the three-year Phase 2 effort will continue through FY 2021 by conducting further research on the FY 2020 tasks.

In FY 2021, ANL plans to perform in depth studies to improve electrochemical properties of electrospun materials and establish in-situ process optimization for R2R ES by correlating the insight gained from the Argonne APS in-situ X-ray analysis with real-time process/property monitoring of laboratory ES. The goal is to achieve desirable device performance in the context of energy generation, conversion, storage, and improved electronic devices through a combined materials engineering, process development, and advanced characterization approach.

ANL will develop LLZO nanofiber-conductive polymer composite electrolytes using slot-die coating technology, which will address the low density associated with cold-pressed LLZO pellets. ANL will focus on improving electrochemical properties of LLZO fibers through doping and/or microstructure engineering and improving electrolyte-electrode interface and fiber-polymer interface.

ANL will develop ion-exchange membranes for electrochemical separations which allow for the simultaneous separation and transport of charged species using state-of-the-art ion-exchange resin wafer technology that can extract minority compounds (salts, metals, nutrients) with low pressure pumping and low voltage requirements. ANL will re-design the ion-exchange wafer based on electrospun dual-fiber membranes that contain well-mixed anionic and cationic fibers or laminated architectures and will expect to demonstrate a more homogeneous porosity distribution and higher ionic conductivity and energy efficiency.

ANL will demonstrate electrospun heterogeneous particle-on-fiber meso-structures used for energy conversion applications, such as fuel cells and CO_2 conversion. Development will be around material system selection (e.g., ionic conductive polymers and 2D catalytic nanostructures), R2R ES recipe optimization, and catalytic property evaluation (e.g., activity, selectivity, and electrochemical stability).

ANL will make an exploratory ink formulation and conduct a printing study for printed electronics technology development. Printed electronics is an emerging technology that enables inexpensive manufacturing of size, weight, and power sensitive electronic devices. The technical challenges that hinder industry adoption of printed electronics include the lack of ink choices that are specific to R2R printing processes (viscosity, surface tension, wettability, drying, etc.), resolution and feature size control during high-speed R2R production, precise registration between layers at a high speed, and reliability and repeatability of electronic devices made by R2R manufacturing. ANL will perform exploratory ink formulation studies for conductive, dielectric, and semiconductive inks using ANL in-house fabricated nanomaterials, polymers, and organic solvents. Ink and printing process co-development and co-optimization will be conducted based on aerosol jet printing and flexographic printing techniques, which will be validated by a fully printed logic device. The knowledge developed under this task will be shared with the other laboratory participants to promote a collaborative R&D effort for printed electronics.

ORNL will continue research on multilayer coatings with PEMFC and LIB electrodes as example technologies. In collaboration with NREL, coating parameters for bilayer and tri-layer PEMFC cathodes and LIB for high energy cells as well as multilayer film consolidation will be optimized, and baseline data will be provided to SNL for their multilayer drying-solidification models. An experimental setup will be developed to record the mass of coated electrodes during drying over time at various conditions. Drying parameters for optimized multilayer film consolidation will also be provided to SNL. Devices will be fabricated and tested to evaluate the impact of multilayer structures and processing conditions.

ORNL will collaborate with NREL and LBNL on formulation chemistry for multilayer architectures with support from Argonne's APS and ORNL's Spallation Neutron Source, and High Flux Isotope Reactor. PEMFC ink rheology studies will be conducted with varying solvent type, ionomer content, solids fraction, etc. Optimized solid weight fractions will be provided for PEMFC inks and experiments will be performed on aqueous LIB cathode slurry rheology to optimize solid weight fractions and develop additives for thick, crack-free coatings. Surface chemistries will be characterized for colloidal dispersions (zeta potential, surface tension, wettability) and multilayer coatings using these dispersions will be characterized to understand inter-particle and inter-layer interactions. Electrochemical characterization will be performed for the multilayer coatings for energy conversion and energy storage applications.

ORNL will support efforts at ANL on ES scale-up with SSBs and solid oxide fuel cells as example technologies. In coordination with ANL, LLZO, Al-LLZO, lithium-aluminum-titanium-phosphate, and polyethylene oxide (PEO)/ceramic-composite fiber spinning scale-up will be developed for SSB cathode scaffolds and densified electrolytes. ORNL will provide ANL with formulations for electrospun garnet and garnet-PEO electrolytes. Composite cathodes for SSB will be synthesized and characterized based on these electrolytes. ORNL will demonstrate electrospun yttria-stabilized zirconia electrolyte fibers and composite fibers for solid oxide fuel cells and provide fiber electrolytes to other laboratory participants.

ORNL will collaborate with SNL and LBNL on drying physics studies. Measurement of heat- and mass-transfer coefficients as a function of solvent type and solids loading will be made and the experimental data will be provided to LBNL and SNL to support their modeling studies. Additionally, efforts will be focused on ultraviolet and electron beam curing and energetic post-processing. Multilayer structuring via solventless processing or high-speed curing of low-solvent-content dispersions. This will include determining the speed rate for the curing of low-solvent-content dispersions and application-agnostic, high-speed coating of

multipurpose dispersions (i.e., carbon-black/ceramic/radiation-curable binder/co-solvent). The intent is to develop electromagnetic post-processing of dispersions and colloids to reduce manufacturing cost and energy consumption. ORNL will determine the manufacturing advantages for the ultraviolet (UV)/electron beam curing processing.

NREL will collaborate with ORNL on experiments for multilayer coatings with PEMFC and LIB electrodes and bilayer and tri-layer energy conversion and storage material structures for high performing cells and with ANL on advanced characterization of these materials. Coordination with SNL and LBNL will be on broad multilayer coating process window studies using generic polymer dispersions and polymer-particle colloids and rheology studies to support broad multilayer process studies and modeling. NREL will collaborate with SNL on coating parameter and drying protocol optimization for multilayer film consolidation and dispersion-substrate interaction studies.

NREL will coordinate with ORNL, ANL and SNL on formulation chemistry for multilayer architectures and ink characterization with support from the Argonne APS, the Spallation Neutron Source, and the High Flux Isotope Reactor. This will include energy conversion and storage material ink formulation, rheology, and characterization studies to understand solvent, binder, active material, and additive effects as well as inter-layer interface behaviors. In conjunction with these efforts, NREL will coordinate with ANL on ES scale-up by conducting energy conversion material nanofiber ES studies including fiber characterization and device fabrication/testing.

NREL will interact with SNL and LBNL on R2R modeling and drying physics studies. This will include correlation of drying conditions and protocols to multilayer coating defects and materials distribution and interfaces in multilayer coatings. NREL will participate in the development of models to include model development for electrospinning materials and processes by contributing ink, coating, and drying experimental data. NREL will perform device fabrication and testing to evaluate the impact of multilayer structures and processing conditions and develop in-line NDE, metrology, and defect detection development for multilayer structures.

Other FY 2021 efforts by NREL will include coordination with ORNL on experimental and ANL and ORNL on advanced characterization of materials processed by UV and electron beam curing and energetic post-processing of dispersions and colloids to reduce manufacturing cost and energy consumption. NREL will contribute to a new area of research for flexible electronics with micro- and nano-structuring at ANL and SNL. This will involve exploratory studies of conductive and insulating ink formulation and deposition.

LBNL will provide modeling support for formulation chemistry of multilayer architectures by conducting dilute mixing experiments with a particle size analyzer and constructing a flow cell for microscope observation, including image processing workflow, of dilute dispersions to make quantitative observations about dilute dispersion structures. Drying physics studies will include using the coating experiment setup to simulate manufacturing conditions and observing concentrated dispersions using microscopy and radiography. Modeling efforts will include developing a component clumping and breakup model based on mixing experiments with a sub-model for component clumping at rest to collect data for populating the drying models. These models will describe the dispersion structure evolution at rest and undergoing drying (microscopy and image analysis) to obtain additional data for the drying models.

SNL will continue to produce models and workflows for single and multilayer slot and slide die coating simulations. With rheology studies complete for exemplar MEAs and fuel cells complete, SNL will focus on coating operability window prediction workflows together with user-interface tools. SNL models will support coating trials at NREL and ORNL by providing pre-trial coating process parameter selection and guidance.

These will include expanding to IrO_2 inks. A full particle-polymer-solvent, multilayer continuum drying model will be completed with a companion experimental setup and include particle effects previously developed.

SNL will complete multilayer slide flow stability analysis in support of NREL experiments. Coating window(s) for all factor-space single- and multilayer slide-die coating trials scheduled at NREL will be finalized and provided to NREL. Workflow documentation for multilayer slide die coating model development and simulation, together with validation studies, will be completed. SNL will complete demonstration simulations for three-layer slide-die coating with representative fuel cell layer constructions, including IrO_2 inks to leverage a HFTO-funded project. The modeling tool set will be expanded to include IrO2 ink formulations. User-interface for single-layer slot-die coating simulations will be demonstrated, and SNL will train a wider user-base within the R2R collaboration. A publication on multilayer slide coating mod/sim with accompanying validation will be submitted.

SNL will finalize coating window(s) for all formulations and provide modeling support to ORNL for a two-layer coating trial with a 10-20 μm membrane overlayer. The model extension to the multilayer case will be completed. A table-top drying experimental setup will be completed, and studies will be performed to replicate published drying experiment data. Goma 6.0 development will continue to handle colloidal and active particle transport (diffusivity and hindered transport properties) and a DAKOTA wrapper for parameter estimation will be integrated into GOMA. Models will be validated using the SNL table-top drying setup to generate experimental data.

CRADA projects

Efforts for the CRADA projects with agreements negotiated in FY 2018 continued into FY 2020 to meet contractual and programmatic requirements. This included the following efforts:

- Navitas Systems, Inc. - Navitas Systems, Inc. partnered with ORNL and NREL to demonstrate R2R production of an advanced separator for lithium-ion batteries. Project completed in March 2020.

- SolarWindow Technologies, Inc. (SWT) – SWT partnered with NREL and ANL to demonstrate diffractive multiplexing for high-throughput R2R laser patterning of flexible OPV modules. Project completed in September 2020.

- Nel Hydrogen - Nel Hydrogen partnered with NREL, ORNL and ANL to research R2R manufacturing of advanced (low loading, direct coated onto membrane) electrolysis anodes for low-cost hydrogen production. This project started in FY 2020 and will continue into FY 2021. Integration of new catalyst material. Ink formulations and gravure cylinder configurations need to be optimized to achieve the target loading of 0.5 mg/cm^2. Nel Hydrogen will test several IrO_2 materials from different suppliers and select one for their applications. NREL and ORNL will develop inks to integrate a new IrO_2 catalyst material and provide samples to Nel Hydrogen for electrochemical testing. Scattering studies will be conducted to understand if new catalyst material changes interparticle interactions. NREL will assist Nel Hydrogen with transitioning their process to Kodak by translating the ink and process recipes developed in the laboratory to Kodak for pilot coating trials. Kodak will provide information from their coating trials including data on the web tension used and the acceptable amount of strain at the pre-production scale. Using inputs from Kodak, NREL and ORNL will reformulate inks as needed. NREL will perform a scoping study of existing QC diagnostic techniques to inspect materials supplied by Nel Hydrogen for electrode loading and/or thickness uniformity. A technique will be demonstrated to show sufficient sensitivity to inspect for a loading variation of <10%.

Potential New Efforts

Future efforts should address key barriers in the areas of (1) materials and substrates, (2) novel processing of flexible electronics, (3) multicomponent slurry formulation and processing, (4) drying and curing technologies, (5) material deposition and R2R coating techniques, (6) quality control, in-situ evaluation, process control and optimization, (7) predictive modeling and simulation to guide experimental efforts, and (8) data science and machine learning development to more quickly achieve the above developments. Some potential new efforts for all the R2R Collaboration laboratories to address these barriers and technology challenges are listed below.

Materials and substrates

- Investigate novel printable and coating materials and substrates to enable the design of optical mechanical, electrical, thermal, and chemical properties which include new nanomaterials, polymer development, polymer functionalization, substrate selection and functionalization, and circular economy for new material/substrate design. Efforts include functionalization methods for polymer substrates, additive R2R processes for novel substrates (e.g., ceramics, glass, advanced polymers), deposition of high-temperature materials on low-temperature substrates, and high-speed, low-cost R2R processes.

- Investigate additive R2R processes (e.g., thin films, coatings, 3D structures) relative to new devices and applications. Address the challenges of material incompatibilities between additives, polymers, and curing processes, as well as between different coating/printing layers for multi-layer devices. Develop new processes that enable high-temperature curing or thermal treatment of materials on low-temperature substrates (e.g., using a rapid photonic curing process). Improve process compatibility during complex high-speed low-cost R2R manufacturing.

- Develop digital twin and machine learning frameworks and models and in-situ product quality and process parameter monitoring and control systems to improve coating and printing process automation and self-optimization.

Novel processing of flexible electronics

- Develop ink formulation for enhanced electronic and mechanical properties (e.g., electroactive polymers, polymer interfacial strength and adhesion, 2D nanomaterials, particle-free inks) using machine learning accelerated polymeric and nanocrystalline material design and fabrication in combination with an advanced structural/microstructural study by hard X-ray and electron holography.

- Develop compatible conductive, semiconductive, and dielectric inks and integration pathway for complexed multilayer device fabrication using in-situ X-ray imaging of ink printing at the Argonne APS. Develop correlations between ink formulation, printing parameter, and printing quality for aerosol jet and flexographic printing. Establish an understanding of liquid printing hydrodynamics.

- Leverage ANL’s ongoing research on destructible and degradable polymers and polymer semiconductors to demonstrate recyclable printed electronics devices with controllable deconstruction and excellent electronic performance and printability. Demonstrate a scalable synthesis of the recyclable polymeric ink materials and a scalable process for R2R manufacturing of recyclable printed electronic devices.

- Establish a pathway to realize materials, processes, and devices needed for the co-design and co-development of printed electronics devices.

- Develop printed logic and/or memory devices to demonstrate complementary metal–oxide–semiconductor printability and neuromorphic computing to enhance microelectronic integration density and computing capabilities.

- Conduct in-situ and operando X-ray imaging and electrical and mechanical property measurements of devices to investigate the microstructure root-cause of transient electrical property degradation of printed flexible and stretchable devices during bending, folding, and stretching.

Multicomponent slurry formulation and processing

- Address slurry processing effects on slurry properties, R2R processing conditions, and device performance.

- Utilize diagnostic and material characterization to understand the properties of slurries for multi-layers, and substrates, and research the compatibility between slurries for multi-layers coated simultaneously or separately, slurries and substrates, and substrate and R2R processing.

Drying and curing technologies (alternate solvent removal processes)

- Correlate drying protocols and microstructure and performance of film with the impact of variables, including solvent(s), solvent content, drying temperature, duration and methods, component homogeneity, and microstructure and performance of the films will be investigated.

- Create mathematical models to simulate removal of solvent and guide optimization of drying protocols.

- Evaluate thermal budget and cost of the drying processes for R2R applications.

Material deposition and R2R coating techniques

- Form novel structures or multi-layer films by traditional methods.
- Elucidate the relationships between material forms and deposition processes and process-induced morphology and performance using computational and experimental capabilities.
- Develop and validate innovative new deposition techniques, including vapor or gas phase deposition, chemical bath deposition, and integration of traditional R2R processing with additive manufacturing.

Quality control, in-situ evaluation, process control and optimization

- Address the lack of understanding of critical coated-layer defects that are formed during R2R processing and their impact on device performance.

- Develop novel in-line and in-process measurements of interest for key technologies of interest. Focus on in-line measurements for defect detection, layer property and thickness measurement, physical resolution for thin films and structured coating maximization, and inter-layer defects. Focus on in-process measurements being thermal-, optical-, electrical-, and species-sensitive techniques.

- Develop and demonstrate novel process-control and feedback methodologies.

Predictive modeling and simulation to guide experimental efforts

- Develop microscale models that would include the fundamental interactions within the dispersions and slurries using model and real single particles for development of inter particle potentials.

- Develop mesoscopic models that would be based on upscaling techniques such as dissipative particle dynamics and phase field modeling from the microscale models to examine agglomeration and phase coalescence.

- Develop a hierarchical homogenization model that is based on particle morphology and aggregation dynamics to predict the rheology of the slurry and other properties of the dried slurry.

- Develop a macroscopic model, based on the mesoscopic/homogenization model, for R2R tool design and operation that can be used in commercial tools such as COMSOL software.

Machine learning for R2R printed electronics

- Accelerate ink materials development and polymeric material design and fabrication using machine learning.

- Investigate functional nanofiber, nanoparticle and 2D material synthesis at scale.

- Utilize machine learning to make printed devices recyclable.

- Conduct in-situ studies for promoting scalable precision printing and coating using machine learning techniques and methods.

- Conduct defect and interface studies for microstructure optimization within a multilayer print that would use machine learning to minimize defects at the micro level.

- Optimize electrical and mechanical property control for non-planar surface printing using a machine learning approach.

Technology Transfer Paths

For the core program tasks, technology will be transferred through collaboration with industry and companies with CRADA contracts and the DOE team will work closely with any companies to ensure technologies are accepted for commercialization. General results for the research efforts of the R2R Collaboration program were presented at conferences, symposia, peer reviews and during direct contact with industry and the commercial sector. Specific research was reported in technical journals and through patent applications.

The models and simulations will be extended to encompass not only materials discovery, but also to accelerate materials synthesis and fabrication applicable to industry. This effort leverages the R2R processes and technologies at ORNL, the engineering expertise and research facilities such as the Materials Engineering and Research Facility and the Argonne APS, and the metrology, R2R processing, and device fabrication and testing capabilities at NREL, in conjunction with the materials design computational efforts of SNL and LBNL. SNL continued to provide open access to the upgrades for the modeling and simulation tools to industry, all National Laboratories, and academic partners.

Results

Novel R2R Deposition System Based on ES Technology and Advanced/In-Situ Characterization and Testing (ANL Lead Laboratory)

The goal is to develop a R2R ES platform that is applicable to a truly vast range of materials, such as solid-state lithium battery electrolytes and electrodes, ion transport media for fabrication of water filtration and purification membranes, reusable N95 facepiece filter media, and fuel cell membranes. Advanced ES ink characterization at the Argonne APS using SAXS and USAXS, as well as exploratory study of ink formulation for R2R printed electronics were also performed within the context of new ink materials development for R2R manufacturing.

R2R ES Platform Development

There are currently a few barriers to commercialization of ES: (1) ES is mostly limited to filtration applications produced in single-step, batch processes; (2) advanced materials used in electronics, fuel cells and batteries that require continuous, post-ES processing; (3) complex multi-step physiochemical processes that create challenges transferring technology from the bench to commercial production; and (4) time-consuming material transfer process steps. Capabilities that can address these technical barriers need to be developed.

This effort focused on the physics, methodologies, and equipment required for multilayer coatings applicable to a truly vast range of materials including functionalized membranes and porous media, ion transport media, water filtration and purification media, electrochemical active layers, catalytic membranes, etc. The objective of this task was the development of a R2R ES platform that is capable of synthesizing multilayer composite membranes. The development of this highly versatile deposition process will enable significantly improved device quality (as compared to conventional deposition methods) and productivity for a wide range of high-performance applications.

Tool Development for Scalable Synthesis of Composite Fiber Membranes

Research was conducted to develop composite membranes that can incorporate multiple fiber materials. A significant improvement was demonstrated in scalable polymer nanofiber production using R2R ES processing. Although this new ES system can fabricate hybrid membranes with different nanofiber material layers, its design layout has limitation in terms of intermixed composite membrane synthesis, such as the ion-exchange membranes described in the Advanced Nanofiber Materials Development for Water Purification Applications section below. To develop scalable composite nanofiber membranes, a multi-nozzle co-ES system was designed, as shown in Figure 2. The design contains two nozzle stands that face a rotating drum from each side of the drum. Each nozzle rack has an arch-shaped arm that can hold four bars of nozzles. The arch design ensures all nozzles stay equal distance to the drums surface. The nozzle racks are mounted on opposite sides of the drum, which enables deposition of different material systems at the same time without electric field interference. In addition, nozzles on each bar can have their own power supply and syringe pump and thus can each deposit a different precursor. This further increases the number of nanofiber materials in the composites. On the other hand, the co-spinning process enables well-intermixed nanofibers of different materials, which allows more uniform distribution of functionalities.

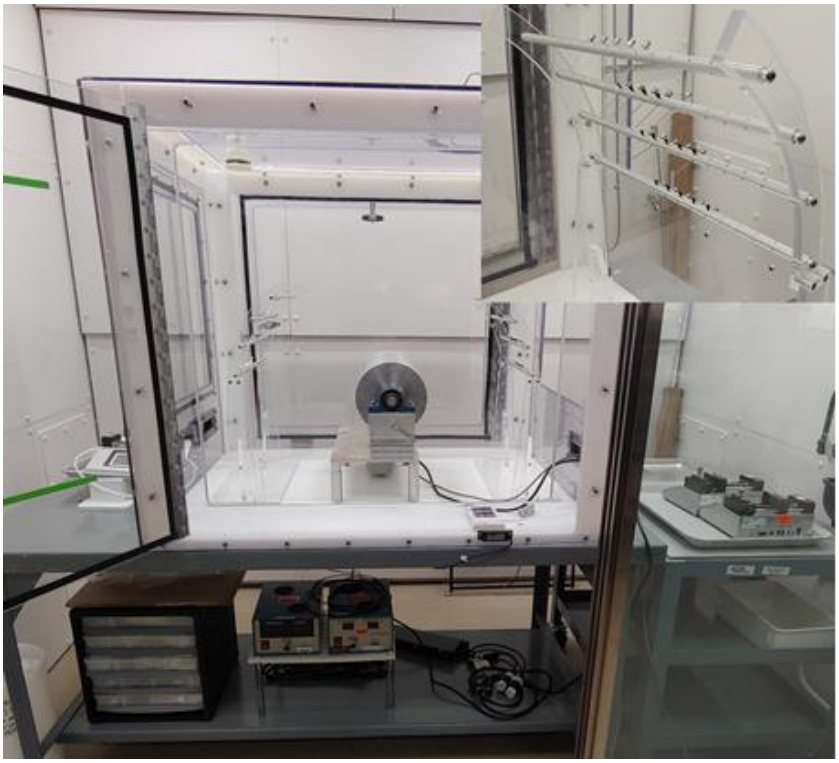

Figure 2. Multi-nozzle co-ES system that contains four bars of nozzles at each side of a rotating drum. Source: ANL

Advanced Nanofiber Materials Development for Battery Electrolyte Applications

Battery nanofiber formation through in-situ APS characterization

In FY 2019, ANL developed ES recipes to fabricate polymer precursor nanofibers of LLZO solid-state electrolyte materials. Research in FY 2020 was performed to convert precursor nanofibers to LLZO fibers and to achieve an in-depth understanding of LLZO crystallographic information and its temperature evolution. In-situ simultaneous SAXS, WAXS and CO_2 measurements during precursor nanofiber annealing was conducted at the Argonne APS. The electrospun precursor fibers were prepared with a composition that has excess lithium (~10% excess as compared to the stoichiometric LLZO composition) to compensate for any lithium loss during the annealing process. The annealing was made between 25 °C and 900 °C with a heating rate of 10 °C/min and 5 °C/min in the temperature ranges of 25-400 °C and 400-900 °C, respectively. O_2/He gas was flowed through a sample capillary tube during annealing to ensure sufficient O_2 supply for polymer oxidation.

The SAXS and WAXS 2D images at various temperatures are shown in Figure 3(a). The 2D WAXS image can be converted to conventional 2θ X-ray diffraction (XRD) profiles using the relationship q=4, as shown in Figure 3(b). As seen in Figure 3, the polymer precursor nanofibers are amorphous in the temperature range of 25-500 °C. $La_2Zr_2O_7$ was first formed in the polymer fibers, which converted to cubic phase LLZO at 500 °C. The cubic LLZO was stable between 600-800 °C and decomposed at above 800 °C. Figure 4(a) shows the CO_2 peak during annealing, and Figure 4(b) shows the integrated intensity of the X-ray peaks associated with the SAXS data (2θ=2.5°-3.5°), $La_2Zr_2O_7$ (2θ=27.7°-29.1°), and cubic LLZO (2θ=16.3°-17.1° and 2θ=33.3°-34.5°). The overlap of the CO_2 and SAXS peaks indicates that polymer oxidation led to morphological changes in fibers and polymer oxidation was correlated with metal oxides formation. Specifically, polymer oxidation preceded any metal oxide phase. $La_2Zr_2O_7$ formed after the majority of the polymer oxidized, as indicated by the shoulder in CO_2 peak and onset of the $La_2Zr_2O_7$ X-ray peak at around 450 °C. The cubic LLZO formed at

the depletion of all the polymers in the fibers at ~600 °C. This study revealed the kinetics of LLZO formation from the polymer precursors.

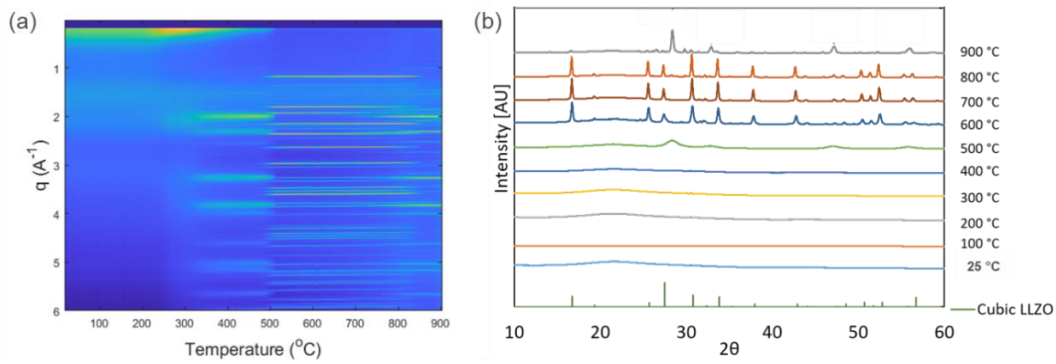

Figure 3. (a) 2D SAXS-WAXS data and (b) 2θ XRD profiles of nanofibers during annealing between 25 °C and 900 °C. Source: ANL

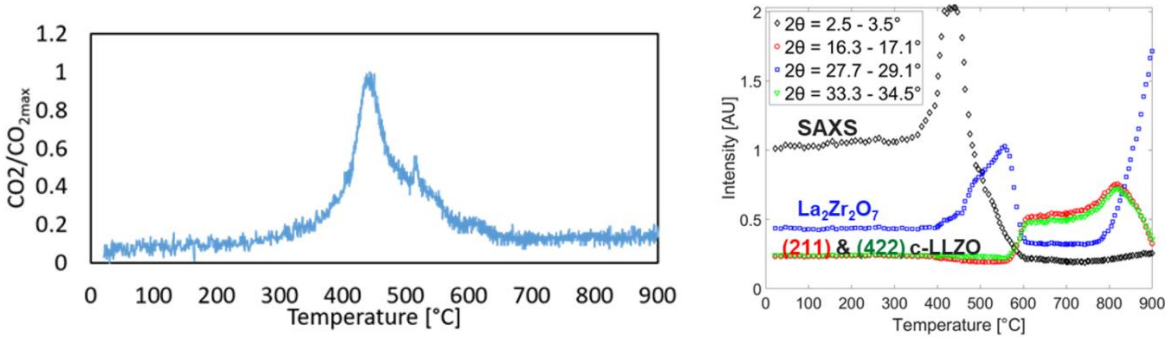

(a) (b)

Figure 4. (a) Changes of CO_2 intensity with annealing temperature and (b) integrated intensity of X-ray peaks associated with SAXS, $La_2Zr_2O_7$, and cubic LLZO (c-LLZO) at various temperatures during annealing. Source: ANL

The knowledge gained from the in-situ X-ray study was applied to LLZO nanofiber fabrication using a laboratory furnace. Cubic phase LLZO nanofibers were successfully obtained after 700 °C annealing, as confirmed by powder X-ray diffraction, as shown in Figure 5. The XRD also indicated the existence of a small amount of Li_2CO_3 in the sample.

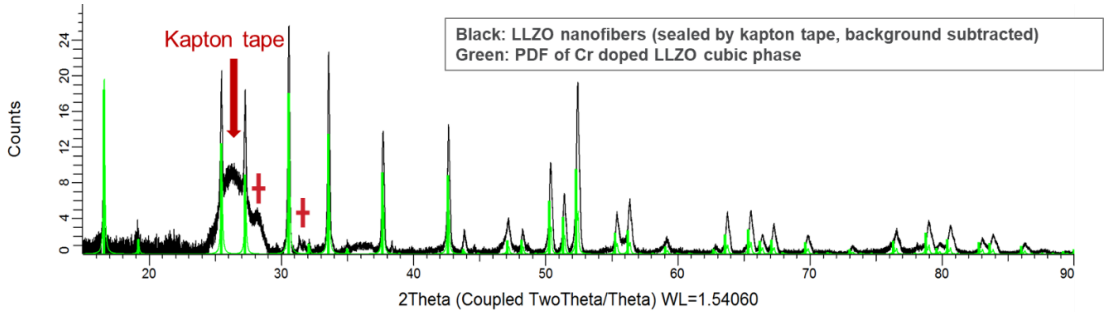

Figure 5. XRD profile of LLZO fibers annealed using lab furnace, which was consistent with the X-ray profile of Cr-doped cubic LLZO (green peaks). The broad peak in the 2θ range of 25° - 29° was associated with Kapton® tape used for XRD sample preparation. The peaks at 2θ=29° and 31.5° (marked by a red cross) were consistent with the X-ray peaks of Li_2CO_3. Source: ANL

Battery nanofiber property optimization

The XRD characterization of the furnace annealed LLZO indicated the presence of Li_2CO_3 in the sample. To verify this observation, TEM imaging and Raman spectroscopy was performed. Surface Li_2CO_3 of 5nm thickness was clearly revealed by TEM, as shown in Figure 6(a). This was also confirmed by a small Raman peak at 150 cm^{-1}, as shown in Figure 6(b). Since Li_2CO_3 is not Li-ion conductive, removal of the surface Li_2CO_3 layer is necessary to achieve good ionic conductivity of LLZO fibers. Thus, a second nanofiber annealing was performed in an argon atmosphere and XPS analysis was used to examine Li_2CO_3 elimination. The XPS results for fibers before and after argon annealing are presented in Figure 6(c).

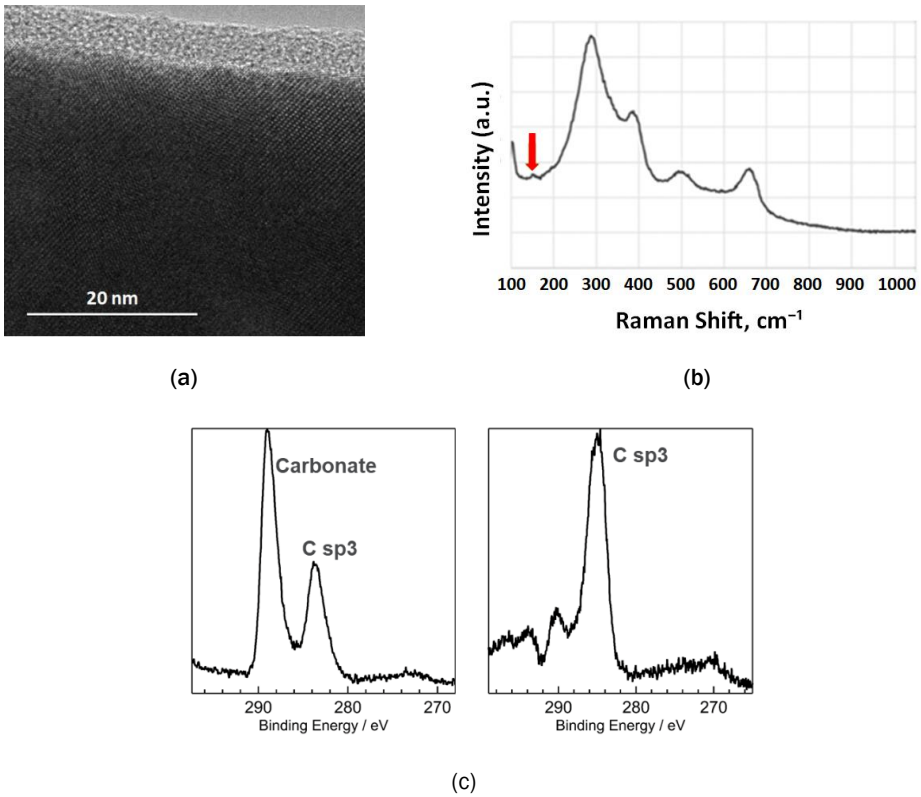

Figure 6. (a) High-resolution TEM image of a LLZO nanofiber annealed at 700 ˚C showing a thin surface layer corresponding to the lithium carbonate (Li_2CO_3) phase, (b) Raman spectra of the same sample that confirmed the presence of Li_2CO_3 (indicated by the Raman peak at 150 cm-1 and marked by the red arrow); (c) C 1s XPS spectra of LLZO nanofibers before (left) and after (right) annealing in argon. The CO_3 peak associated with the Li_2CO_3 disappeared after annealing, indicating the removal of Li_2CO_3 from sample surface. Source: ANL

Nanofiber-based battery device demonstration

Using the knowledge gained from the above studies, an experimental protocol was established that can be used to fabricate high quality c-LLZO fibers. Large quantities of LLZO fibers were synthesized for LLZO electrolyte pellet and symmetric Li/LLZO/Li cell fabrication and characterization. The composition of the annealed LLZO nanofibers was characterized by a microwave digestion method as $Li_8La_3Zr_{1.8}O_x$ (at.%).

A densified LLZO pellet of 0.25 inch diameter was made by cold pressing of LLZO nanofibers at room temperature using a higher pressure of 400 MPa. Before pellet making, lithium carbonate was removed from the LLZO fibers and the purity of cubic LLZO phase was examined and confirmed by XRD and XPS. The resulting pellet had a packing density of 60%. This density was significantly lower than the high-temperature sintered LLZO electrolyte where the density can reach >85%.

The pellet was then assembled into a Li/LLZO/Li symmetric cell for electrochemical property characterization. EIS measurements of the cell showed a high impedance at room temperature, indicating a low ionic conductivity of the LLZO pellet. The ionic conductivity was slightly improved at 100 °C, showing a value of 1.3 x10^{-5} S/cm, as can be seen in Figure 7. The low ionic conductivity is likely attributed to the low packing density of LLZO pellet, which can be addressed by hot pressing of LLZO fibers or preparing a fiber-polymer composite pellet. These solutions and Li film coating by e-beam or sputtering at the LLZO pellet and Li foil interface will be examined in terms of interfacial resistance reduction during future experiments.

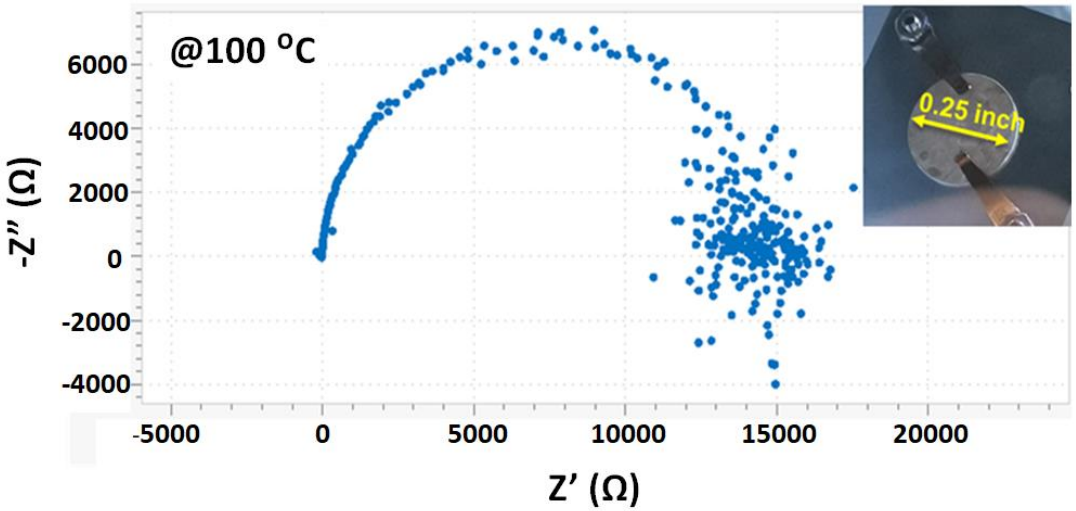

Figure 7. EIS of Li/LLZO/Li symmetric cell at 100 °C. Inset shows the photo of the LLZO fiber pellet. Source: ANL

Finally, the new ES recipe scale-up was demonstrated not only for ANL's recipes but also for an ORNL recipe associated with LLZO precursor fiber fabrication. This indicated good transferability of the ES recipes and processing knowledge between systems.

Advanced Nanofiber Materials Development for Water Purification Applications

ES recipe development for cationic and anionic fiber synthesis

ES was used to fabricate a membrane for water purification applications. Cation- and anion-exchange ionomers were electrospun to fabricate a nanofiber-based electro-deionization wafer. First, the cation and anion-exchange ionomers were independently electrospun to determine fiber morphologies. The two ionomers were then co-electrospun to produce a mixed-fiber mat, and the conductivity of all three types of fiber mats – pure cationic nanofibers, pure anionic nanofibers, and a cationic/anionic mixed fiber mat – were determined in salt water. Nafion, a perfluoro sulfonic acid ionomer, was dispersed into a mixture of alcohol and water. The structure of Nafion is shown in Figure 8(a) where proton conduction is facilitated through the terminal sulfonic acid sites on the ionomer's side chains. A small amount (1 wt.% relative to the Nafion content) of PEO, molecular weight = 600 kDa) was added to enable ES. The Nafion nanofibers were electrospun onto the lab-scale electrospinner leading to a porous fiber mat consisting of cation-exchange ionomer fibers. Sustainion, an alkaline ionomer, was prepared in a similar fashion (dispersion the ionomer into a mixture of alcohol and water and adding 1 wt.% PEO to enable ES). The polymer structure of Sustainion is shown in Figure 8(b) where anion-conducting properties are due to the fixed cationic side on the polymer's side chain. Scanning electron microscope (SEM) images of the nanofibers shown in Figure 11 indicate that well-formed nanofibers of both ionomers were obtained from the ES process. Nafion nanofibers had fiber diameters of 213 ± 49 nm as shown in Figure 9(a), whereas the Sustainion nanofibers had diameters of 711 ± 140 nm as shown in Figure 9(b).

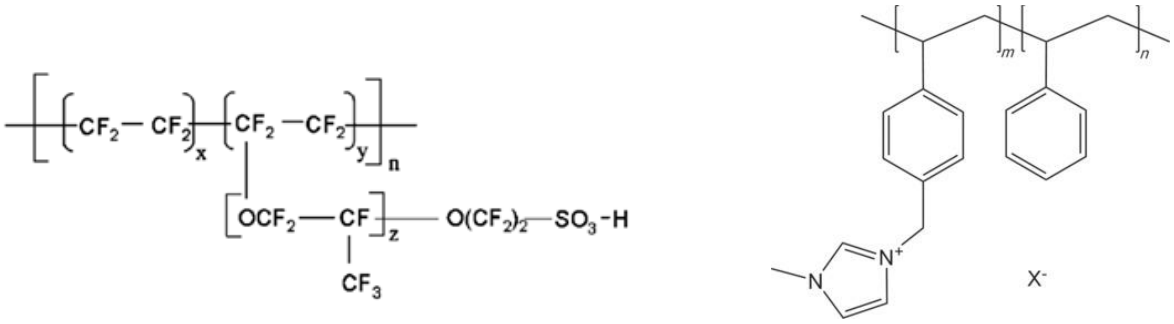

(a) (b)

Figure 8. Polymer structures for (a) Nafion and (b) Sustainion. Sources: [7] [8]

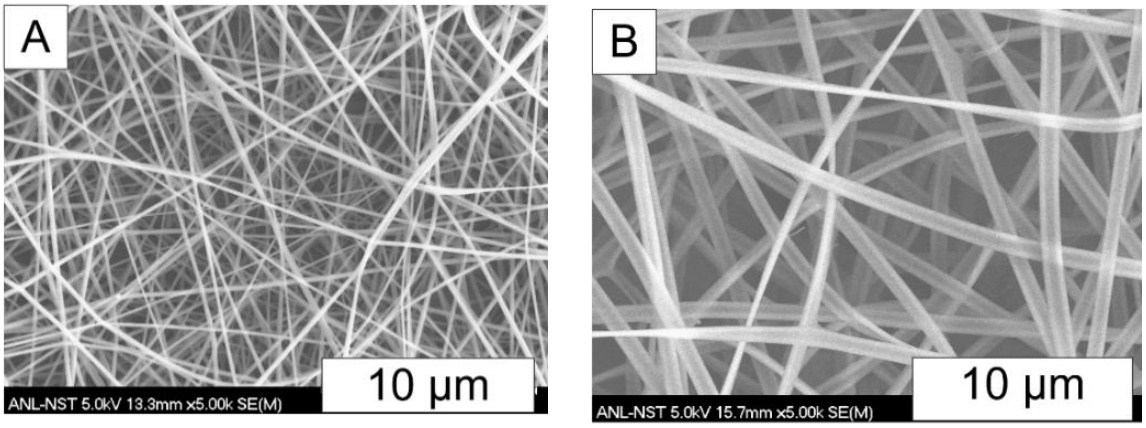

Figure 9: Plan-view SEM images of electrospun (a) proton-conducting Nafion nanofibers and (b) anion-conducting Sustainion nanofibers. Source: ANL

Dual-fiber ion-exchange membrane synthesis

A mixed-fiber mat consisting of Nafion and Sustanion was prepared by co-ES the ionomers onto a common target with a 1:1 weight ratio. The ES precursors were prepared as described previously. Adjustments to the ES conditions were required due to the geometry of the bench-top ES unit. SEM images of the mixed-fiber mat shown in Figure 10(a) indicate that well-mixed fibers of the two ionomers were obtained. The SEM and energy dispersive X-ray spectroscopy (EDS) elemental mapping of the mixed-fiber mat are shown alongside the SEM image as Figure 10(b) and Figure 10(c) where regions containing fluorine and nitrogen are highlighted in blue and purple, respectively. The structure of Nafion consists of a fluorocarbon backbone and side chains that terminate with a sulfonic acid group. In contrast, Sustainion contains a hydrocarbon backbone and side chains which contain nitrogen functionalities. Based on the EDS mapping, the Sustainion fibers correspond to the thicker fibers in the SEM images which is consistent with the differences in fiber diameter observed for the independently electrospun Nafion and Sustainion.

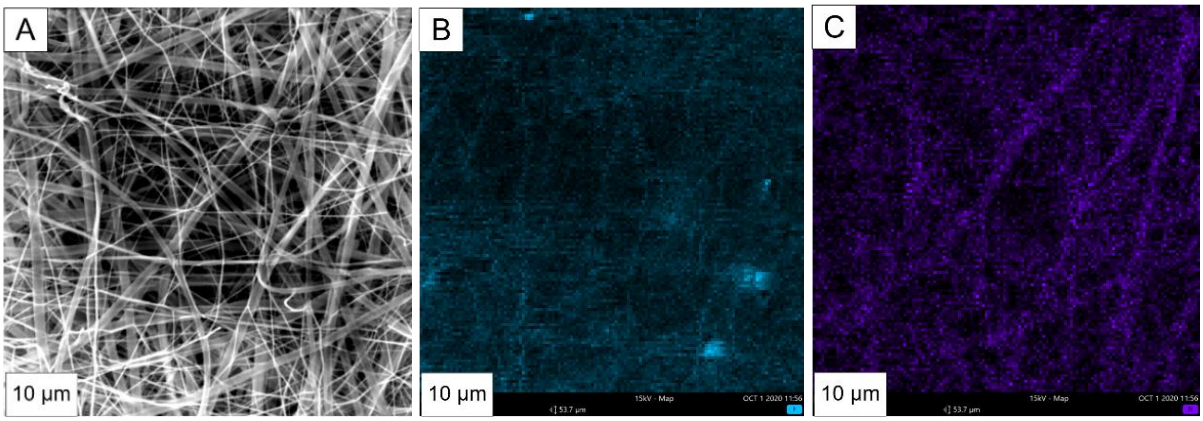

Figure 10: (a) Plan-view SEM image of co-electrospun Nafion and Sustainion nanofibers; (b) and (c) SEM-EDS elemental mapping of fluorine and nitrogen, respectively, taken from image (a). Source: ANL

Ionic conductivity of the nanofibers mats was determined using a two-electrode cell. A fiber mat was mounted between the electrodes which was allowed to equilibrate in 0.08 M NaCl while the impedance and phase were measured. The equilibrated impedances for the as-spun Nafion nanofiber mat, Sustainion nanofiber mat, mixed-fiber mat, a commercial cation-exchange film, and a commercial anion-exchange film were measured and converted to ionic conductivity as shown in Table I. The mixed fiber mat exhibited a slightly lower ionic conductivity as compared with the commercial ion-exchange polymers. This can be due to the differences in porosity between the commercial (dense films) and in-house made electrospun membranes (porous) or ion-exchange capacity of the materials (i.e., the amount of charged sites per mass ionomer). Additional experiments are planned to understand the cause.

Table I: Ionic Conductivity of Commercial Ion-Exchange Membranes and Electrospun Fiber Mats in 0.08M NaCl

Material	Conductivity (mS/cm)
Commercial anion exchange membrane	2.803
Commercial cation exchange membrane	1.762
Nafion fiber mat	0.255
Sustainion fiber mat	0.333
Mixed-fiber mat	0.357

DOE Basic Energy Sciences COVID-19 Support

The global outbreak of SARS-CoV-2 has generated a continuous demand on N95 facepiece respirators. This demand cannot be fully satisfied by the existing supply chain. Thus, there is a critical need to reuse the N95 respirators after decontamination and to extend the use time of a respirator before it can be disinfected at the end of day. ANL team converted the R2R ES tool to a platform for reusable N95 filter media development to support the DOE Basic Energy Sciences Office National Virtual Biotechnology Laboratory program [9]. Electrospun filter media can provide high filtration efficiencies when tested with salt spray and di-ethyl-hexyl-sebacate (DEHS) oil particulate, as shown in Figure 11. Electrospun media with a filtration efficiency greater than 95% was fabricated that did not show efficiency degradation after ten cycles of autoclaving or bleach spray disinfection, as shown in Figure 12. These electrospun filter media also incorporated antiviral function by introducing antiviral ingredients in the nanofibers.

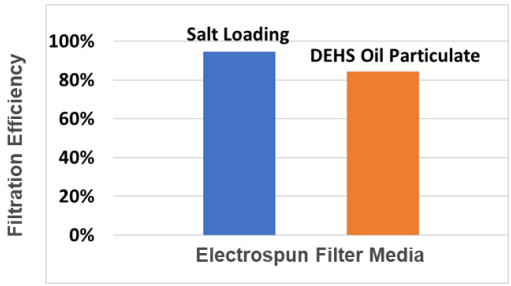

Figure 11: Filtration efficiency measured for electrospun filter media by salt loading and DEHS oil particulate tests using a face velocity of 23 cm/s. Source: ANL

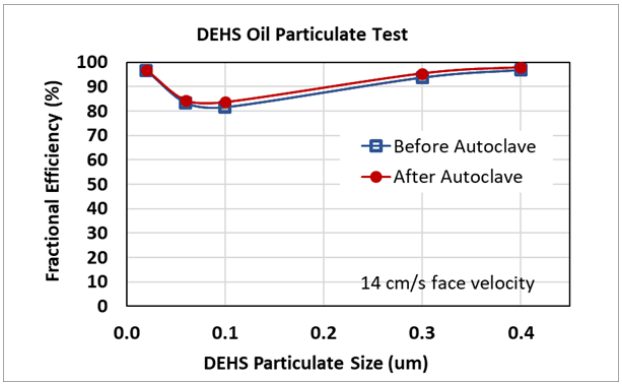

Figure 12: Filtration efficiency of electrospun filter media before and after autoclaving disinfection measured by DEHS oil particulate test using 14 cm/s face velocity. Source: ANL

Figure 13 shows antiviral testing based on bacteriophage Phi6, a SARS-CoV-2 virus surrogate. During tests, the "antiviral" electrospun fibers were examined together with two control samples. Control I samples were regular electrospun fibers. This cohort was exposed to Phi6 phage for 15 minutes with the "antiviral" fiber samples before being transferred to a bacteria culture. The antiviral tests showed a reduced bacteria population for Control I samples after six hours of bacteria culturing, indicating a phage attack on the bacteria in these samples (e.g., Control I did not kill phage). Control II was a bare bacterial solution that did not contain any fibers. This sample was not exposed to bacteriophage Phi6 and showed bacteria duplication over time. The fact that the "antiviral" fibers showed a similar behavior for Control II but were different from Control I suggests that they effectively destroyed the phage and indeed had antiviral effects.

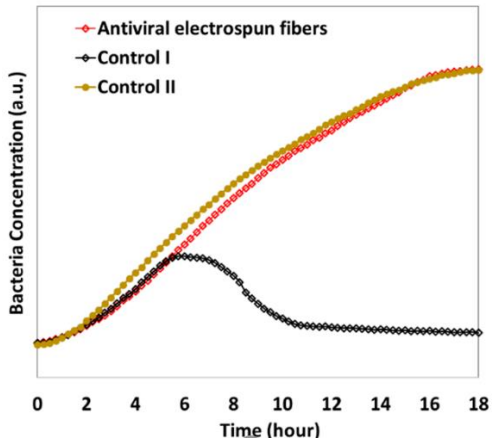

Figure 13: Test results for the antiviral electrospun fibers and two control samples. Source: ANL

The ANL team will collaborate with BiOAID™ to commercialize a reusable facepiece respirator. Figure 14(a) shows a prototype reusable respirator made with ANL electrospun filter media and Figure 14(b) show the BiOAID™ N95 reusable face mask.

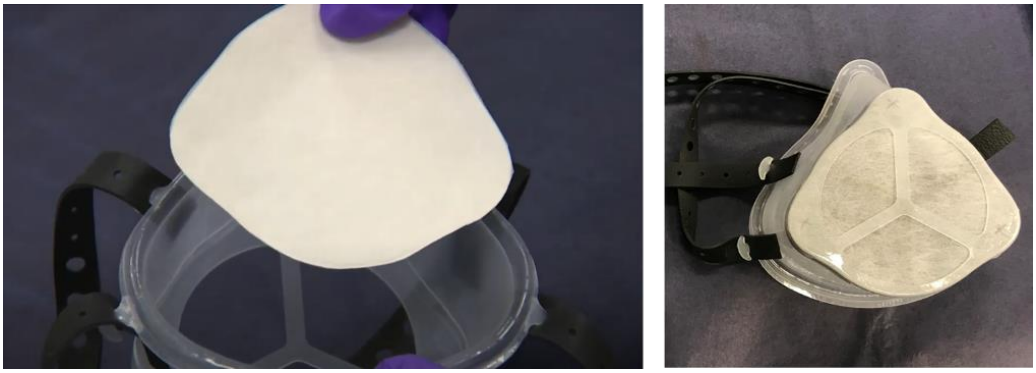

(a) (b)

Figure 14: Photographs of (a) a prototype reusable N95 face piece respirator that contains ANL electrospun filter media and (b) a BioAID™ mask shell. Source: ANL and BiOAID™ [10]

Advanced Ink Characterization

Advanced X-ray analysis for ES ink development and characterization

ANL supports NREL in the development of catalyst-ionomer-solvent ink compositions and processing techniques for efficient R2R fabrication of energy conversion device electrodes while also optimizing the performance and lifetime of these electrodes in the device and minimizing ink processing time. Specifically, SAXS and USAXS were utilized to analyze the ink agglomerate structures to determine the ink microstructure evolution as a function of ink composition, ink mixing method, and mixing time. These data are to support the rheology and performance data taken at NREL for inks and membrane-electrode assemblies made using inks processed by the same methods, respectively.

A catalyst ink formulation consists of catalyst powder or catalyst/support powder and ionomer dispersed in an alcohol-water mixture. The interactions between the catalyst ink components, catalyst-ionomer-solvent, and the ink microstructure play a key role in the microstructure evolution of the electrode during fabrication, which has significant impact on the fuel cell performance. In recent research, a nanofiber morphology utilizing an electrospinning electrode fabrication method was found to result in improved electrode performance compared to conventional fabrication methods (e.g., hank painting, ultrasonic spraying, and screen printing) due to improvements in catalyst utilization, proton conductivity, and gas transport. The electrospun electrodes were also found to be more durable than conventional electrodes during cell performance testing.

The ES process utilizes a catalyst ink containing not only catalyst, ionomer, and solvent, but also a high molecular weight carrier polymer to enable the creation of stable fibers. The concentration and molecular weight of the carrier polymer in the ink formulation have been empirically optimized for the ES process. NREL found that the fiber stability and dynamics of the ink during the ES process, which dictate the fiber characteristics, are strongly influenced by the rheology of the inks. However, there have been no studies of how the carrier polymer interacts with the catalyst ink components or on the influence of ink structure on the rheological behavior of the inks.

NREL and ANL investigated the carrier polymer interactions with catalyst ink components and the influence of this interaction on rheological properties of the inks, both in shear and extension, using a rotational rheometer in combination with dynamic light scattering and USAXS/SAXS. The ionomer solutions and Nafion

membranes for the 9-ID beamline studies at the Argonne APS are listed in Table II. The catalyst inks were comprised of catalyst powders of platinum nanoparticles on a Vulcan carbon support, ionomer dispersed in normal propyl alcohol (nPA) – water (H_2O) mixture, and a carrier polymer of PAA.

Table II. Ionomer Solutions for USAXS/SAXS/WAXS Studies

Sample No.	Sample ID	Sample Description
1	I1	0.24 wt% ionomer: 10% nPA-H_2O
2	I2	0.24 wt% ionomer: 25% nPA-H_2O
3	I3	0.24 wt% ionomer: 50% nPA-H_2O
4	I4	0.24 wt% ionomer: 75% nPA-H_2O
5	I5	0.24 wt% ionomer: 90% nPA-H_2O
6	MEM1	Pristine Nafion 212
7	MEM2	Nafion 212 coated with the solvent
8	MEM3	Nafion 212 soaked in solvents

As shown in Figure 15, shear rheology suggests a strong influence of PAA concentration on the ink microstructure. The PAA can induce flocculation of the catalyst particles and stabilize agglomerates. Figure 16(a) shows the USAXS profiles for the Pt/Vulcan-ionomer-solvent inks as a function of PAA concentration. Particle populations shift to smaller size with increasing PAA concentration, consistent with the trend in dynamic viscosity with PAA concentration, as shown by the slurry particle size data in Figure 16(b). These results are consistent with rheology data from NREL discussed later in this report. An optimal PAA concentration was found that minimizes the extent of flocculation of catalyst particles in the ink. The comparison of shear rheological behavior with extensional rheology and processing behavior in ES as a function of PAA concentration and further USAXS/SAXS studies on this same set of inks will be the focus of future work. This work also supported the implementation of ink recipes and operating parameters co-developed by ANL, ORNL, and NREL on the benchtop ES tools toward the development of the R2R ES process at ANL.

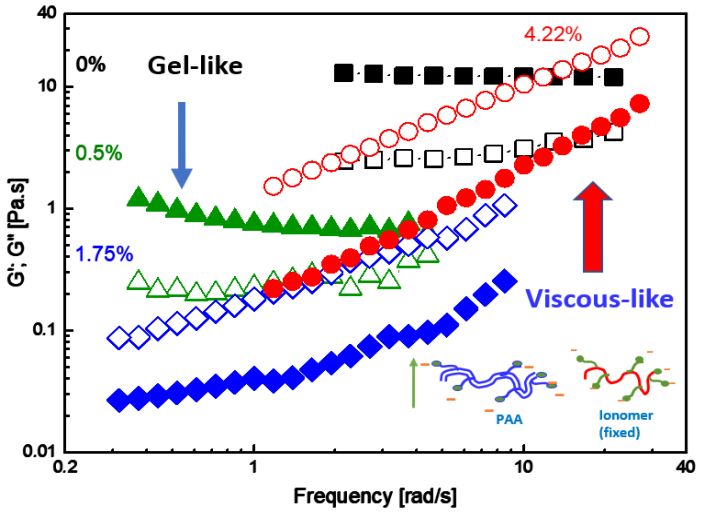

Figure 15. Effect of PAA concentration (10% Pt-Vulcan, 0.34% Ionomer) on dynamic viscosity. Source: ANL

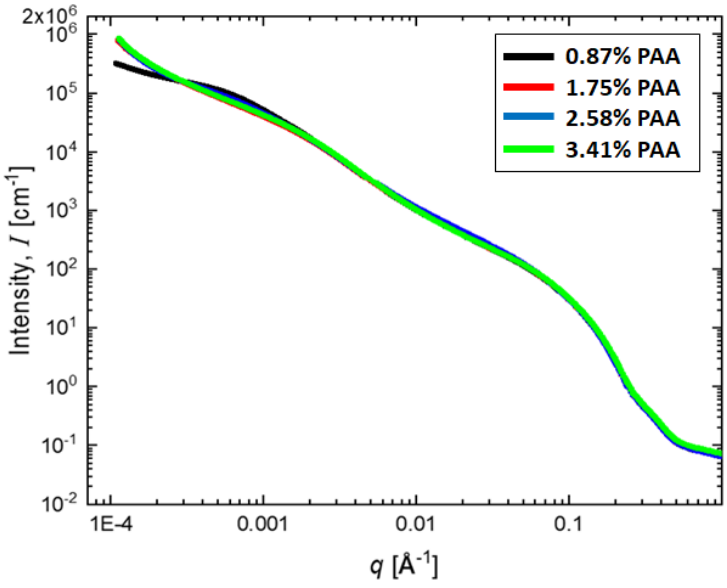

(a)

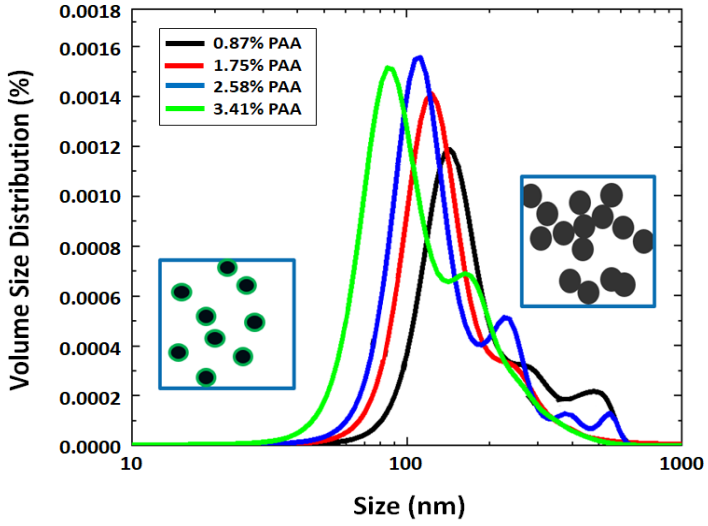

(b)

Figure 16. (a) USAXS profiles and (b) size distributions for varying PAA concentrations. Source: ANL

Seedling Effort for Printed Electronics

The goal of this task was to study the feasibility of printable electronics within the R2R program. The first step was to develop inks that can be used for various printing technologies, such as aerosol jet and flexographic printing. During the printing process, several parameters can be adjusted to modify printing quality, such as ink dilution, temperature, and ink flow rate. These parameters have large implications on the printability of the ink being used, so initial efforts were to understand ink rheological properties. Copper (Cu) nanoparticle solutions with 12.5 wt% base polymer, 14 wt% base polymer, and 13.5 wt% polymer with 10 wt% Cu nanoparticles (NP) were prepared at two different mixing times. Figure 17 shows viscosity as a function of shear rate for these solutions. The results indicate that all solutions had a shear-thinning behavior as would be expected. However, the solutions with nanoparticles in them were more viscous than the base polymer solutions.

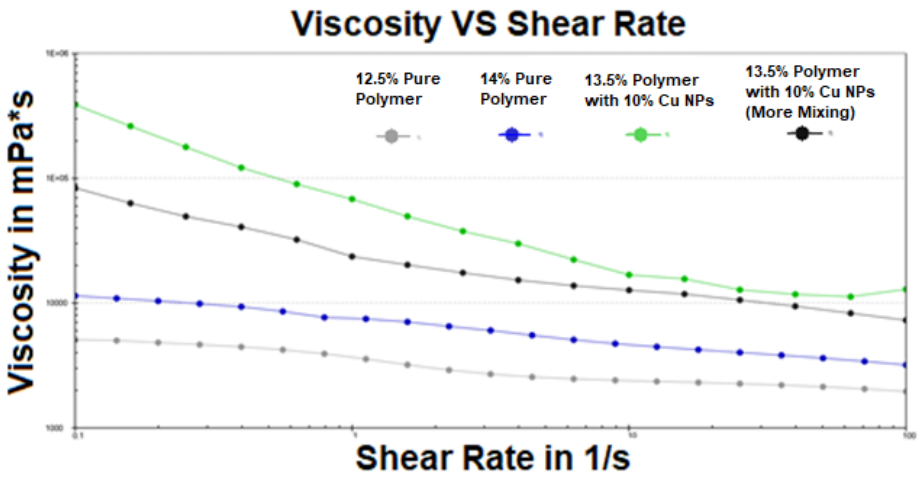

Figure 17. Viscosity curve of ink solutions. Source: ANL

In addition to viscosity, amplitude sweep tests were performed for these solutions to characterize storage moduli and loss moduli of the samples at different shear strains as shown in Figure 18. This test can tell the deformation behavior of the solutions. The results showed significant difference between the base polymer and nanoparticle containing solutions, where the former showed identical storage and loss moduli, while the latter had a higher storage moduli than the loss moduli. In general, a higher storage moduli is a feature associated with a more solid-like sample. Thus, the experimental results indicated that the nanoparticle ink recipe needs to be modified to improve fluidity.

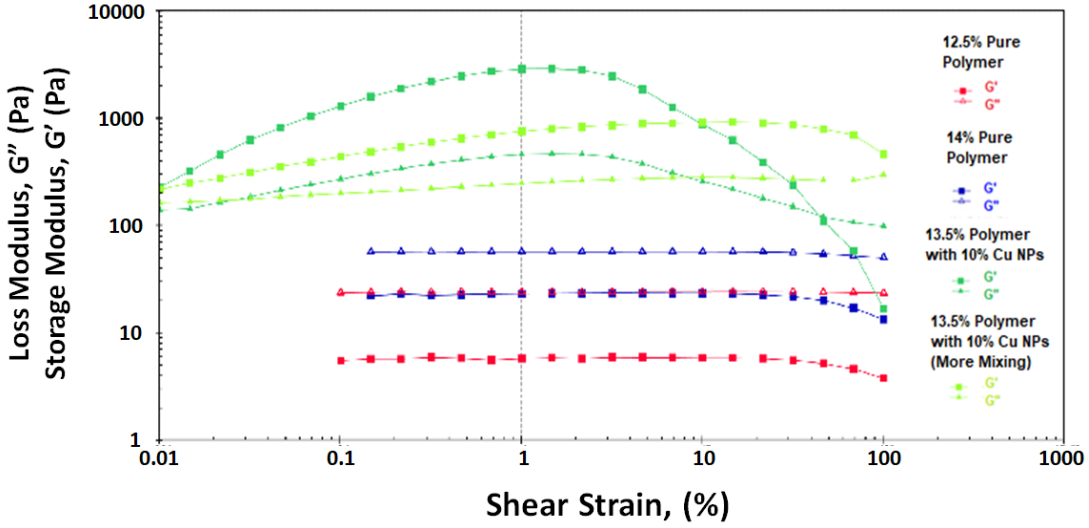

Figure 18. Loss and storage moduli for 12.5% and 14% pure polymer and 13.5% polymer/10% Cu nanoparticle ink solutions. Source: ANL

Education, Information Dissemination, Publications, and Technology Transfer

Two university graduates were hired and trained on the ES equipment and fully participated in filter media development using the ES technology. The new graduates will participate in broader ES-related R&D for R2R processing. The research also led to one conference publication, one patent application, and two joint peer-reviewed papers. A CRADA with a company in terms of technology transfer of the reusable N95 filter media is under development.

Colloidal Chemistry, Surfactant Research, Slurry Processing, Deposition and Drying/Curing Methods (ORNL Lead Laboratory)

Colloidal Chemistry and Slurry Processing

A slurry with the 8 wt.% Pt/C composition listed in Table III was slot-die coated onto a GDL using combinations of line speed, ink extrusion rate, gap between the die lips and substrate, and vacuum levels. XRF determination of the Pt loading at each parameter set allowed a determination of the relationship between each of the parameters and the Pt loading as shown in Figure 19. As expected, the Pt loading increases with increasing pump speed.

Table III. Composition of Fuel Cell Ink for 6 wt.% and 8 wt.% Slurries

Component	Concentration (wt.%)	Concentration (wt.%)
Pt/C	8.00	6.00
Water	56.25	61.50
Nafion D2020	19.16	14.37
n-propanol	16.59	18.13
Total	100.00	100.00
Solid Content	12.02	9.02

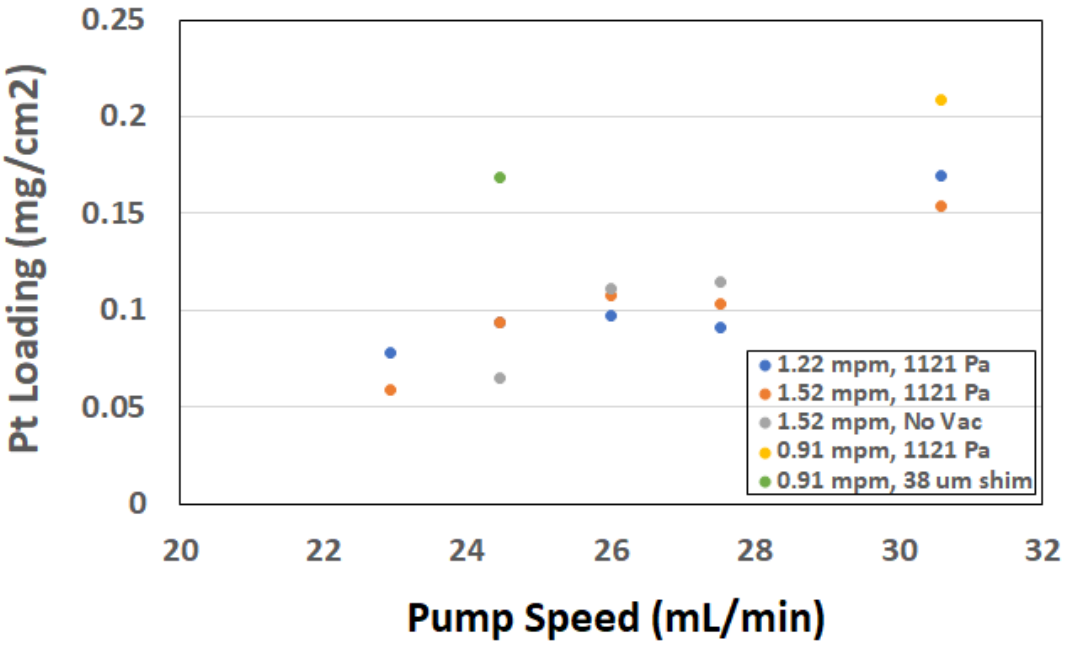

Figure 19. Pt loading of catalyst layer coatings with various coating parameter sets. Source: ORNL

A reliable coating of 0.1 mg_{Pt}/cm^2 across multiple electrodes was achieved using coating parameters of 4.6 mL/min pump speed, 1.52 m/min line speed, 1121 Pa vacuum, and a 12.7 µm gap between the die lips and substrate corresponding to a wet film thickness of 30 µm. However, the small gap size relative to the wet coating thickness results in the ink wetting the die face and may be the cause of coating non-uniformities. A

SEM image of the cross section of one of the earlier coatings with 0.1 mg_{Pt}/cm^2 loading (coated with the narrow gap) is shown in Figure 20. The 1.23 μm coating dried to form a bilayer but it did not penetrate the MPL. With the desired wet thickness for optimal Pt loading known, the coating parameters can be adjusted to a wider gap in conjunction with mathematical modeling to achieve a more uniform coating bead and improve coating uniformity and reliability.

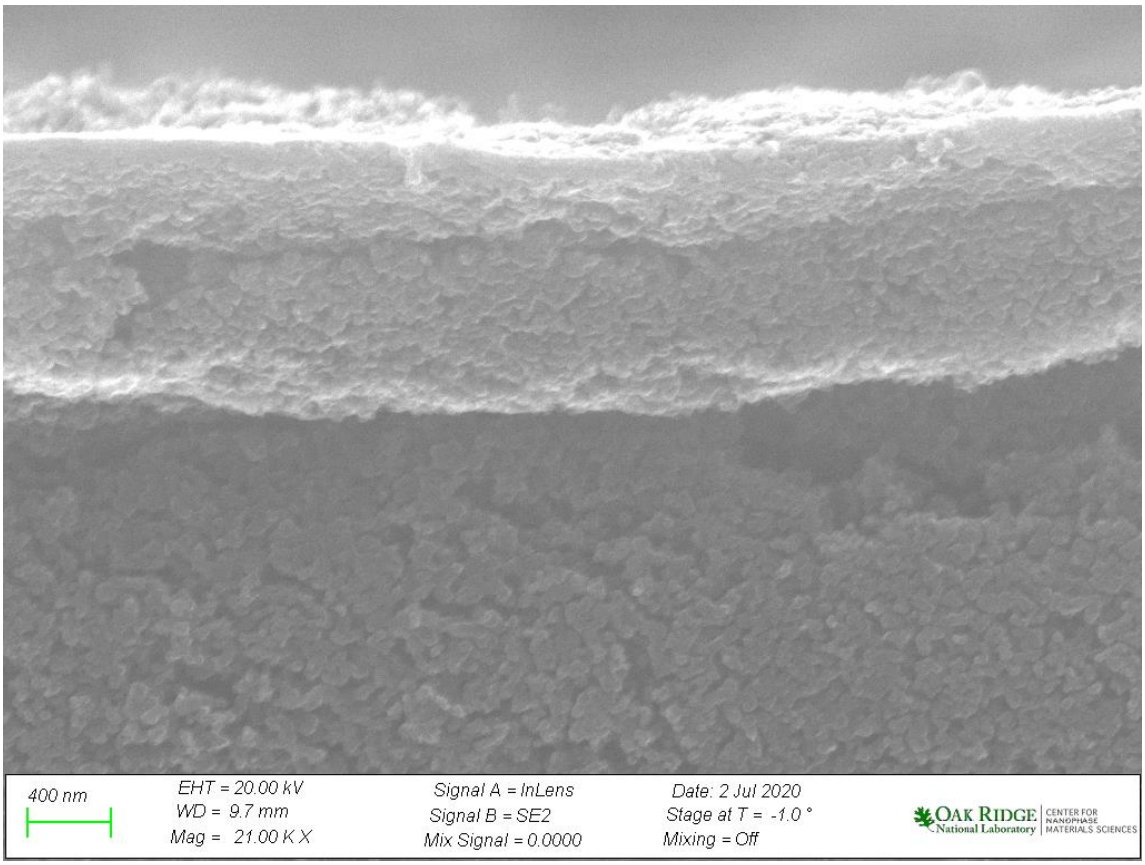

Figure 20. SEM image of a cross section of the slot-die coating with 0.1 mg_{Pt}/cm^2 loading. Source: ORNL

Solvent contact angle measurements on a GDL

Initial trials of catalyst layer coatings at wider gaps in an attempt to achieve more uniform coatings resulted in ribbing or rivulets in the coating, indicating an unstable coating bead. These trials were performed with the same line speed, pump rate, and vacuum pressure that were used for the narrow gap coating. The narrow gap may force the ink to wet the entire surface while the water-based ink may have difficulty in coating the hydrophobic MPL surface at wider gaps. To investigate the effect of solvent on ink wetting, static sessile drop contact angle measurements of 1-propanol and ethanol solutions with water were performed.

Figure 21 shows that lower alcohol content (higher water content) results in higher contact angles, which is expected due to the hydrophobic MPL surface. The 1-propanol has higher dispersion forces than the shorter-carbon-chain ethanol, so it has higher contact angles than ethanol. Contact angles less than 90° indicate wetting. Therefore, the 29.5 mass percent 1-propanol solvent system in the ORNL ink should bead up on the MPL surface rather than wetting it. However, the ink also contains the Nafion binder, which should act as a surfactant to lower the contact angle and improve wetting. Future work will consist of measuring contact angles of the inks with and without Pt/C.

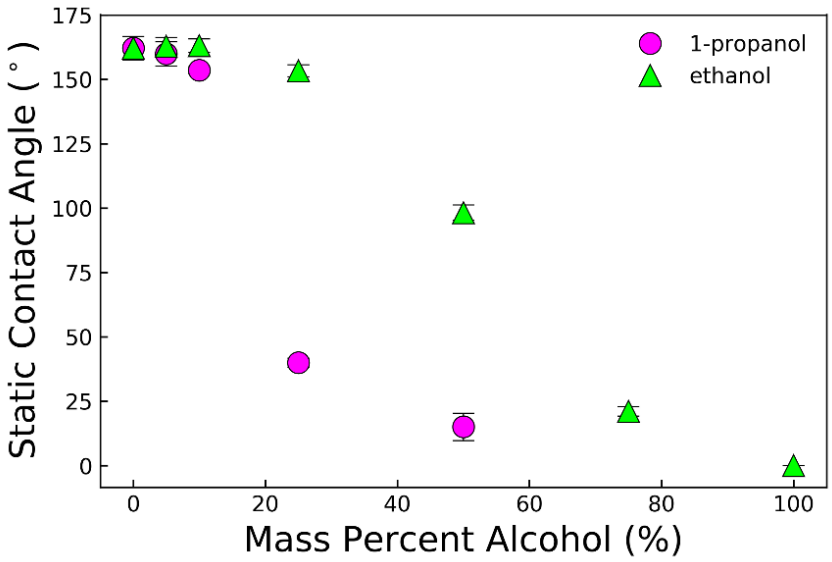

Figure 21. Sessile drop static contact angle measurements of water-alcohol mixtures on a GDL/MPL substrate. Error bars represent the standard deviation of five measurements. Source: ORNL

As seen by the data in Figure 21, a mixture of 25 wt.% 1-propanol in water has a static contact angle on the GDL of 40°. However, the dispersion media of the 8 wt.% Pt/C catalyst layer ink is 28.5 wt.% 1-propanol in water and the ink has a contact angle of 75° on the GDL, which is higher than expected for the dispersion media composition. The measurement was difficult to perform due to the high viscosity of the ink. The addition of the Nafion ionomer was expected to contribute to decreasing the contact angle due to its role as a surfactant, but the high viscosity of the ink due to the presence of Pt/C decreased the apparent contact angle.

Catalyst ink rheology measurements

ORNL conducted experiments for doctor blade coating of inks with 6 wt.% Pt/C but the experiments did not include a comparison in rheology between the 6 wt.% and 8 wt.% Pt/C formulations (compositions listed in Table III above). Subsequent experiments showed that the shear viscosity of the lower solids-loading 6 wt.% Pt/C ink is lower than that of the higher solids-loading 8 wt.% Pt/C ink, as expected and as shown in Figure 22.

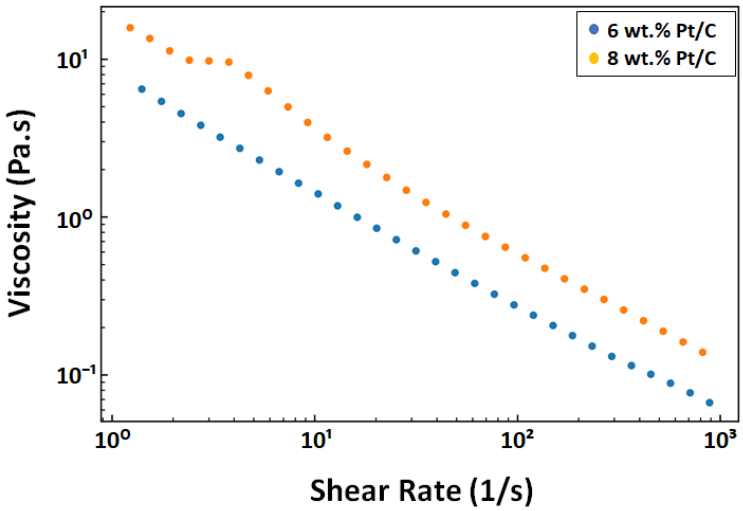

Figure 22. Ink rheology showing viscosity differences between 6 wt% and 8 wt% Pt/C cathode electrocatalyst ink contents. Source: ORNL

Neutron scattering experiments

SANS data was collected for 56 ball-milled ink samples with low solids-loading. The samples included:

- Controls that do not contain ionomer, Pt, or Pt/C
- Two different types of carbon (Vulcan and high surface area carbon (HSC))
- 4-6 levels of deuteration for contrast variation

A software package being developed to analyze and model the data will be used to determine the size of ionomer particles in the inks and how they vary with ink composition.

Deposition and Drying/Curing

Mixing with a blade disperser and a rotor-stator disperser

Slurries with the composition listed in Table IV were mixed at 10,000 revolutions per minute (rpm) for 15 min in an ice bath with a Netzsch Model 50 motor and the Hi-Vis blade-type mixer head labeled "Netzsch" shown in Figure 23(a) and an IKA Works T25 motor with a S25N-25F rotor-stator mixer head labeled "IKA" as shown in Figure 23(b).

Table IV. Composition of Fuel Cell Ink for 8 wt% Slurry

Component	Concentration (wt.%)	Mass (g)
Pt/C	8.00	8.00
Water	56.25	56.25
Nafion D2020	19.16	19.16
n-propanol	16.59	16.59
Total	100.00	100.00
Solid Content	12.02	

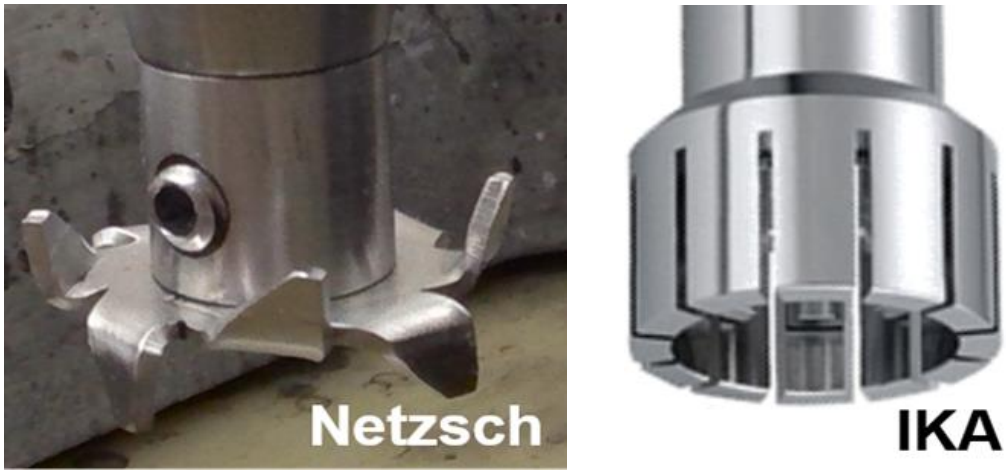

(a) (b)

Figure 23. (a) A Netzsch blade-type mixer head and (b) an IKA S25N-25F rotor-stator mixer head. Source: ORNL

The slurries were coated onto a Freudenberg GDL and dried in 59 °C air on a bed and then at 115 °C overnight. A SEM image of the GDE for the Netzsch mixer head is shown in Figure 24(a) and indicates that the particle aggregates range from 1 to 21 μm. A SEM for the IKA 25F mixer head is shown in Figure 24(b) and indicates that the particle aggregates range from 1 to 12 μm which are significantly smaller than the

Netzsch-mixed slurry coating. There are also significantly fewer aggregates in the IKA-mixed samples, resulting in a more uniform coating. The IKA coating may have higher activity due to the increased surface area resulting from breaking up the aggregates.

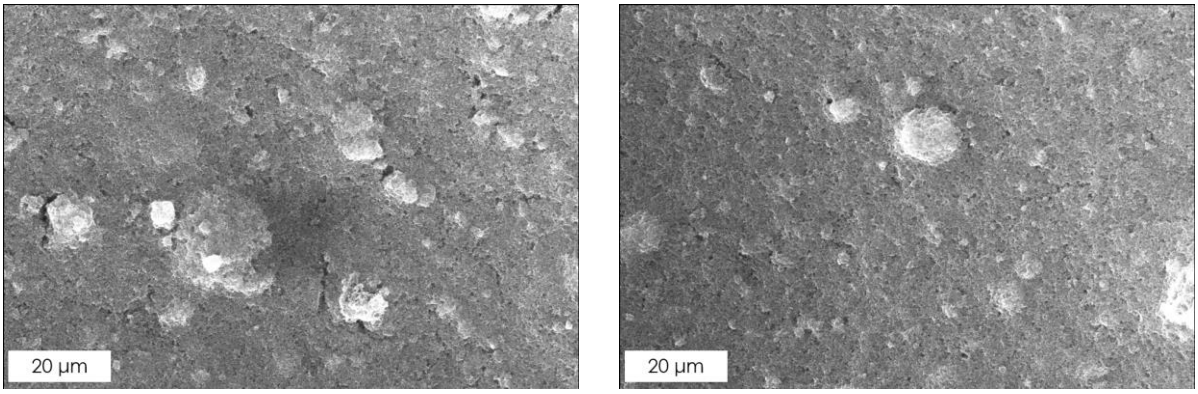

(a) (b)

Figure 24. (a) SEM image of a coating mixed with the Netzsch mixer head and (b) SEM image of a coating mixed with the IKA 25F mixer head. Source: ORNL

Rheology was used to study the shear viscosity profile of the inks. The ink mixed with the Netzsch mixer head exhibited shear thinning viscosity behavior after 15 minutes of mixing as expected, as seen by the solid red line in Figure 25, and the ink mixed with the IKA 25F mixer head also exhibited a shear thinning viscosity behavior after 15 minutes of mixing, nearly identical to that of the Netzsch-mixed ink, as seen by the solid black line in Figure 25. These results indicate that the disperser geometry has little impact on the shear viscosity of the ink. The red dashed line in Figure 25 represents mixing with the Netzsch mixer head for 2.5 hours and the black dashed line is for mixing with the IKA 25F for 1 hour. Interestingly, while the viscosity did not change with mixer type in the 15-minute-mixing study, the viscosity seems to decrease with mixing time. Further studies are needed to determine whether this trend is preserved when more slurry mixing parameters are added.

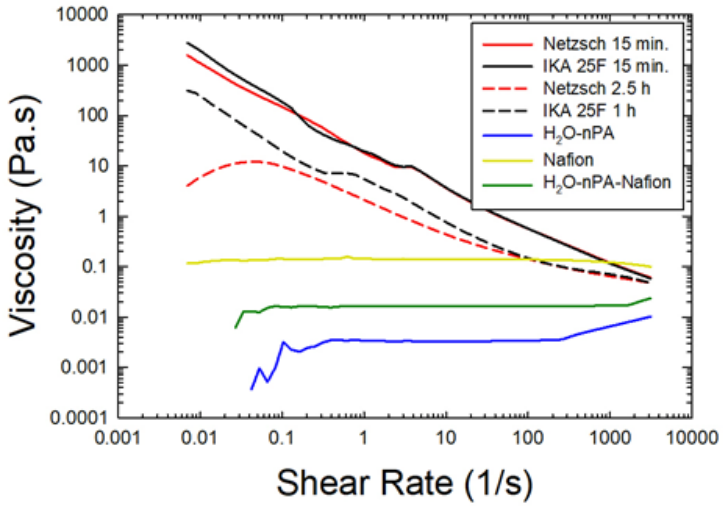

Figure 25. Shear viscosity profiles of fuel cell inks and their non-active constituents. Source: ORNL

R2R slot-die coating for a GDL

The target Pt loading for a GDE is 0.1 mg_{Pt}/cm^2 based on ORNL and NREL collaborations. A GDE with 0.18 mg_{Pt}/cm^2 was previously achieved, so efforts continued to try to decrease the Pt loading. The ink composition

was the same as that in Table IV above except 250 mL were prepared for the slot-die coatings rather than 100 mL as in the mixing study discussed above. The ink extrusion rate and line speed were varied as shown in Table V to achieve the target Pt loading.

Table V. Slurry Mixing and Coating Parameters with Coating Characterization

Mixer type	Mixing time (min.)	Line speed (ft/min.)	Small pump speed (rpm)	Extrusion rate (mL/min.)	Coating thickness (μm)	Pt loading, XRF (mg_{Pt}/cm^2)	Pt loading, mass (mg_{Pt}/cm^2)
Netzsch	140	4.0	20	5.7	3.3	0.16	0.14
Netzsch	140	4.5	20	5.7	4.1	0.19	0.17
Netzsch	140	5.0	20	5.7	4.0	0.13	0.08
IKA	60	4	20	5.7	3.3	*No data*	0.11
IKA	60	5	20	5.7	1.8	*No data*	0.10
IKA	60	4	15	3.9	*No data*	*No data*	0.02
IKA	60	5	15	3.9	*No data*	*No data*	0.00*

*The mass difference between the coated and uncoated samples was too small to reliably detect.

All slurries were mixed at 10,000 rpm. The extrusion rate given in Table V was calculated by a calibration curve of mineral oil extrusion/time at several pump revolution rates. The coating thickness given in the Table V is determined by measuring and averaging the coating thickness in several locations in a cross-sectional SEM image. An example of an SEM cross section for the Netzsch-mixed slurry coated at 20 rpm (5.7 mL/min and a 4.5 ft/min line speed is shown in Figure 26. The Pt loading was determined by two methods: (1) XRF spectroscopy which was completed at NREL and (2) mass difference between several known areas of coated and uncoated GDL. Both measurements (where available) are given in Table V. The mass difference method of Pt loading determination seems to generally underestimate the Pt loading. The thickness and Pt loading of the coatings made from the Netzsch-mixed slurries had larger variability than is typical for slot-die coating. This is likely due to over mixing and damaging the catalyst particles and/or starting the coating immediately after the shear mixing completed. The slurry and the coating of Netzsch-mixed samples both had significant amounts of bubbles present.

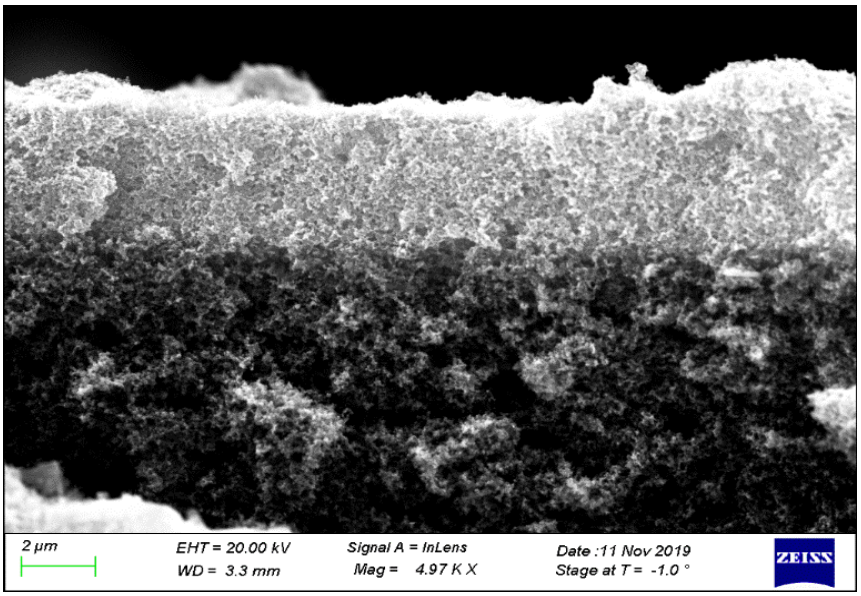

Figure 26. SEM image for a cross section of coating mixed with the Netzsch mixer and coated at 20 rpm and 4.5 ft/min. Source: ORNL

Dual slot-die coating of a catalyst layer and a Nafion overlayer

A dual slot die was also used to simultaneously coat catalyst ink and a Nafion ionomer overlayer onto the GDL. This may be the first dual slot-die coating of this kind. Prior NREL studies showed that sprayed GDEs require an overlayer. This was the basis for attempting a dual-layer R2R configuration. Previous experiments also determined that the single-layer R2R GDEs performed as well as or better than the sprayed GDEs with an overlayer at least at low percentages of solids. The dual slot-die trial was intended to validate that the same effect occurs with a high percentages of solids in the inks and coating. Though not clear in all SEM images of cross sections of the dual layer coating, some clearly show a smooth overlayer on top of the catalyst layer as can be seen in Figure 27. In-situ electrochemical evaluation at NREL determined that catalyst layers without ionomer overlayers (spray or dual slot-die coated) performed better than catalyst layers with ionomer overlayers. The dual layer slot-die catalyst layer coating produced catalyst layers with ionomer equivalent weight (EW) gradients for a catalyst layer and a membrane overlayer. Improvement in the multilayer coating process was demonstrated with the elimination of the Nafion overlayer coating as shown by the polarization measurement curves in Figure 28.

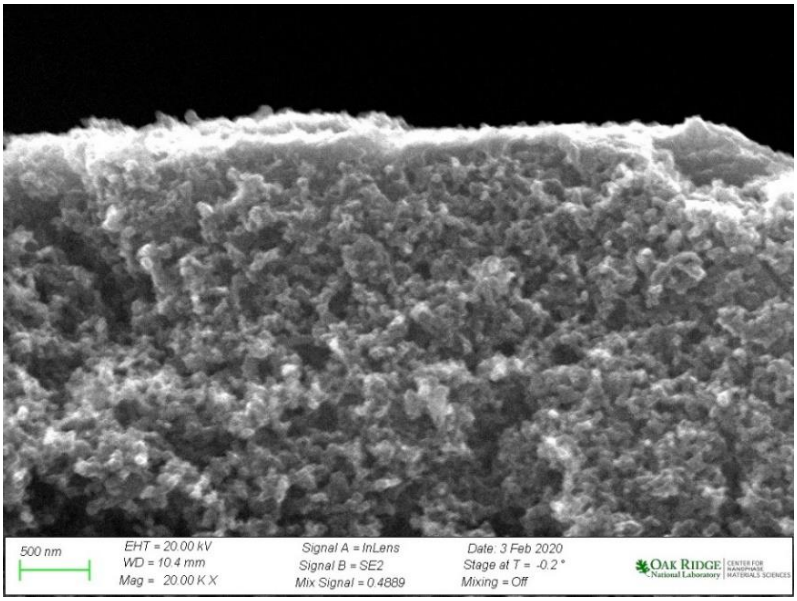

Figure 27. SEM image of a cross section of the dual layer slot-die coating of a catalyst layer and ionomer overlayer. Source: ORNL

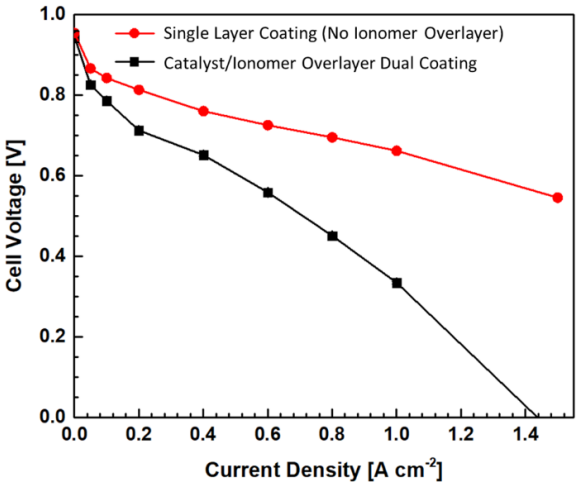

Figure 28. Polarization measurement curves for the catalyst layer with and without an ionomer overlayer. Source: NREL

Uniform slot-die coated PEMFC catalyst layer

ORNL experimented with fuel cell electrode coatings to explore the effects of high-solids content inks. Several issues have occurred previously that were mainly related to high solids although NREL had coated lower solids inks with minimal issues. Understanding the resulting morphologies and optimizing high-solids inks will have the benefit of reduced energy consumption during drying. Although the target catalyst layer loading of 0.1 mg_{Pt}/cm^2 was achieved, the variability in the Pt loading across the GDL substrate was greater than 10% (standard deviation / mean). One hypothesis for the high variability was that the gap between the die lips and the substrate was smaller than the wet thickness of the coating. This was tested by performing slot-die catalyst layer coatings at larger coating gaps. The modeling team at SNL and UNM predicted that a decrease in the line speed and an increase in the vacuum level would be needed to achieve a stable coating at a larger coating gap. A defect-free coating was achieved at a 0.5 ft/min line speed, and XRF measurements at NREL confirmed that the variation in Pt loading was much lower than had previously been achieved with the small coating gap. Table VI gives the mean Pt loading ($\bar{x}$), standard deviation (s), and the coefficient of variation ($s/\bar{x}$) for many trials of slot-die PEMFC catalyst layer coatings. The values that are not highlighted represent coatings made with coating gaps smaller than the wet coating thickness. The highlighted values represent coatings made with gaps larger than the coating wet thickness. The coatings with the larger coating gaps have much smaller Pt loading variations (4-7%) than the coatings with the smaller coating gaps (Pt loading variation typically 10-40%). Unfortunately, the Pt loading is too high with the larger coating gaps due to equipment limitations of vacuum and ink pump rate. A new vacuum and pump was needed to achieve the appropriate 0.1 mg_{Pt}/cm^2 loading with the larger coating gaps.

Table VI. Pt Loading for Slot-Die PEMFC Catalyst Layer Coatings

Mean Pt Areal Loading $\bar{x}$ (mg/cm^2)	Pt Loading Standard Deviation s (mg/cm^2)	$s/\bar{x}$
0.159	0.0340	21.4%
0.192	0.0320	16.7%
0.128	0.0510	39.8%
0.0785	0.0224	28.5%
0.0585	0.0197	33.7%
0.166	0.0141	8.5%
0.155	0.0291	18.8%
0.20883	0.0450	21.5%
0.1735	0.0153	8.8%
0.1525	0.0200	13.1%
0.094	0.029	30.9%
0.098	0.038	38.8%
0.092	0.009	9.8%
0.094	0.035	37.2%
0.107	0.012	11.2%
0.103	0.025	24.3%
0.065	0.011	16.9%
0.112	0.024	21.4%
0.114	0.018	15.8%
0.169	0.026	15.4%
0.351	0.024	6.8%
0.342	0.014	4.1%

Improvement of slot-die vacuum backpressures

Increasing the coating gap will result in a more stable coating bead and a lower loading variation. However, the SNL collaboration team predicted that the defect-free coating parameter window for the high-solids slurry required higher vacuum backpressures to support the slot-die coating bead than were possible with the ORNL R2R coating machine. A new blower was installed on the R2R coating machine and vacuum pressures greater than 10 in. H_2O were achieved at coating gaps where the maximum vacuum pressure was previously~3 in. H_2O. Other coating trials confirmed that the vacuum pressure was adjustable and stable.

R2R ES Recipe and Platform Development Support

Scale up of the electrospun LLZO nanofibers

ORNL collaborated with ANL to study several solution formulations and ES parameters. Thin and uniform LLZO nanofibers were obtained using lithium, lanthanum, and zirconium nitrate precursors that were dissolved in water and acetic acid at a molar ratio of 7.7:3:2, respectively. [11] [12] Polyvinylpyrrolidone (PVP, molecular weight 1,300,000) was used to electrospin the fibers using a feed rate of 0.16 ml/h, a voltage of 18 kV, and a working distance of 13 cm. ANL used this recipe and process to successfully reproduce the results by ORNL with the objective of scaling up the LLZO nanofiber formulation using the large scale ES setup at ANL.

Aqueous-based Al-LLZO formulations were processed using an experimental ES setup where the speed rate and the concentration of the precursor solution were increased. The Li:La:Zr molar ratio of 7.7:3:2 was used with a 10% excess of Li to account for the Li loss during calcination. Initially, 2 mmol zirconium oxynitrate, 7.7 mmol lithium nitrate, 3 mmol of lanthanum nitrate hexahydrate and 0.27 mmol aluminum nitrate nonahydrate were dissolved in 12.5 mL deionized water. The reactants were then mixed overnight, and this solution was labeled “Solution 1”. PVP was dissolved in acetic acid at 15 wt.% concentration using magnetic stirring overnight. This solution was labeled “Solution 2”. Equal volumetric amounts of Solutions 1 and 2 were mixed for 12 h before ES with needle diameter of 0.6 mm, a feed rate of 0.3 mL/h, a voltage of 18 kV, a collector speed of 400 rpm, and a needle-collector distance of 13 cm.

Nanofiber annealing

Electrospun fibers were annealed to remove the PVP polymer and to crystalize the LLZO phase and several batches of Al-LLZO nanofibers were synthesized. To increase the yield of the ES process, the concentration of the Al-LLZO precursors in the water solution was doubled. A multi-step annealing process was used to anneal the fibers where the temperature ramp was 120 ^oC for 1.5 h to remove the remaining water and acid, then 350 ^oC for 1 h to remove the PVP, and finally 700 ^oC for 1, 2, and 3 h to crystalize the Al-LLZO phase. Different annealing times were used to study the effect of annealing time on the Al-LLZO crystal structure and therefore, to determine the annealing time that is required to achieve the cubic phase. After annealing, the fibers were rapidly removed from the furnace and allowed to cool. SEM images of the fibers prior to annealing are shown in Figure 29 where the diameter of the fibers is 100-200 nm. SEM images of the Al-LLZO fibers after annealing at 700 ^oC for 1, 2, and 3 h are shown in Figure 30, Figure 31, and Figure 32, respectively. The annealed fibers coalesce and form nanostructured ligaments.

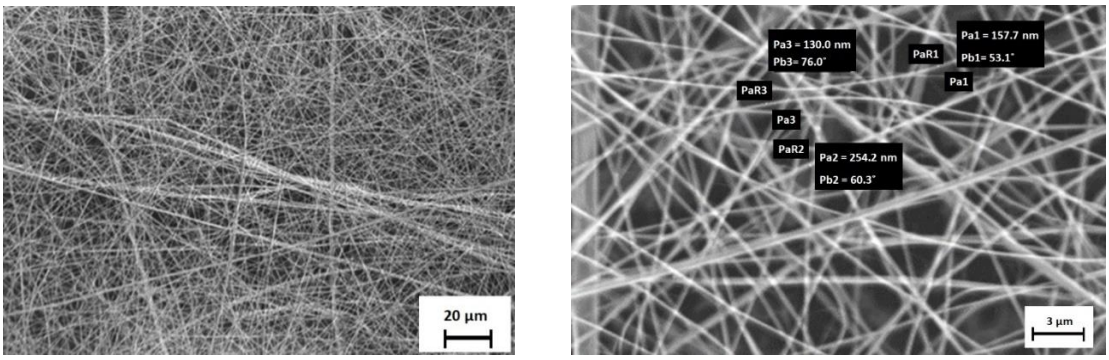

Figure 29. SEM images of Al-LLZO fibers before annealing with diameters of 100 to 200 nm. Source: ORNL

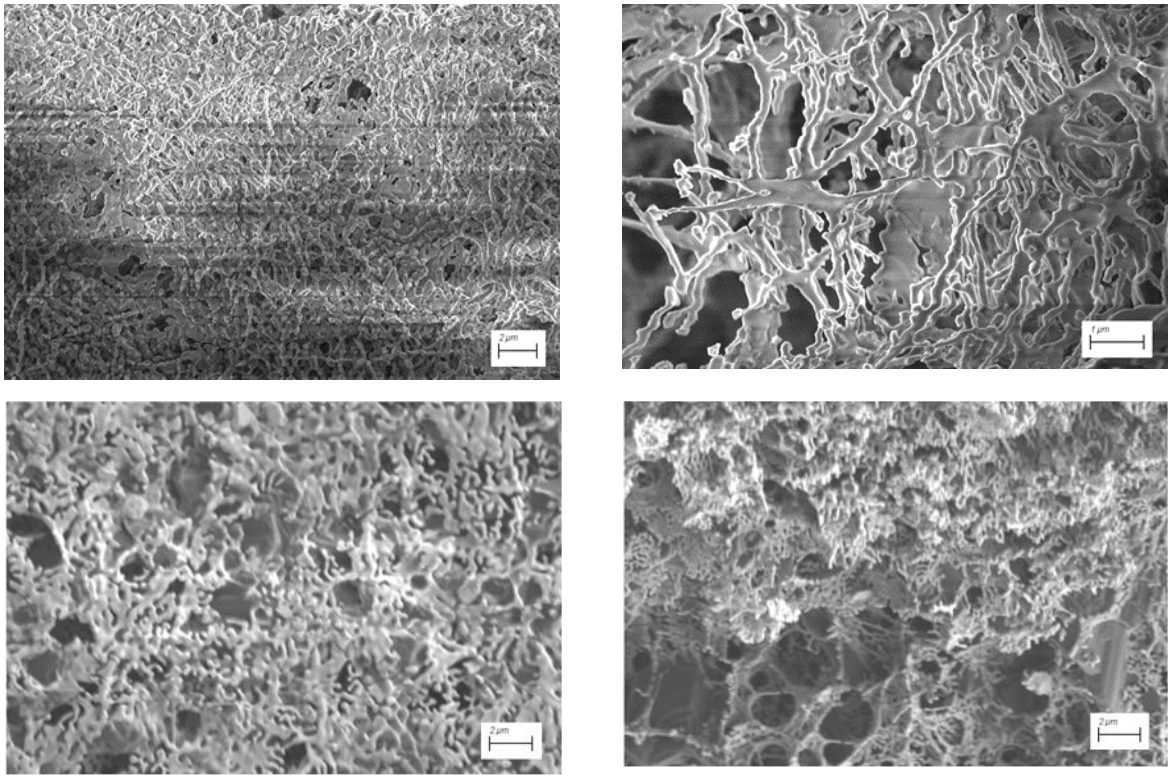

Figure 30. SEM images of Al-LLZO fibers annealed at 700 ^{o}C for 1h. Source: ORNL

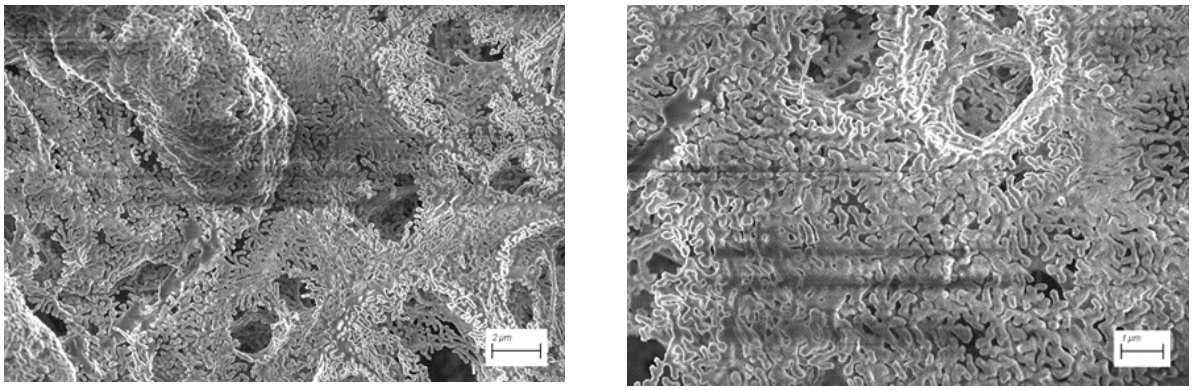

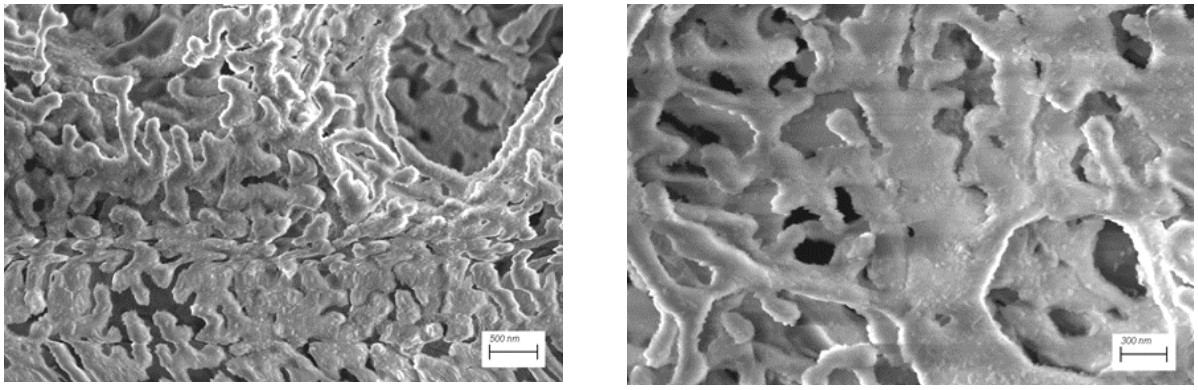

Figure 31. SEM images of annealed Al-LLZO fibers at 700 °C for 2h. Source: ORNL

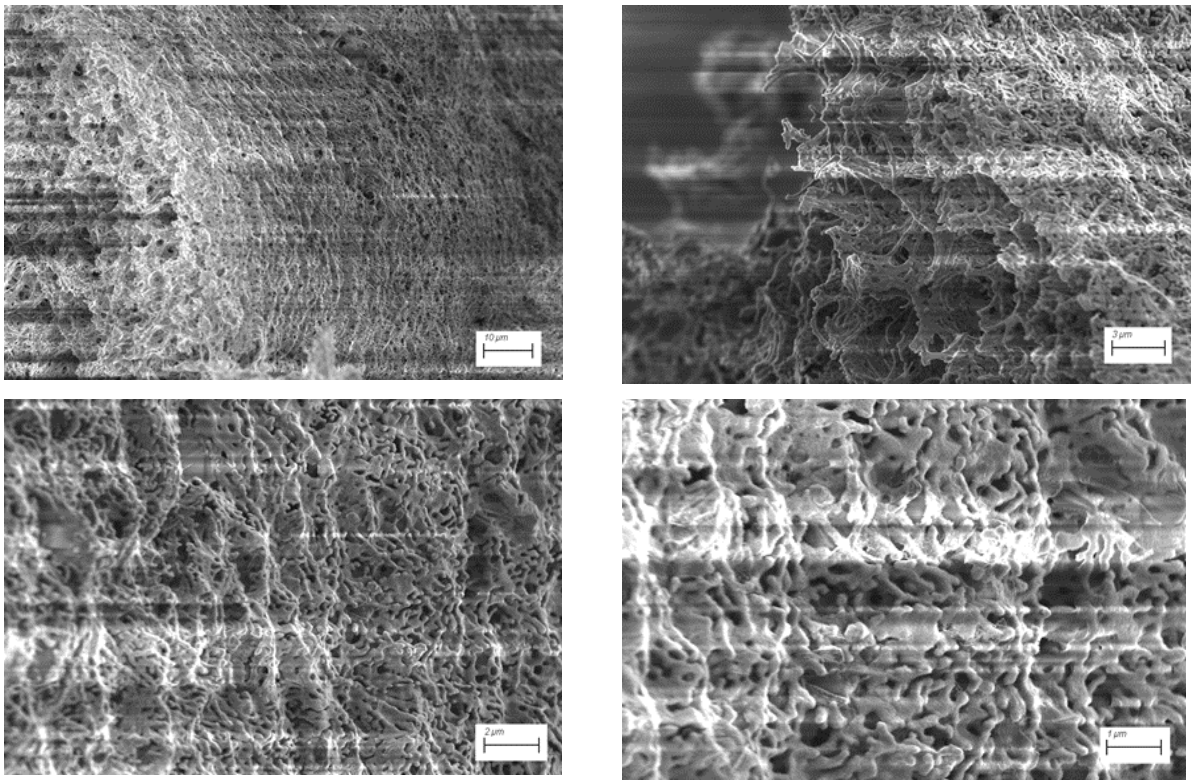

Figure 32. SEM images of the annealed Al-LLZO fibers at 700 °C for 3h. Source: ORNL

No significant change in the fiber morphology was obtained for the three different annealing times. The XRD plots are shown in Figure 33. The peaks of the 1 h annealed Al-LLZO are slightly shifted and are closer to the tetragonal phase. One hour was not adequate for the Al-LLZO to crystalize in the cubic phase. The 2 h and 3 h annealed samples are in the cubic phase. The unassigned peaks are mainly due to carbonates and are present in all samples. The fibers must be annealed in argon to remove the carbonates and increase their conductivity.

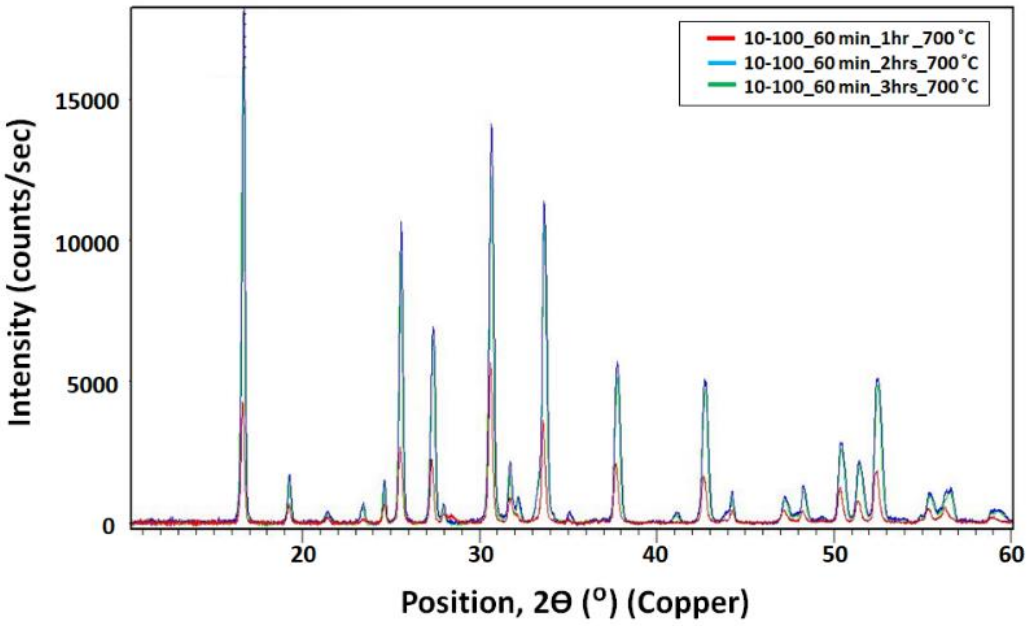

Figure 33. XRD plots for annealed Al-LLZO fibers. Source: ORNL

Impedance measurements

For the electrical measurements, an Al-LLZO pellet was sintered at 900 °C for 12 h to form the cubic phase as shown by the XRD plot in Figure 34(a). The conductivity at 25 °C was $5x10^{-6}$ S/cm for a pellet with a relative density of 55% as shown by the impedance plot in Figure 34(b). The low conductivity can be attributed to the low density of the pellet and the formation of carbonates.

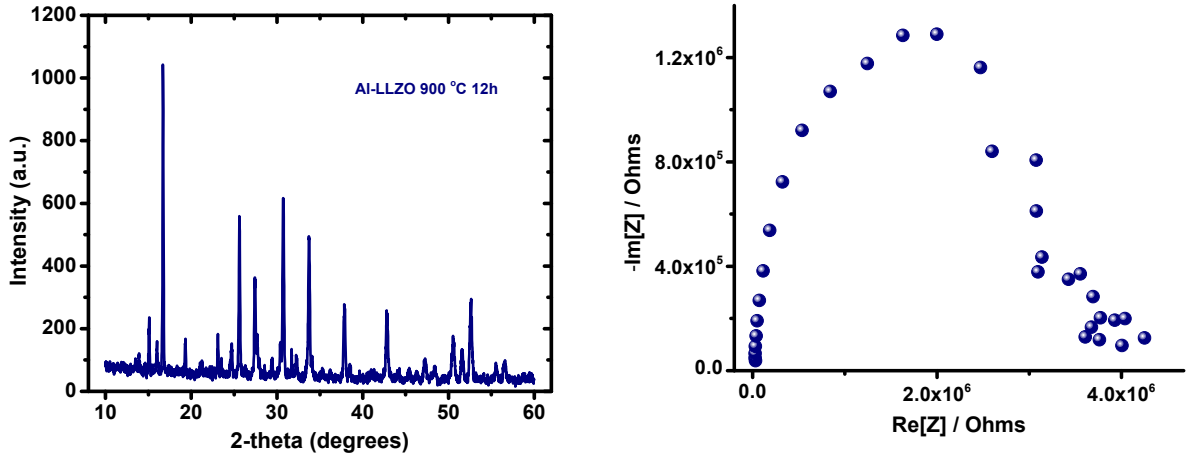

(a) (b)

Figure 34. (a) XRD plot of the Al-LLZO sintered at 900 °C for 12 h. (b) Impedance plot of the same pellet. Source: ORNL

Coin cells based on composite cathodes were assembled and tested. Calcined Al-LLZO scaffolds of porous fibers and coalesced ligaments were used as additive materials in the cathode formulations. The structure of the Al-LLZO scaffolds according to our previous studies are shown in Figure 35(a) and Figure 35(b), and a representative XRD pattern of the Al-LLZO cubic phase are shown in Figure 35(c).

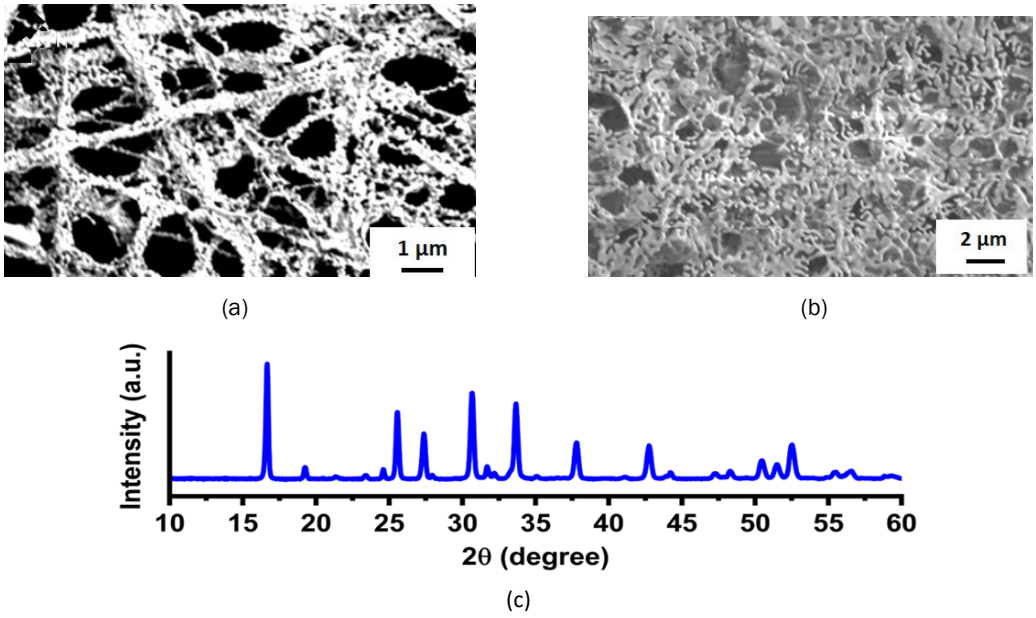

Figure 35. SEM images of Al-LLZO scaffolds of (a) the porous fibers and (b) the coalesced ligaments. (c) A representative XRD pattern of the Al-LLZO cubic phase. Source: ORNL

Three full cells were tested: (1) a control cell without Al-LLZO additives, (2) a cell with porous fiber scaffolds, and (3) a cell with coalesced ligament scaffolds. The cathode formulations were as follows:

Control:
NMC 6:2:2 (BASF): 90 wt%
Carbon black (Small Denka): 5 wt%
PVDF: 5 wt%

Coalesced ligament scaffolds:
NMC 6:2:2 (BASF): 86 wt%
Al-LLZO: 4.7 wt%
Carbon black (Small Denka): 4.7 wt%
PVDF: 4.7 wt%

Porous fiber scaffolds:
NMC 6:2:2 (BASF): 86 wt%
Al-LLZO: 4.7 wt%
Carbon black (Small Denka): 4.7 wt%
PVDF: 4.7 wt%

Full cells were made using Gen 2 electrolyte (lithium hexafluorophosphate, $LiPF_6$), a Li disc for anode, and a separator. The charge discharge curves at different C-rates and the impedance spectra during the first cycle are shown in Figure 36. The interfacial resistance is similar for all samples (less than 5 Ω for the bulk electrolyte resistance and approximately 30 Ω for the interfacial resistance contributions). The composite cathodes exhibit more noticeable power law contributions, in the low frequency regime, which is indicative of a more pronounced ion diffusion mechanism. The charge-discharge profiles are almost identical for low C-rate where the charge and discharge occur over a long period of time and the Li diffusion within the composite cathode is sufficient and does not require Li-conductive additives. At higher C-rates a marked improvement in the specific capacity is evident for the cells based on composite cathodes (due to their enhanced Li conductivity) and especially for the cathode filled with porous Al-LLZO fibers. This behavior is better illustrated in Figure 37 where the summarized discharge specific capacities are presented for all measured C-rates. The superior performance of the composite cathodes based on highly porous Al-LLZO fibers can be attributed to their high aspect ratio and light weight due to their porous features.

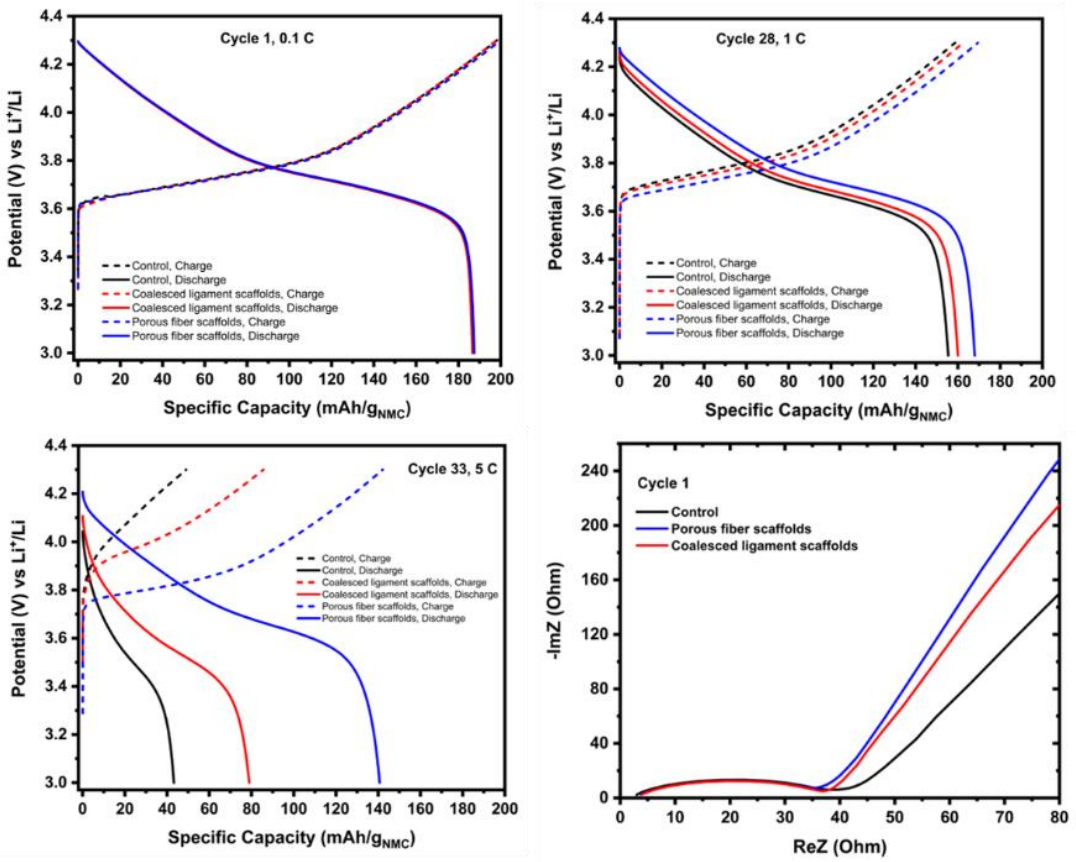

Figure 36. Representative charge-discharge cycling and impedance spectra for the coin cells based on composite cathodes. For comparison, the spectra of the control cell are also presented. Source: ORNL

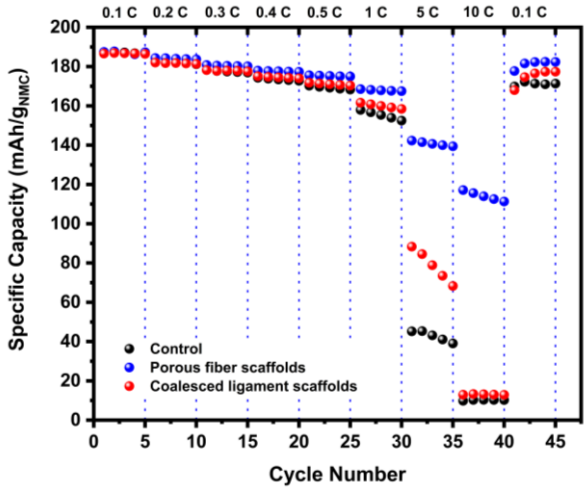

Figure 37. A summary of the C-rates for the cells tested. Source: ORNL

Coaxial LLZO/PAN fibers

Coaxial LLZO (sheath) /PAN (core) fibers were electrospun using the experimental setup shown in Figure 38(a). The diameter of the fibers is approximately 100 nm as shown in the SEM image in Figure 38(b). The LLZO precursors were dissolved in a water-based solution whereas, PAN was dissolved in dimethylformamide

(DMF). The immiscibility of the LLZO and PAN precursor solutions led to the formation of beads as shown in Figure 38(c) and at a higher magnification shown in Figure 38(d).

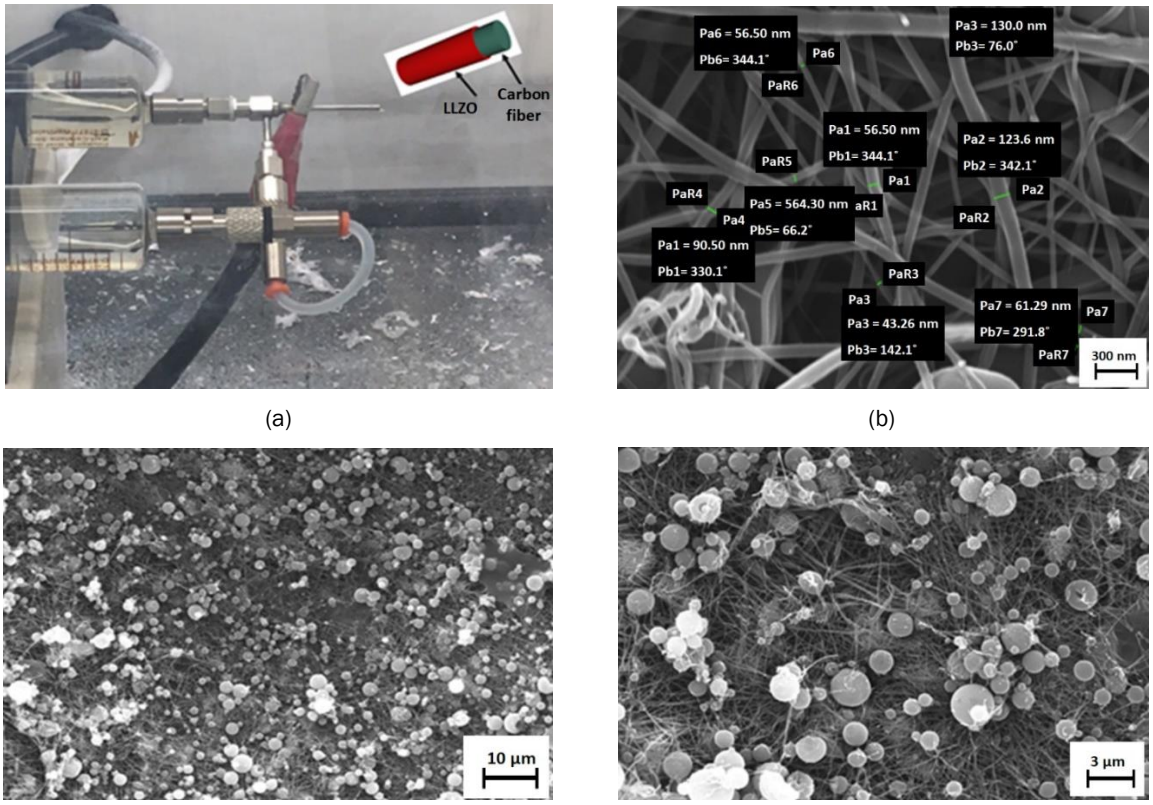

(a) (b)

(c) (d)

Figure 38. (a) Experimental setup for ES of coaxial LLZO/Pan fibers, (b) SEM image of the coaxial fibers with an approximate diameter of 100 nm, and (c) and (d) SEM images showing bead-like structures formed by the immiscibility of the LLZO and PAN precursor solutions. Source: ORNL

The DMF-based formulations for both precursor solutions required optimizing their concentrations to be suitable for ES without the formation of phase-separated structures. Two solutions were mixed and remained in a vial for a week to test their miscibility. The mixed solution shown in Figure 39(a) is homogeneous without any visible signs of phase separation. The cast solution shown in Figure 39(b) had a film that was formed after drying on a hot plate at 100 ^{o}C. No signs of LLZO precursor aggregates were observed.

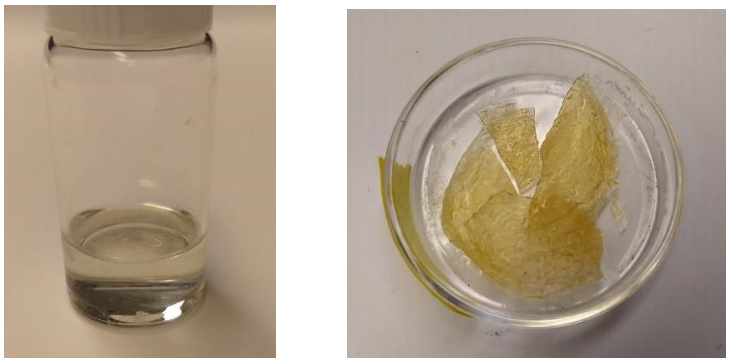

(a) (b)

Figure 39. (a) Mixed LLZO and PAN precursor solutions after one week and (b) the cast film of the mixed solution. Source: ORNL

Composite Al-LLZO/PAN electrospun nanofibers

ORNL collaborated with ANL to perform small-scale studies on different materials that can be synthesized using the R2R ES platform. Hybrid composite nanofibers were developed that were based on Al-LLZO and carbon nanofiber. The purpose of the study was to synthesize nanofibers with electronic and ionic conductivity using PAN as the carbon fiber precursor. Composite Al-LLZO/PAN nanofibers were synthesized according to the DMF-based formulation that was described above. In solution 1, stoichiometric amounts of $Zr(OCH_2CH_2CH_3)_4$, $LiNO_3$, $La(NO_3)_3$, $Al(NO_3)_3$ were dissolved in acetic acid and DMF. In solution 2, PAN was dissolved in DMF (7 wt%). Equal volumetric amounts from solutions 1 and 2 were mixed and the final solution was stirred for 48 h. The ES parameters used were a 20cc syringe with a diameter of 20 mm, a Hamilton 91022 22 gauge needle with an inner diameter of 0.41 mm, a feed rate of 1.0 ml/h at a distance of 12 cm, and a voltage of 18 kV. SEM images of the as-spun Al-LLZO/PAN fibers are shown in Figure 40(a) at a lower magnification and Figure 40(b) at a higher magnification. The diameter of the fibers was found to vary from approximately 800 nm to 1.4 µm.

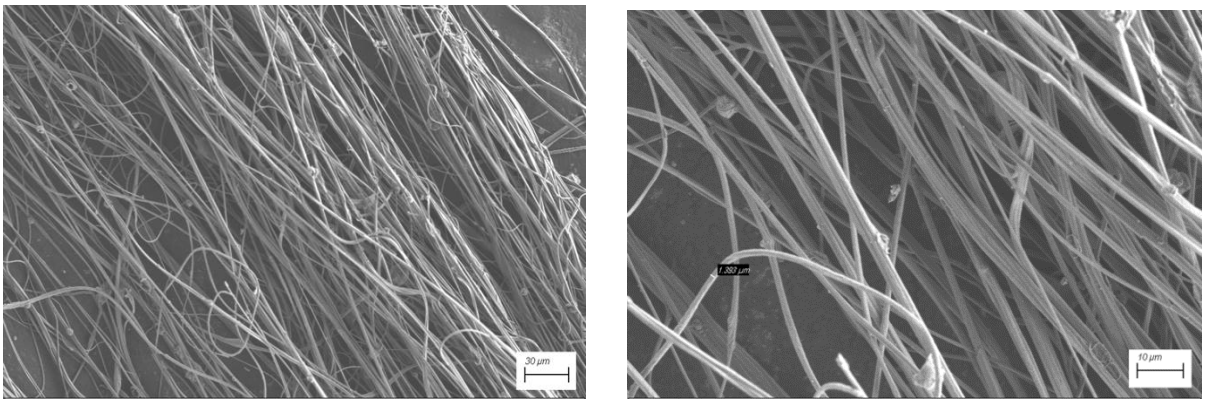

(a) (b)

Figure 40. (a) SEM image at low magnifcation and (b) higher magnification of composite LLZO/PAN electrospun fibers. Source: ORNL

The Al-LLZO/PAN fibers were stabilized and carbonized according to the following procedure: Annealing at 280 °C for 3h in air, annealing at 700 °C for 1 h, annealing at 1000 °C for 1 h, and cooling down to 300 °C. The annealing and cooling was performed under an argon flow of 0.4 standard liters per minute and after the argon was turned off, the fibers were allowed to cool to room temperature. SEM images of the carbonized fibers are shown in Figure 41(a) at low magnification and Figure 41(b) at higher magnification where the diameter of the carbonized fibers is less than 800 nm.

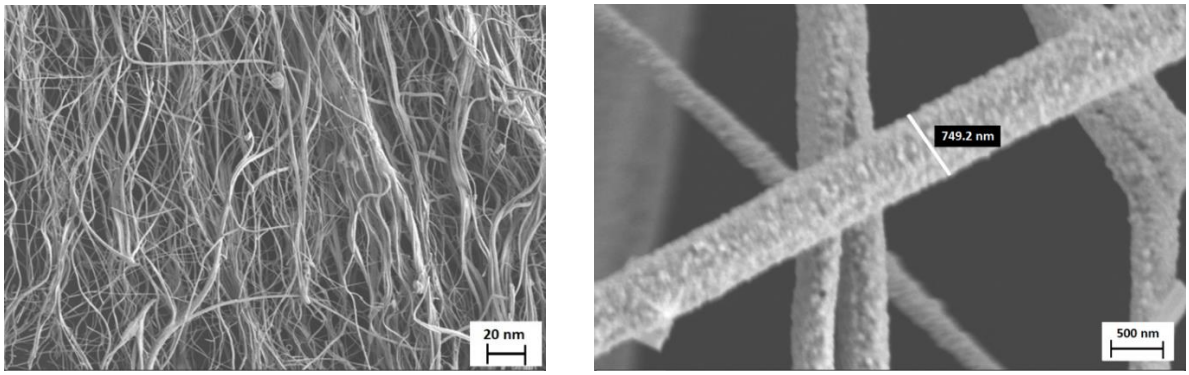

(a) (b)

Figure 41. SEM images of the carbonized Al-LLZO/PAN fibers at (a) low magnification and (b) higher magnification. Source: ORNL

EDS was performed on the carbonized fibers to verify the presence of the C, O, Al, La, and Zr elements. The fibers were mounted on carbon tape. The scanned area and the elemental map are shown in Figure 42. The Al-LLZO is uniformly distributed on the carbon fiber structures. The corresponding EDS spectrum is shown in Figure 43.

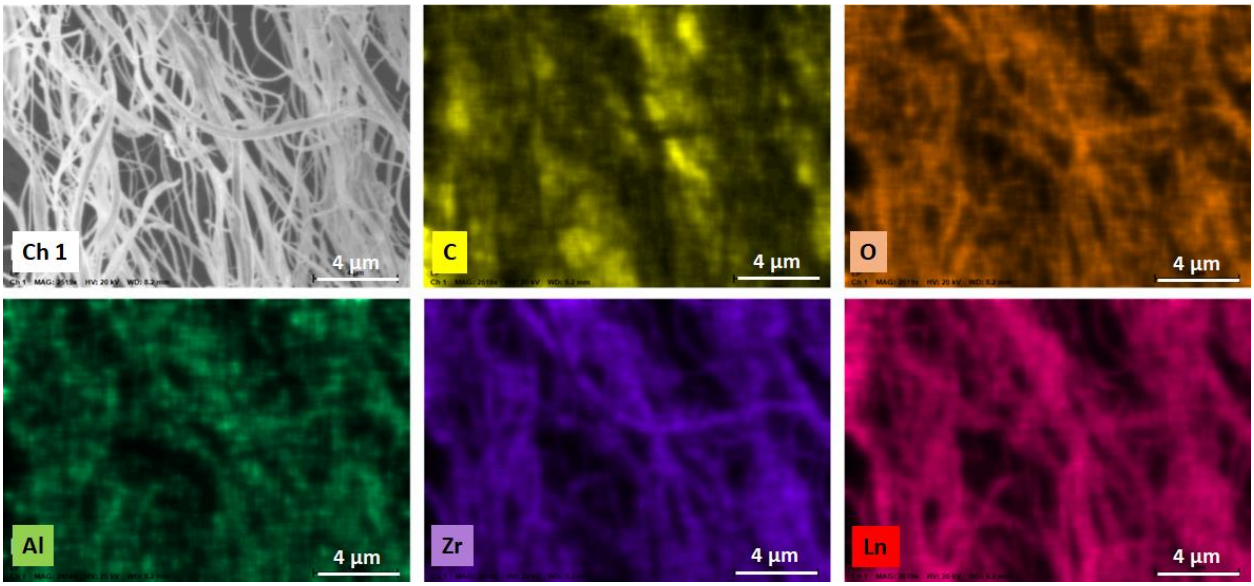

Figure 42. Elemental map of the carbonized Al-LLZO/PAN fibers according to the EDS analysis. Source: ORNL

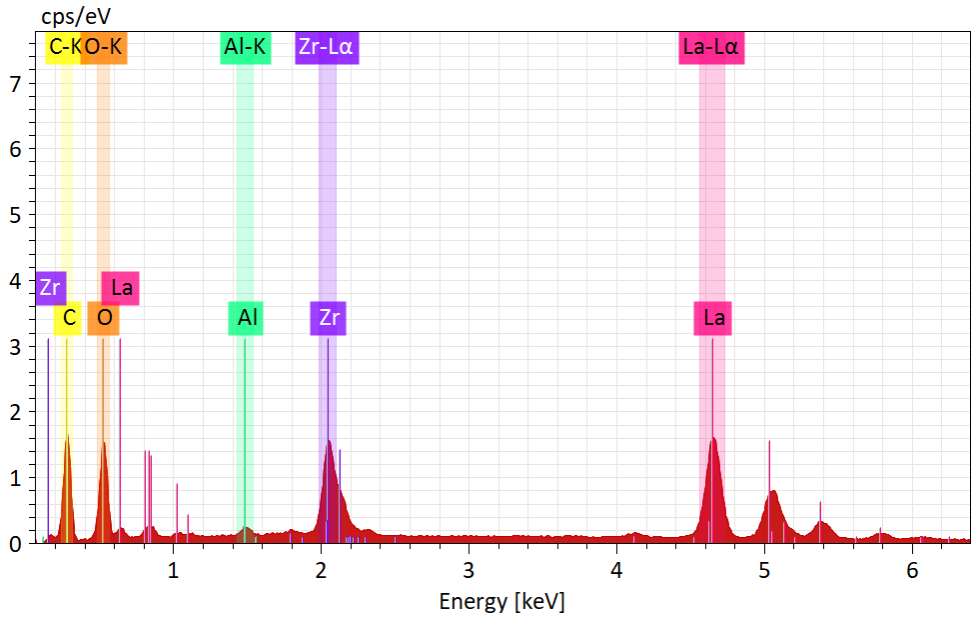

Figure 43. EDS spectrum for the elemental analysis of the carbonized Al-LLZO/PAN fibers. Source: ORNL

Education, information dissemination, publications, and technology transfer

A manuscript summarizing the progress on the ES formulations was completed with the title of "Nanostructured ligament and porous fiber LLZO ceramic scaffolds synthesized at low calcination temperature for solid-state batteries" and submitted to *Applied Surface Science*.

Physics and Methodologies for Multilayer Coatings/Deposition; Fabrication and In-Situ Testing of Prototype Components and Devices; and Novel Non-Destructive Evaluation, Quality Control and Metrology (NREL Lead Laboratory)

Cutting-Edge Coating and Deposition Science for R2R Applications

R2R slide die development

The receipt of the multilayer (ML) slide die from a U.S. manufacturer, Allied Die, was significantly delayed by six months which impacted the research schedule. During this time, the design of the support and lifting modifications to a commercially available industrial cart for the die were completed and readied for build-out upon receipt of the die. Also, other ancillary pumping and die support hardware were obtained.

The three-layer slide die was received in mid-February 2020. Frequent communications and meetings were held with Allied Die to complete additional design and infrastructure activities associated with the use of the slide die. Figure 44(a) and Figure 44(b) show two design drawings and Figure 44(c) is a photograph of the slide die. Upon receipt, the die lip, the insert part where the flow of inks down the slide transitions into the coating bead and onto the moving web, was not designed correctly. The design was for curtain coating rather than bead coating. Figure 45(a) shows the curtain coating design with a bullnose turn of the flow to vertical prior to dropping the flow into the air, forming the 'curtain'. Figure 45(b) shows the bead flow lip as a straight extension of the slide, which intersects at an approximately 30˚ angle with the backing roll. While the original part is not the desired design, it provides the ability to explore slide curtain coating in the future which could be useful for certain applications. NREL coordinated with SNL extensively to explore the patent and publication literature in order to validate the bead coating lip design details.

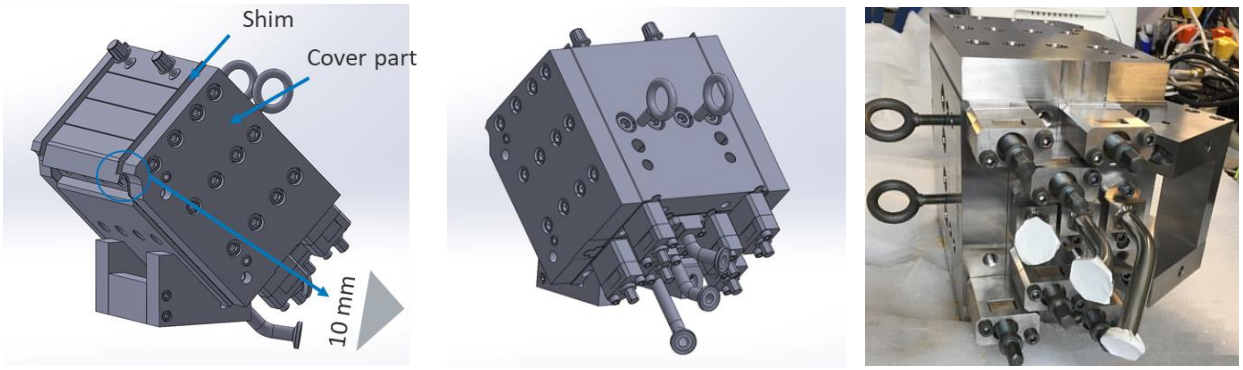

(a) (b) (c)

Figure 44. (a) The design drawing for the side view of the three-layer slide die showing the three slide manifolds (roughly horizontal in the image) on the face of the slide, (b) the design drawing of the end view of the slide die, and (c) an image of the slide die laying on its side from the rear. Source: NREL

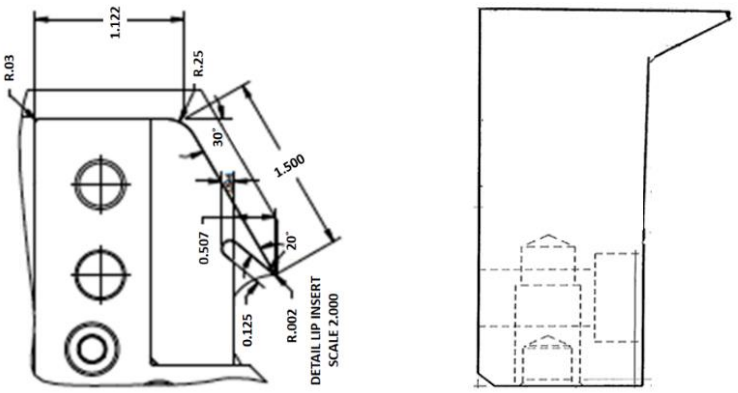

(a) (b)

Figure 45. Design of (a) curtain coating lip and (b) bead coating lip. Source: NREL

During the inspection and setup of the slide die, an issue with die side-plate bolts was discovered. As shown in Figure 46, the threading for several bolts was misaligned, so the die was returned to Allied Die for re-machining of the threads in the side plates. The die was also received with flow inlets that would not allow proper mounting in our coating station. These flow inlets were redesigned, and new inlets were machined.

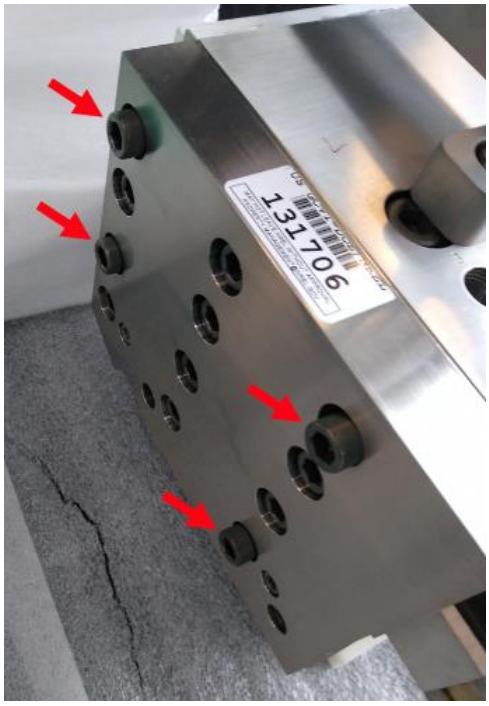

Figure 46. Bolt threading misalignment on the die side plate. Source: NREL

A lift cart for moving and placing the 90-plus pound slide die required design and machining of specialty parts for an extension arm to facilitate motion of the die into the coating enclosure or hood or a cabinet for storage. Also, a base plate for the in-hood experimental setup was machined. Figure 47(a) shows the design for the extension arm and Figure 47(b) shows the die lifting bracket design. A schematic of the extension arm assembly with the slide die attached is shown in Figure 48(a) and the actual assembly extending the slide die into a laboratory hood is shown in Figure 48(b) . This design will continue to be improved and further modifications will be made.

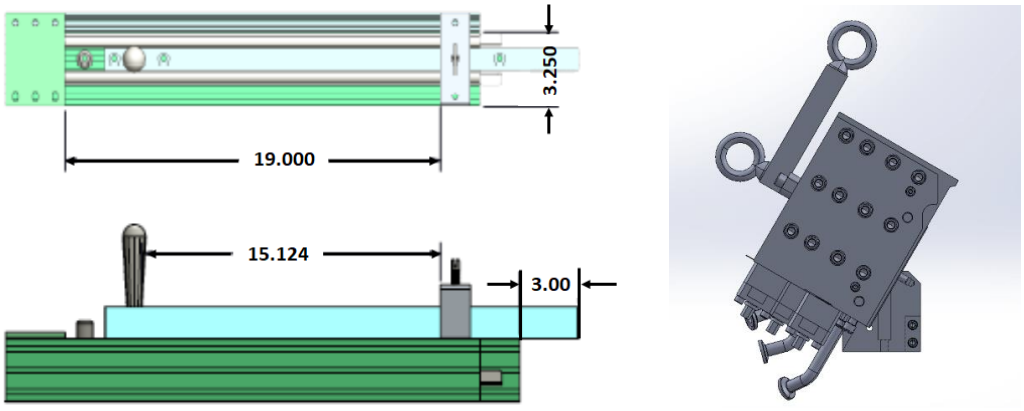

(a) (b)

Figure 47. Design of (a) the extension arm and (b) the die lifting bracket. Source: NREL

(a) (b)

Figure 48. (a) The design of extension arm with the attachment of the slide die at right and (b) the actual slide die lift cart extending the slide die into a hood. Source: NREL

Before the die could be used in an actual coating configuration such as a coating station, a method was needed that could provide an inexpensive way of performing flow visualization experiments. Methodologies presented in the ML coating literature were explored for coating flow visualization. Strong collaboration and coordination with SNL on the development of a continuum ML slide die model (which did not exist in the literature), and a method of flow visualization to help validate the outputs of the model was developed. Various camera and lens types were evaluated, and similar equipment already existing at NREL were identified for initial use. To support the intended flow visualization aspect of the broad ML coating effort, as well as post-coating microscopy of the various target dried ML structures, relevant dye materials were explored for use with the low-cost, flexible-property "dummy inks" previously developed. Rheology of the PEO polymer dummy ink was performed to identify suitable dye loadings and to verify that addition of the dye does not appreciably change the behavior of the ink. Figure 49(a) shows the polymer ink with blue and red dies of different loadings and Figure 49(b) shows the rheology results for the different percentages of die used. No significant change to the ink rheology is seen in the high-shear region of interest. The miscibility of the inks after drop-casting were also evaluated and the inks were seen to be immiscible for short times.

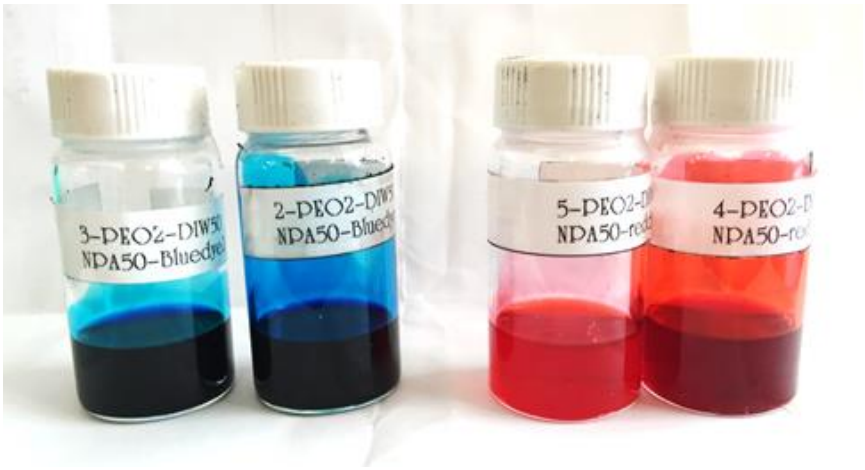

(a)

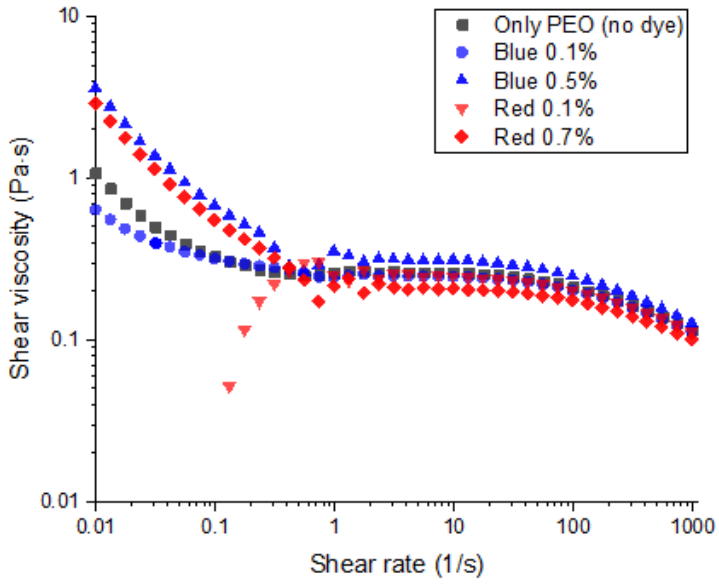

(b)

Figure 49. (a) PEO solution with blue and red dye and (b) rheology of PEO with added dye. Source: NREL

Upon completing assembly of all die components and ancillary equipment, multilayer flow testing was initiated in the hood setup to explore coating stability as a function of layer thickness and ink properties using dyed 'dummy' inks. The slide die was installed in a fume hood to perform flow experiments with different numbers, flowrates, and formulations of inks. Coupled with flow imaging, this provided extensive initial information about stable slide flow configurations and conditions. Figure 50(a) provides an illustration of the fume hood flow experiment setup and Figure 50(b) shows the actual slide die installed in a hood for initial flow testing. The newly machined flow inlets were installed, and the die was made operational for flow visualization experiments. For at least most of these tests, the 'dummy inks' were used to enable easy modulation of ink viscosity, density, and surface tension to explore multi-layer flow interactions and the impact of flowrate and ink properties on slide flow stability. Dyes were added to the dummy inks to enable visualization of the different layers on the slide. This was also an excellent platform to generate data to correlate and validate the SNL coating flow modeling results. In addition to the setup shown in Figure 50, multiple high-resolution cameras were identified at NREL for use in flow imaging, and brackets were obtained to mount the cameras in different configurations.

(a) (b)

Figure 50. (a) The design of the fume hood flow experimental setup for the slide die and (b) the actual equipment for the flow test and visualization setup in the hood. Source: NREL

Single- and two-layer flows were demonstrated using red-and-blue dyed solvent inks and dyed PEO polymer inks as seen in Figure 51 and different flow rates in the two layers were explored. The manifold step heights were adjusted to match expected target layer wet thicknesses. In this regard, NREL coordinated with SNL on theoretical calculations for wet thickness and SNL provided the equations. The imaging of flow stability was performed using a high-resolution camera and flow instabilities were observed before adjusting the manifold heights.

Figure 51. Two-layer slide flow with blue ink in the bottom layer and red ink in the top layer. Source: NREL

Ink mixing and processing studies

The impact of ball milling duration on the coating, drying and crack formation of catalyst inks was investigated. Using a standard Pt/C catalyst ink (e.g., for a PEMFC), inks were milled for 24, 48, 72, and 96 hours and the viscosity of each ink was measured after milling. Small samples were coated on a gas diffusion media (GDM) substrate and dried. Optical microscopy was performed on the dried samples to quantify cracking, as one metric of mixing suitability, and a specially-developed Python algorithm was used to quantify the percentage of the surface covered by cracks. Figure 52(a) shows the optical microscopy and the measured steady-shear viscosity, as a function of milling/mixing time. Clearly the level of cracking increased with milling time, whereas the viscosity decreased. This is an indication that additional milling time decreases the size of agglomerates and leads to lower viscosity, as shown in Figure 52(b), however, the smaller agglomerates lead to smaller pores which lead to larger capillary stresses during the consolidation process, thus leading to more cracks. Figure 53 shows higher resolution SEM images performed by the Colorado School of Mines of the coated electrodes using these four inks which correspond well with the lower resolution imaging.

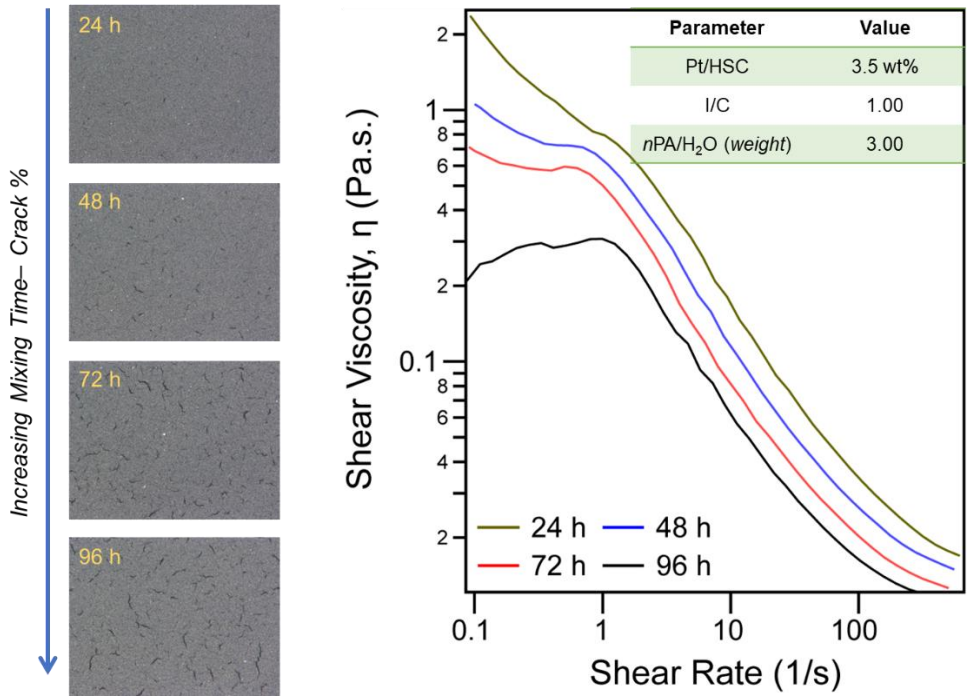

Figure 52. (a) Optical microscopy of coated layers showing increasing cracking with increasing milling time and (b) shear rheology of catalyst inks ball milled for different durations. Source: NREL

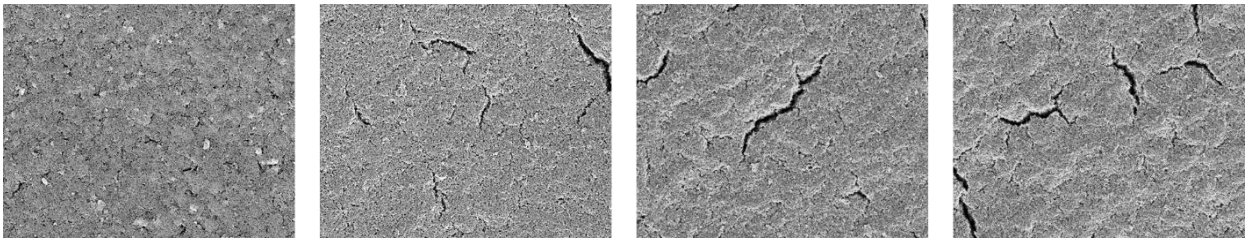

Figure 53. SEM images of coated layers using inks having from left to right 24 h, 48 h, 72 h, and 96 h ball milling time. Source: Colorado School of Mines

Electrospinning ink and process studies

The study of a full electrode (PAA + ionomer + catalyst particles) ink ES process window was conducted and additional rheology measurements to understand the individual contributions of the PAA and ionomer on the level of agglomeration and stability of the full ink were performed. Figure 54(a) shows the impact of PAA addition to the catalyst, where an initial PAA addition of 2% flocculates the particles, and further addition stabilizes the particles. Figure 54(b) shows essentially the same behavior of the ionomer-catalyst (no PAA) inks. The zeta potential measurements of the inks in Figure 55(a) confirm the stabilization of the catalyst particles with addition of either PAA or ionomer, though there is a slight decrease relative to the catalyst-only ink in the full (PAA + ionomer) ink, likely due to pH effects. The diameter measurement shown in Figure 55(b) indicates a difference in conformation and/or polymer-particle interaction between the ionomer and PAA. Interestingly, oscillatory rheology shows a transition from gel-like to liquid-like behavior in the full inks at 10% addition of PAA as illustrated by Figure 56(a) (lower than 10% PAA) and Figure 56(b) (greater than 10% PAA). This transition may impact the spinning quality of the ink. Additional extensional viscosity data for high-PAA inks were received from collaborators at University of Massachusetts, Amherst.

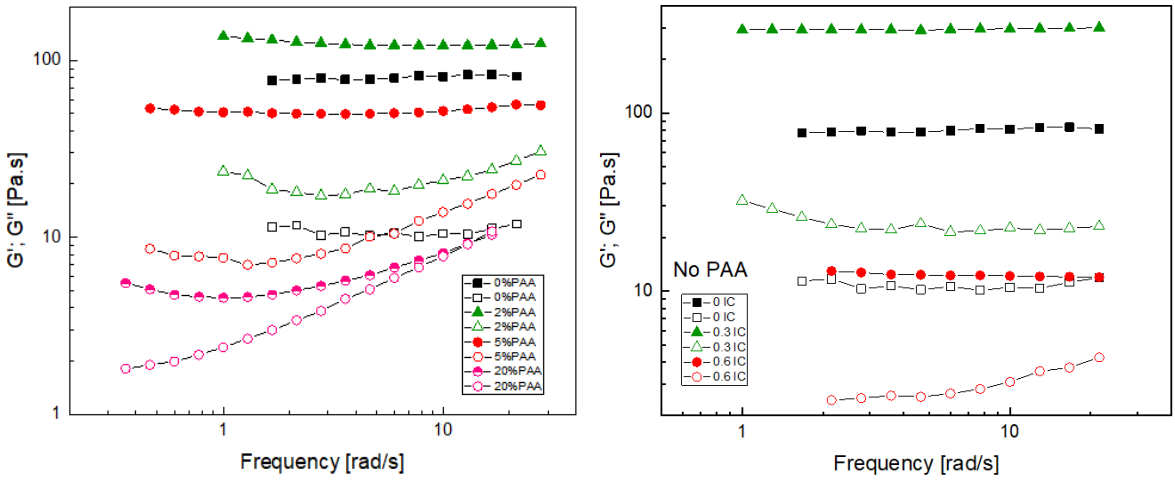

Figure 54. (a) Shear moduli for PAA-catalyst and (b) ionomer-catalyst inks. Source: NREL

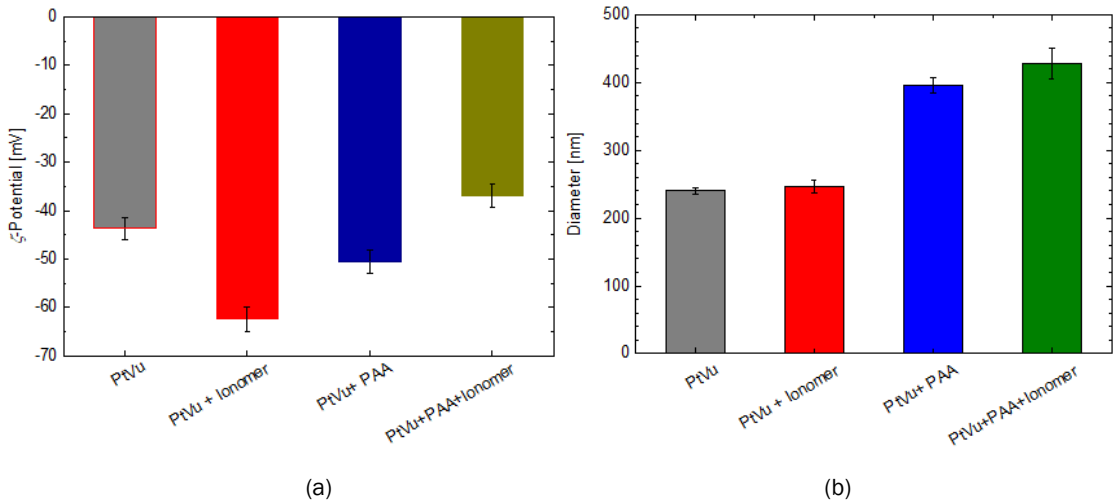

Figure 55. (a) Zeta potential and (b) dynamic light scattering results for catalyst inks. Source: NREL

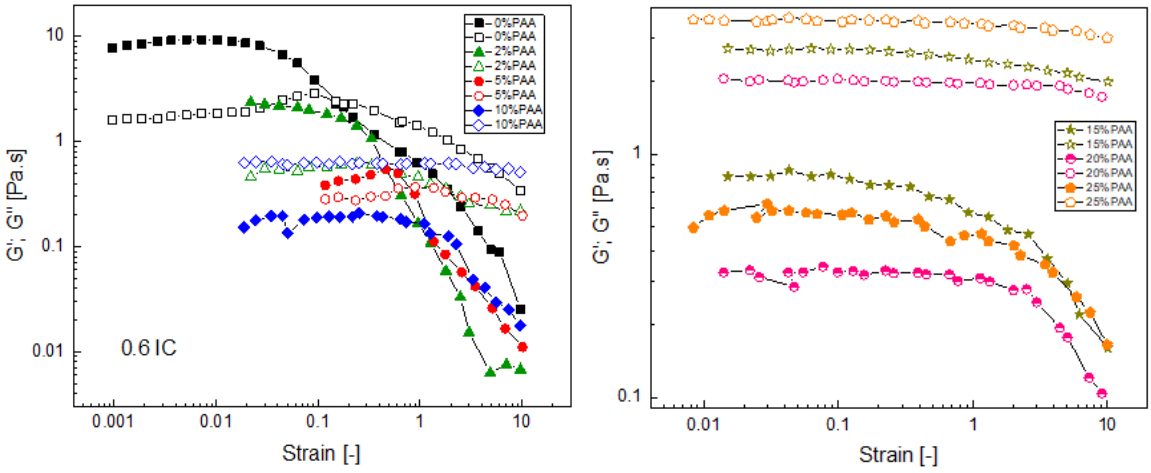

(a) (b)

Figure 56. Shear modulus data for full inks (a) lower than 10% PAA and (b) above 10% PAA. Source: NREL

To further explore the spinnability of full electrode inks, a study was performed to evaluate the effect of the ratio of water to isopropyl alcohol (IPA) in the ink at 10% and 15% PAA, which appear to be the carrier polymer contents that lead to the best fiber formation (15% PAA is what is currently standard for electrode fabrication at NREL). At both levels of PAA addition, water-rich inks tend to lead to large bead formation with fibers, IPA-rich inks tend to lead to much less bead formation with thicker fibers, and a 50:50 mixture tends to result in minimal bead formation with thinner (more desired) fibers. This behavior is shown in the SEM images of Figure 57(a-c) for the 10% PAA case. This study also showed that by going from 10% to 15% PAA addition at a 50:50 solvent ratio, the fiber diameter increases by ~2x. Fiber formation appears to become less stable resulting in broken fibers and sparking at the needle tip is observed. The transition from gel-like to liquid-like behavior of the inks at these PAA additions, which are probably not optimal for electrode formation and processing, is likely related to the observations of the fiber formation. Therefore, cells were fabricated at both 10% and 15% PAA to compare the resulting electrochemical performance of the different fiber morphologies.

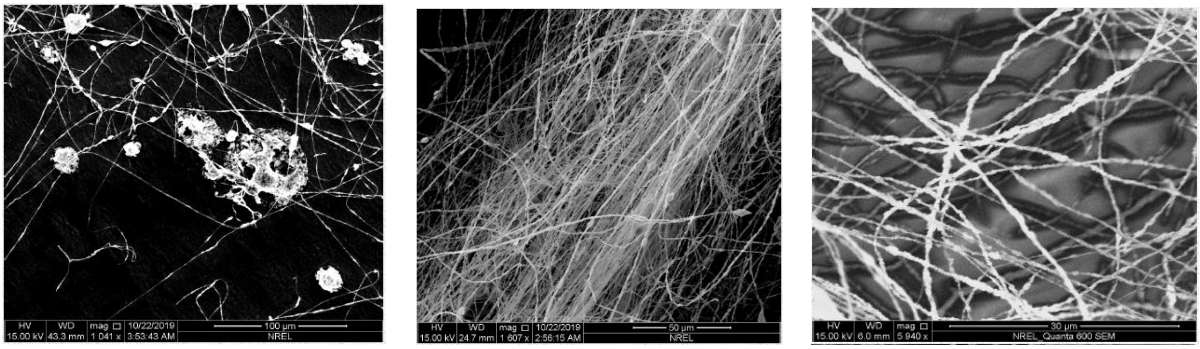

(a) (b) (c)

Figure 57. SEM of electrospun fibers for full inks at 10% PAA and (a) 75% water, (b) 75% IPA, and (c) 50:50 IPA to water. Source: NREL

Additional inks were spun for the full-ink process window study including inks from 2% to 25% PAA. As was seen in the PAA-only process window study, large changes in spinnability were observed across this range. At 2% PAA, only beads are formed – essentially this is a droplet-spraying condition. Fiber formation with

copious beads is observed at 5% PAA. At a 20% and 25% PAA addition, large fibers with large variation in fiber diameter are observed. Similar to the PAA-only ES case, Figure 58 shows a process-window depiction in terms of fiber diameter and the percent of PAA addition for the full inks. Again, a segmented process window was observed as a function of the percentage of PAA going from spraying to large beads and some fibers, to mostly fibers, and finally to very thick and unstable fibers.

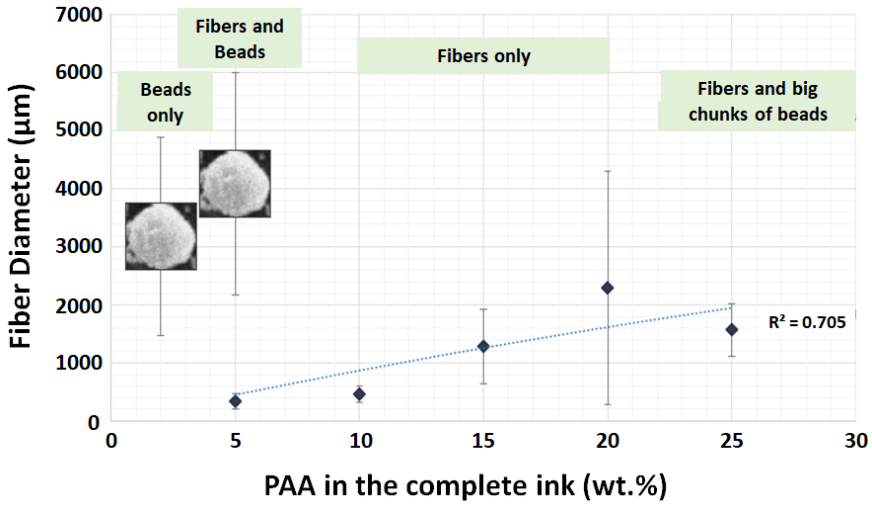

Figure 58. Comparison of the fiber diameter for the full electrode ink process window. Source: NREL

Figure 59 shows the air polarization curves for three PEMFC electrospun electrodes. The trend matches the qualitative fiber-morphology/quality results previously obtained, which showed that the fibers at 10 wt.% PAA provide better quality and incorporation of the catalyst particles into the fibers, even though 15 wt.% PAA has been the standard condition for spinning of these electrodes, both at NREL and within other research groups (e.g., the Pintauro group at Vanderbilt). This result shows the value of the process study performed at NREL where additional process parameters were explored, and improved processing conditions were identified.

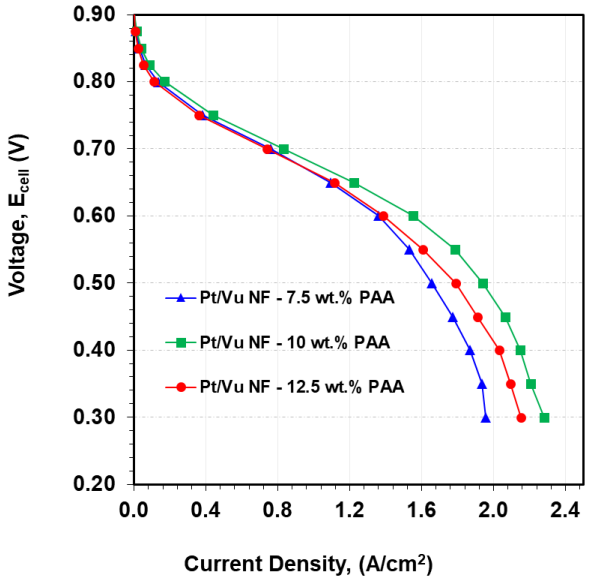

Figure 59. In-situ device testing results for ES PEM electrodes at different PAA carrier polymer concentrations. Source: NREL

In collaboration with ANL for the ES focus area, NREL provided a PAA-only ink formulation to ANL for an initial R2R spinning study. The PAA-only ink was chosen so that ANL could gain experience with the solvents and carrier polymer that NREL was using before trying a full PEM electrocatalyst ink formulation. NREL coordinated with ORNL on a general-purpose SANS experiment at the ORNL neutron source user facility. The experiment was run to understand catalyst ink agglomeration and constituent morphology related to the multi-layer coating studies at NREL and ORNL. NREL also coordinated with other collaborators at ANL on USAXS measurements of ES slurries at the Argonne APS.

Rheology experiments were performed using 3M and Ionomr Innovations, Inc. (a specialty polymer supplier) ionomers toward the goal of developing and demonstrating spinning of electrode slurries with no carrier polymer. Figure 60 shows the new rheology results in black, red and blue for the 3M 375 EW ionomer data at three different solvent mixtures and in green for the Ionomr Innovations, Inc. ionomer data. Figure 61 shows further analysis of this data, whereby the entanglement concentration, C_e, is estimated for each dispersion in Figure 61(a) and then compared for each dispersion in Figure 61(b). PAA, the carrier polymer, has the lowest entanglement concentration (ideal for spinning), but some of the ionomer-only dispersions are similar and these dispersions may be successful in spinning without a carrier. This effort had the intended outcome of eliminating the potential detriment of the carrier polymer to protonic and mass transport resistences within the microstructure of the electrode. Associated with this new study ionomer fibers were spun with no carrier polymer under different process conditions. In an initial study, a dispersion of the 3M 725 EW ionomer was spun at 50% IPA in the dispersion media and 10, 15, and 20 wt.% ionomer for driving voltages ranging from 5 kV to 20 kV. For this ink, at voltages less than 15 kV, no jet was able to be driven from the needle. At 20 kV, a driven flow was obtained but only in the form of droplets and not fibers. In a second study, the same ionomer (1 wt% 3M 725 EW in a 75:25 IPA:water dispersion medium) was spun at different humidity, flowrate and driving voltage conditions giving the results shown in Table VII. A single case was also spun at 10 wt.% but no jet was able to be formed.

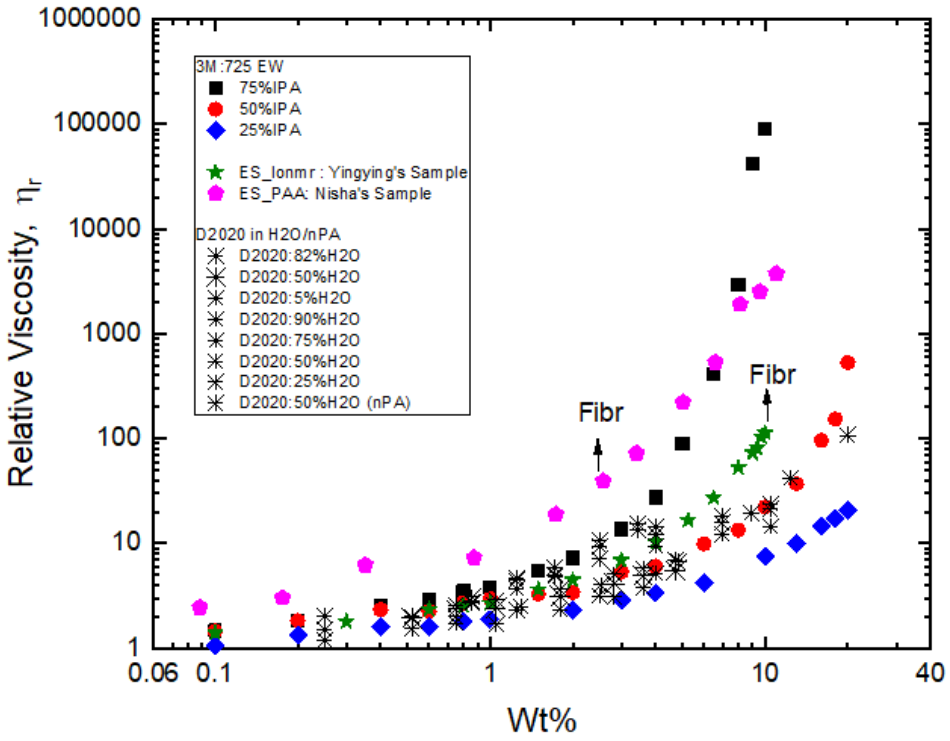

Figure 60. Relative viscosity of ionomer dispersions as a function of weight percent in the dispersion. Source: NREL

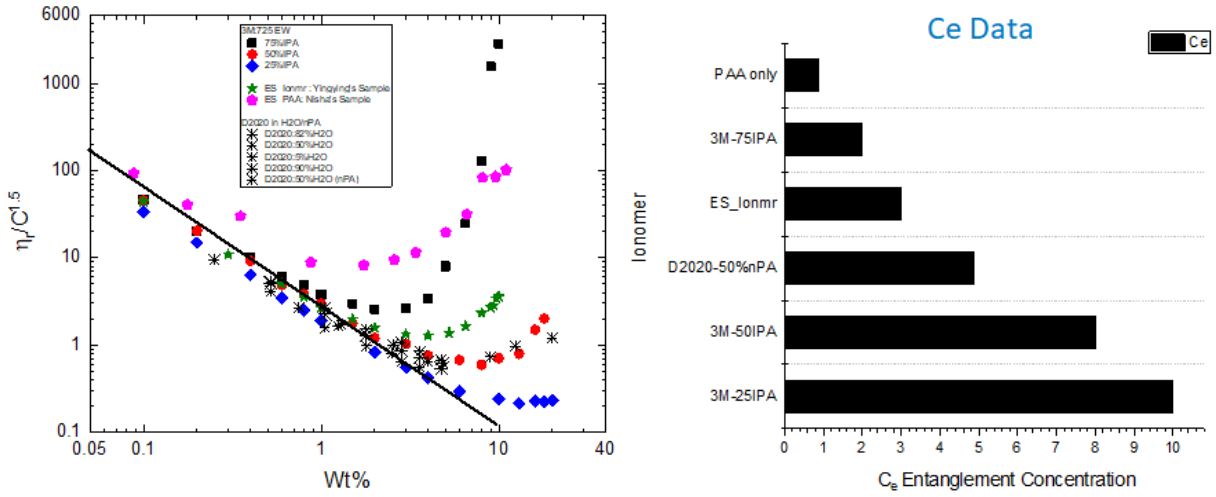

Figure 61. (a) Estimation of entanglement concentration, C_e, (approx. plateau value) for the ionomer dispersions and (b) a comparison of entanglement concentrations for each dispersion. Source; NREL

Table VII. ES Conditions for the New No-Carrier-Polymer Electrode Study

Sample #	Flow Rate (ml/h)	Distance (cm)	Voltage (kV)	Relative Humidity (%)
1	0.2	8	7.5	35
2	0.2	8	10	35
3	0.2	8	15	35
4	0.5	8	7.5	35
5	0.5	8	10	25
6	0.5	8	15	35
7	0.5	8	7.5	20
8	0.5	8	10	20
9	0.5	8	15	20
10	0.5	8	7.5	60
11	0.5	8	10	30
12	0.5	8	15	60

Fabrication and In-Situ Testing of Prototype Components and Devices

NREL fabricated MEAs and performed in-situ testing using R2R slot-die-coated GDEs from ORNL coating runs on October 21, 2019 at three different coating line speeds. XRF measurement were used to evaluate the resulting Pt loading and uniformity of the GDEs. The loadings of the three samples were all between 0.13 and

0.19 mg Pt/cm^2 which is in the typical range of target cathode loading, however, same-sample replicates showed a larger than typical variation in the loading across the surface. Variations of 20% or greater were measured, where typically NREL experiences less than 10% variation. The resulting air polarization performance of the three ORNL samples is shown in Figure 62(a). The performance varies directly with loading, which, all else being the same, would be expected. Also shown are the mass activities (MA) for the three samples. Results are similar for all three line speeds. Figure 62(b) shows the comparison to the current NREL R2R slot-die-coated GDE baseline (no ionomer overlayer) as well as the spray coated (with overlayer) baseline. The ORNL GDE with ~0.19 loading had very similar performance to the NREL R2R baseline with ~0.12 loading.

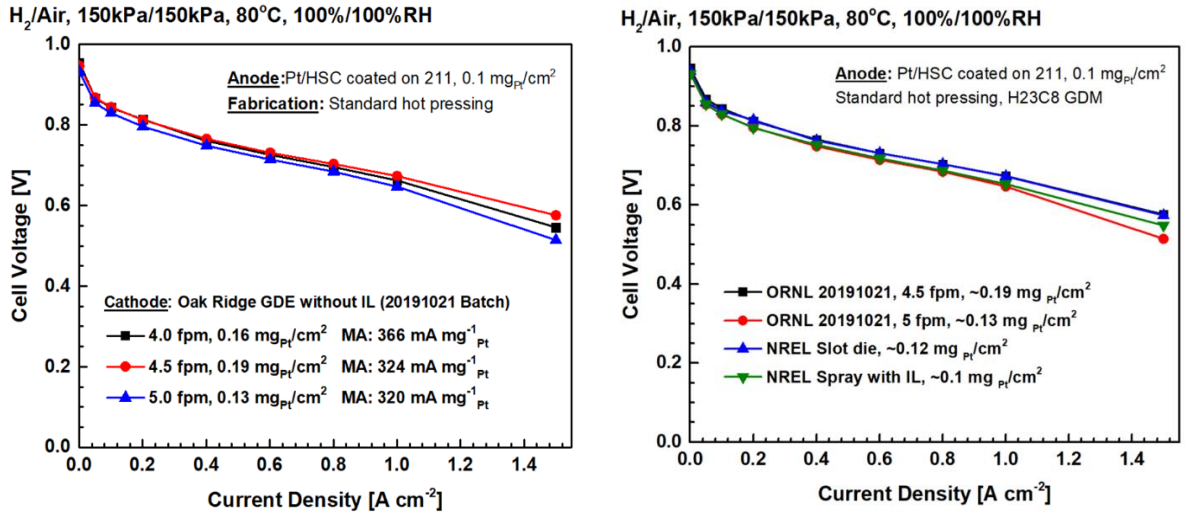

Figure 62. (a) Air polarization performance and (b) a comparison of data for ORNL R2R slot-die-coated GDEs and the NREL baseline coatings at various mass loadings. Source: NREL

XRF measurements were performed to validate catalyst loading and MEAs were fabricated to perform in-situ testing across several runs using the R2R slot-die coated GDEs from ORNL. ORNL's Run 4 was for single-layer GDEs at two different feed rates and two different line speeds. None of the Run 4 MEAs were better than those from the October 21, 2019 ORNL single-layer GDE run. Figure 63 shows the results for two cathode GDEs fabricated at the same line speed and with approximately the same catalyst loading (both MEAs were tested without a cathode ionomer overlayer). ORNL's Run 5 constituted the first R2R coating of a simultaneous dual layer electrode, in this case the catalyst layer with an ionomer overlayer. MEAs were fabricated from several of the test cases at different line speeds and different Nafion feed rates for the overlayer. Figure 64(a) shows a performance comparison between a single-layer MEA from Run 3 to three cases of the GDEs with simultaneous coated overlayer from Run 5, all at approximately the same catalyst loading. None of the overlayer GDEs performed better than the single-layer GDE, which is consistent with prior findings that, with proper ink formulation and coating conditions, the overlayer is not needed in R2R-coated GDEs. However, Figure 64(a) also shows that the two-layer GDE with the least amount (thickness) of overlayer provided the best performance of the two-layer GDEs. This is also qualitatively consistent with a prior NREL study of overlayers on sprayed electrodes, where a minimum overlayer thickness was required, but additional overlayer thickness did not further improve performance and eventually degraded the performance. Electrochemical impedance spectroscopy measurements were also performed for the Run 4 and Run 5 MEAs, and the results shown in Figure 64(b) were largely consistent with the polarization data. In both the Run 4 and Run 5 electrodes, a high level of non-uniformity in the loading as well as the visual appearance of the

electrodes was observed. As a result of these findings, ORNL performed a Run 6 to specifically explore coating uniformity, aspects of their feed pumps, and the die gap. NREL received GDE samples from this run and performed XRF measurements of loading and uniformity. Several samples appeared to have achieved target loading (~0.1 mg Pt/cm^2) and good uniformity.

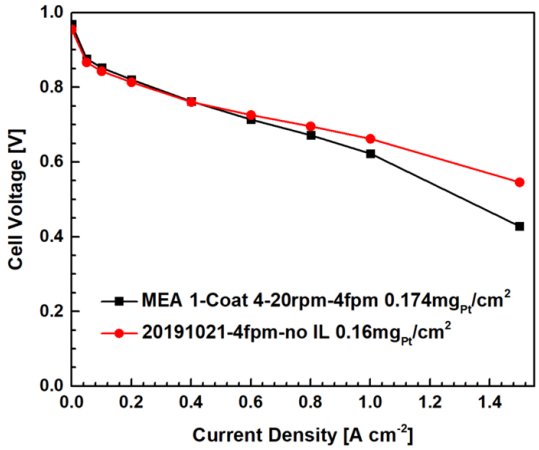

Figure 63. Air polarization curves for the ORNL R2R slot-die coated GDEs comparing Run 3 (red) and Run 4 (black). Source: NREL

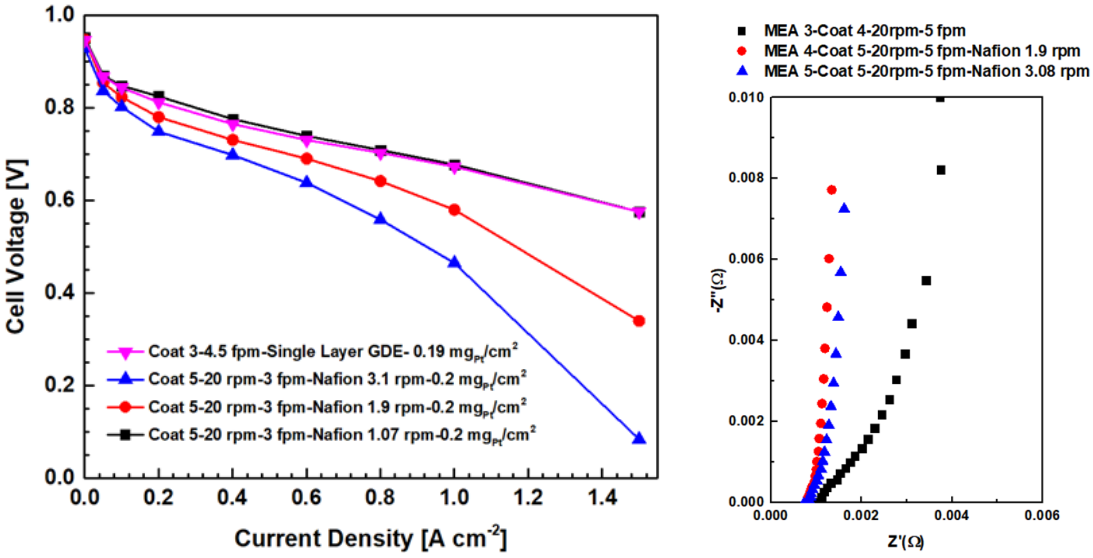

(a) (b)

Figure 64. (a) Air polarization curves comparing the ORNL R2R slot-die-coated GDEs from Run 3 and Run 5 and (b) the electrochemical impedance spectroscopy data showing consistency with the air polarization data. Source: NREL

NREL performed XRF spectroscopy to measure the Pt catalyst loading in the R2R coated GDEs from Run 6 of an ORNL coating run. Loading was measured for two samples each of 11 different single-layer GDE coating conditions. Figure 65 shows the coating parameters and the measured results. Several samples had loadings close to the target of 0.1 mg Pt/cm^2 and were selected for MEA fabrication and in-situ device testing. One of the Run 6 priority electrodes was tested and Figure 66 shows air polarization curves for Run 6 (Coat 6) compared to the NREL spray baseline with no ionomer overlayer, as shown in Figure 66(a), and the NREL baseline R2R slot-die conditions, as shown in Figure 66(b).

Coating Parameters				XRF (mg $_{Pt}$/cm^2) of 1st 50cm^2 electrode	XRF (mg $_{Pt}$/cm^2) of 2nd 50cm^2 electrode
0.0005 in shim	5 fpm	18 rpm	no vacuum	0.115	0.114
0.0005 in shim	5 fpm	17 rpm	no vacuum	0.116	0.107
0.0005 in shim	5 fpm	16 rpm	no vacuum	0.063	0.067
0.0015 in shim	3 fpm	16 rpm	4.1 in H_2O	0.164	0.174
0.0005 in shim	5 fpm	16 rpm	4.5 in H_2O	0.085	0.102
0.0005 in shim	5 fpm	17 rpm	4.5 in H_2O	0.108	0.107
0.0005 in shim	5 fpm	18 rpm	4.5 in H_2O	0.113	0.093
0.0005 in shim	4 fpm	18 rpm	4.5 in H_2O	0.09	0.093
0.0005 in shim	4 fpm	17 rpm	4.5 in H_2O	0.107	0.088
0.0005 in shim	4 fpm	16 rpm	4.5 in H_2O	0.099	0.088
0.0005 in shim	3 fpm	16 rpm	4.5 in H_2O	0.089	0.069

First Priority Second Priority

Figure 65. Catalyst loadings via XRF for the ORNL Run 6 (Coat 6) R2R-coated GDEs. Source: NREL

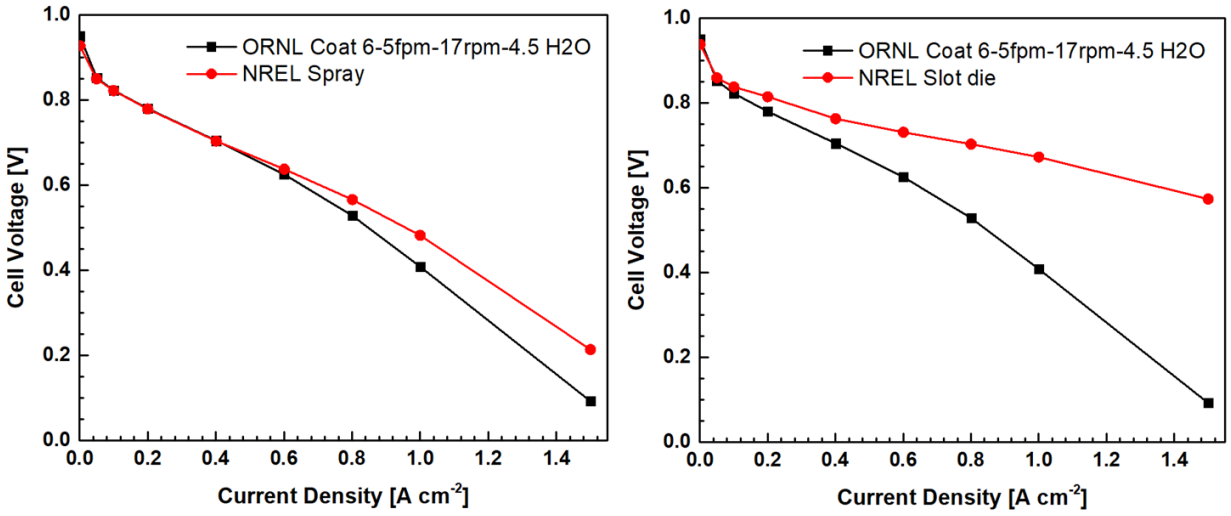

(a) (b)

Figure 66. Air polarization curves for the initial sample from ORNL Run 6 (Coat 6) R2R-coated GDEs compared to the NREL baselines for (a) spray coating and (b) slot-die coating. Source: NREL

Additional XRF spectroscopy was performed to measure the Pt catalyst loading in the R2R coated GDEs from Runs 8, 9 and 10 of an ORNL coating runs. Figure 67 shows the coating parameters and the measured results. In-situ testing could not be performed on these GDEs (during the period of performance of this report) because of test station software issues.

Sample	Pt Loading (mg Pt/cm^2)	Error Bar
2020/08/05 8 wt% IKA 18G	0.150	0.007
2020/08/05 3.5 wt% IKA 18G	0.106	0.01
2020/08/05 8 wt% IKA 25G	0.170	0.019
2020/08/05 8 wt% Netzsch	0.160	0.026

Sample	Pt Loading (mg Pt/cm^2)	Error Bar
Coat 9-50cm^2 electrode 1	0.051	0.004
Coat 9-50cm^2 electrode 2	0.100	0.030

(a)

Sample	Pt Loading (mg Pt/cm^2)	Error Bar
1 mil gap-0.7 fpm-0.69 mL/min-Vac 10-Air dried	0.176	0.021
2 mil gap-0.7 fpm-0.69 mL/min-Vac 10 in H_2O-Air dried **(coated area<50cm^2)**	0.226	0.057
2.5 mil gap-0.8 fpm-0.69 mL/min-Vac 8.5 in H_2O-Air dried	0.202	0.041
2.5 mil gap-0.6 fpm-0.69 mL/min-Vac 8.5 in H_2O-Air dried	0.209	0.019

(b)

Figure 67. Catalyst loadings via XRF for the ORNL Runs 8, 9 and 10: (a) Coat 8 and Coat 9 and (b) Coat 10 R2R-coated GDEs. Source: NREL

Novel NDE, QC, and Metrology Methods

Reverse osmosis membrane studies

NREL continued an exploratory effort to evaluate materials and methods for in-line inspection of ML structures. Commercially available reverse osmosis (RO) membranes, which are multi-layer/multi-functional membranes for water processing, were purchased for evaluation. Using these membranes, cross-sectional microscopy was performed to further understand the layer structure, thickness, and porosity to continue to inform the development of in-line metrology tools for ML structures. Figure 68 shows the ML structure of five different RO membranes. Two layers can be clearly seen: (1) a porous backing layer on the left of each image and (2) the non-porous functional layer on the right. There is a third layer in these constructions, on the surface of the non-porous layer, that cannot be seen at this level of magnification.

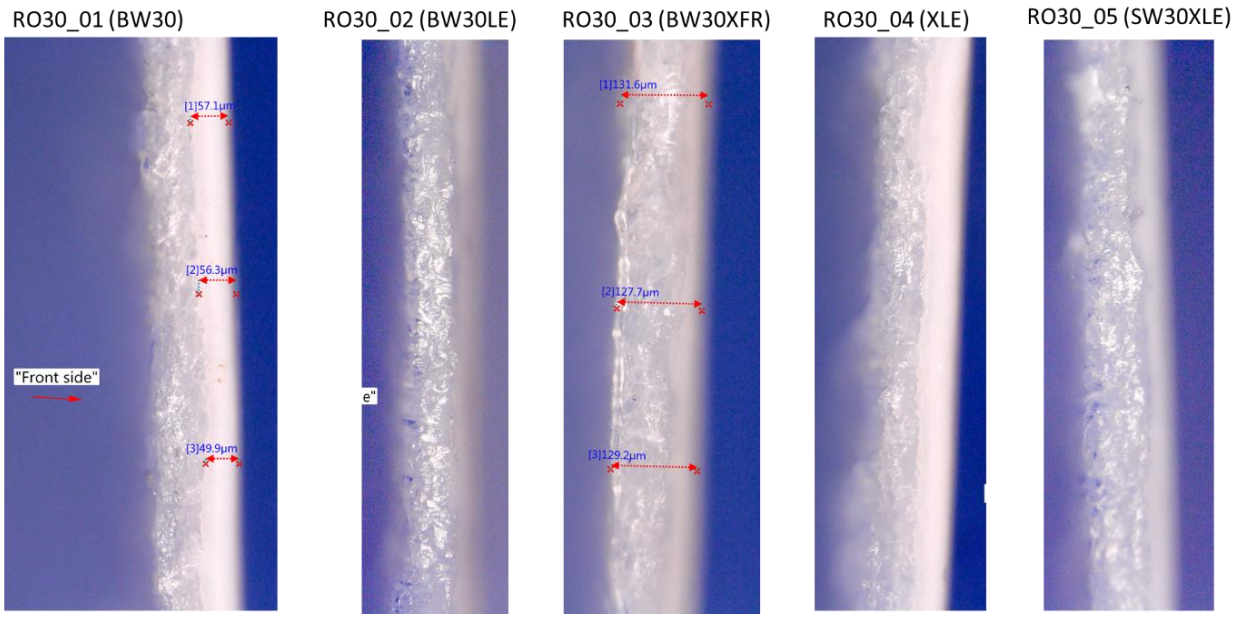

Figure 68. Cross-sectional optical microscopy (300X) of RO membranes. Source: NREL

Additional background information was developed on the materials, structure, and fabrication of RO membranes from a combination of literature, industry documents, and interviews with collaborators at the University of Colorado. Figure 69(a) shows the general structure of these membranes which includes a non-woven polyester support layer shown in Figure 69(b), a dense polysulfone layer shown in Figure 69(c), and a very thin polyamide active layer. The properties of each of these layers can be modulated to provide the target functionality. With this improved background on material structure, reflectance and transmission spectroscopy in the UV-visible wavelength range was performed using a fast spectrometer. Transmission spectroscopy of five different membranes is shown in Figure 70. The overall level of transmission as well as specific peaks around 520 nm and 580 nm appeared to be a function of the membrane properties. Unfortunately, the differences between the different membrane samples are not understood in enough detail to elucidate what property of the membranes this measurement is sensitive to.

(a) (b) (c)

Figure 69. (a) General structure of RO membranes, (b) top-down microscopy of the non-woven polyester layer, and (c) cross-section microscopy showing the polyester layer on the left and the dense polysulfone layer on the right. The polyamide active layer is too thin to be observable by optical microscopy. Source: NREL

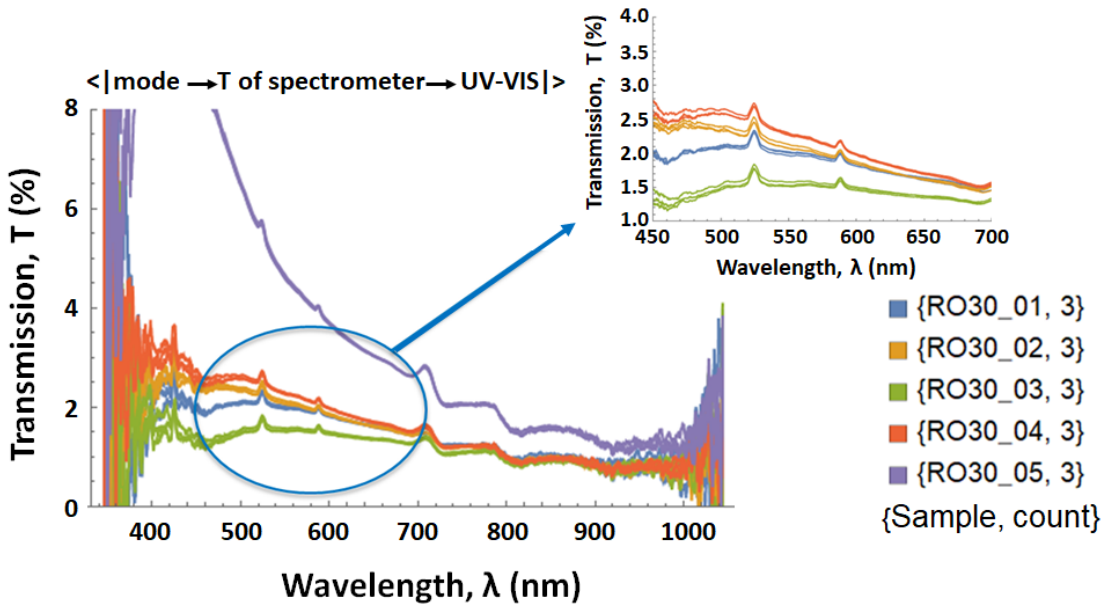

Figure 70. Fast optical transmission spectroscopy of five RO membranes. Source: NREL

IR spectroscopy was performed at higher wavelengths in the IR spectral range of several RO materials of interest. As shown in Figure 71, transmission spectra were obtained across a broad wavelength range that were sensitive to the membrane structure. However, as noted above, the differences in chemistry or structure of this series of membranes is not understood enough to be able to relate the differences in spectral response to specific aspects of the membrane. This work forms a strong basis for future work on RO membranes, for example within the new National Alliance for Water Innovation that supports the DOE Energy-Water Desalination Hub.

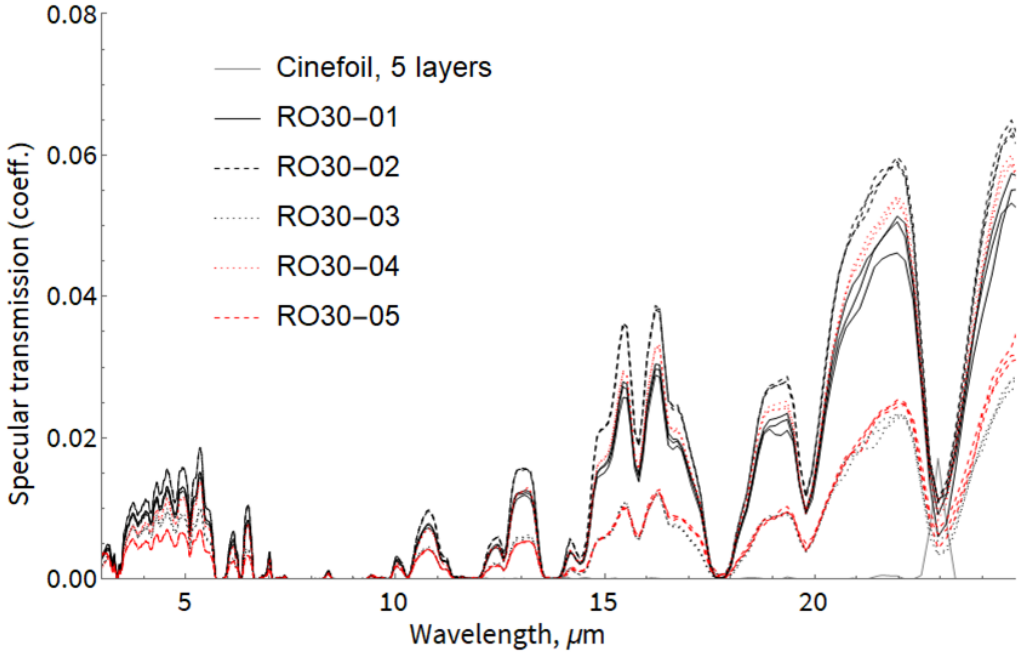

Figure 71. IR transmission spectra of RO membranes. Source: NREL

Spectroscopic methods for NDE of dissimilar layers of multi-layer structures

A literature review of the capacity for penetration of electromagnetic energy into various relevant materials across a range of wavelength from far UV (10^{-7} m) to terahertz (10^{-4} m) was performed. The objective was to begin to understand spectroscopic opportunities to penetrate dissimilar layers of ML structures for metrology. Figure 72 shows a depiction of the initial findings for a variety of specific and representative materials of interest to energy applications. The optical penetration of perfluoro sulfonic acid (PFSA) polymers are much greater than most of the other materials, and interestingly, carbon blacks, which are used in many electrochemical applications, have a wide range of penetration. This information was used as a basis for further development of ML metrology methods and spectroscopy measurements, using a benchtop Cary spectrophotometer, were performed on several film materials of interest for target ML structures.

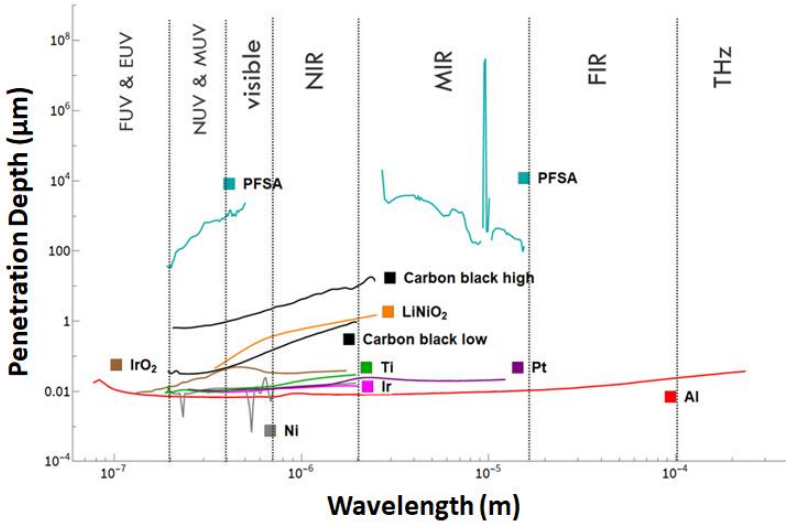

Figure 72. Penetration properties of various materials of interest for ML energy materials. Source: NREL

Two different porous carbon fiber materials were measured, and Figure 73 shows the mid- to far-IR spectra of one of the substrates at two orientations and in three transmission measurement modes. In all cases, significant transmittance was observed which confirmed the possibility of measurement of adjacent sub-surface layers such as a heterogeneous catalyst layer.

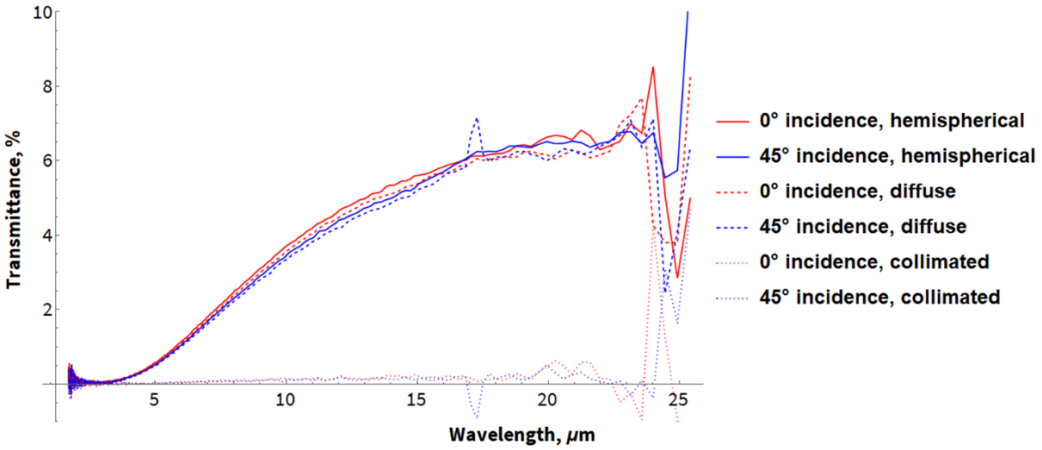

Figure 73. Mid- to far-IR transmission spectra of a porous carbon fiber substrate. Source: NREL

In a second study of coated (three-layer) and uncoated (two-layer) carbon fiber substrates (e.g., GDM), very little differentiation was observed in the resulting IR transmission spectra, and in fact, obtained the curious result that the coated substrates showed higher IR transmission than the uncoated substrates, as shown in Figure 74.

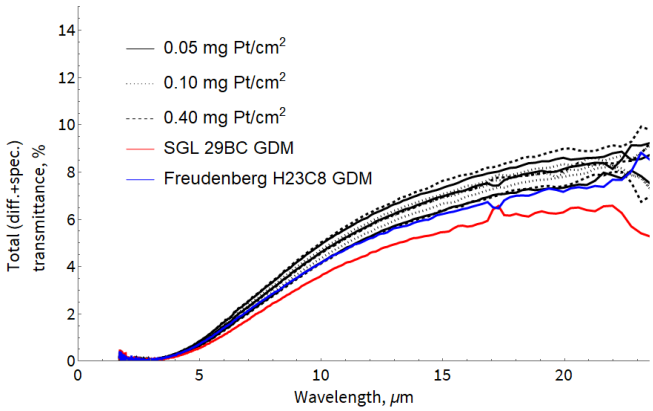

Figure 74. IR transmission spectra of coated and uncoated carbon-fiber substrates. NREL

NREL researchers collaborated with researchers at the Colorado School of Mines to perform ATR-FTIR measurements during the drying of both polymer-only and full catalyst inks. One observation was that the height of the characteristic peak in the spectra did not seem to vary linearly with the known ionomer content, which produced concerns regarding the repeatability of the method. One approach to improve the repeatability was to explore improved methodologies for depositing the inks onto the ATR-FTIR crystal in a way that minimizes Marangoni effects ("coffee ring") and non-uniform drying. Various methods of deposition and various gasketing concepts were explored. The Colorado School of Mines Physics Department faculty provided some insight regarding the unexpected fluorescence response obtained from the ionomer fluorescence spectroscopy measurements.

Efforts continued to improve the ATR-FTIR measurement methodology because of previously observed poor sample formation resulting in no linear relationship between polymer content and the signal. With improved methods, an IR signal was obtained that was proportional to polymer loading as seen in Figure 75. These results indicated potential pathways for polymer-content measurements for both ink and dried active layer quality inspection.

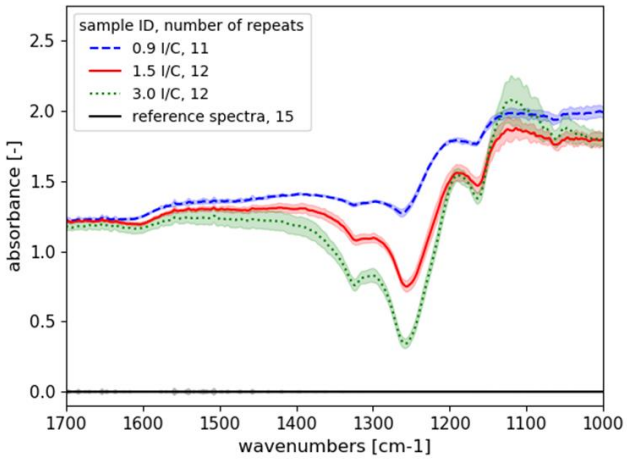

Figure 75. ATR-FTIR spectra of dried heterogeneous inks as a function of polymer content. Source: NREL

Further improvements/understanding of the ATR-FTIR measurement methodology were pursued by exploring scattering and index-of-refraction-matching (the Christiansen effect) spectroscopic behaviors that may be affecting measurements. For example, Figure 76 shows that the indices of refraction for Nafion overlap near the previously measured absorption troughs indicating that the Christiansen effect may be prevalent and thus impact the correlation of the measurement response to the ionomer content in these electrodes. In this case, we see a synergetic behavior, where the Christiansen effect seems to be enhancing the differentiation of the signal relative to ionomer content.

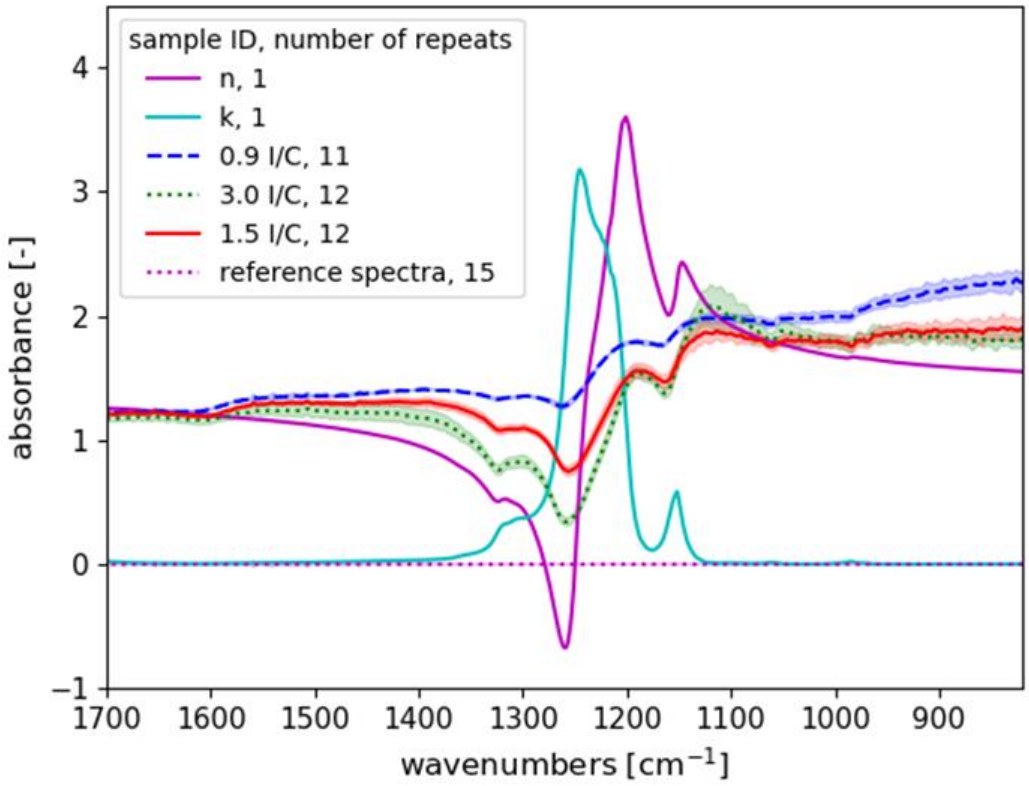

Figure 76. ATR-FTIR spectra of dried heterogeneous inks as a function of polymer content with Nafion indices of refraction overlaid. Source: NREL

Education, information dissemination, publications, and technology transfer

NREL partially supported five post-doctoral researchers and three graduate student researchers in FY 2020. Presentations on the ES process window study and ES rheology work were given at the American Institute of Chemical Engineers and the Materials Research Society meetings in November and December 2019 respectively. NREL researchers (along with SNL and ORNL) participated in the 20th International Symposium on Coating Science and Technology. This is the pre-eminent event in the U.S. for process science related to R2R processing. Several presentations and posters were given by R2R Collaboration members including four from NREL. NREL also co-sponsored the event and hosted a virtual booth for the R2R Collaboration at the symposium. A brochure about the R2R Collaboration was posted on the booth for browsing and download by symposium attendees. NREL coordinated across teams at NREL, as well as with external collaborators, on three papers related to the ES research: (1) ES PEM electrode inks from a process window perspective, (2) ES PEM electrode inks and electrospun electrodes from a device morphology and testing perspective, and (3) a broader process study of the PAA carrier polymer and ionomer inks alone as a baseline.

Macroscopic Mathematical Model of the Drying of a Single Layer Generic Slurry Containing Monodispersed Colloidal Particles, Binder and Solvent (LBNL Lead Laboratory)

Slurry Drying Model

Dispersion mixing

LBNL is conducting research and developing models at the component level for the mixing and drying processes to predict coating manufacturing outcomes. Specifically, methods were developed for producing drying models that incorporate the corresponding component-level experimental results at each step of drying and solidification. This requires detailed observations of the dispersions of interest and fabricating a custom miniature coating drying setup to make observations under simulated industrial conditions. From experience, it is known that the initial conditions for the coating process, i.e., the state of prepared dispersion, effect the final coating properties. This suggests that the internal structure of coating is important. Currently, the initial conditions and internal structure in general are not well-understood for concentrated dispersions. There needs to be a clearer picture of the process before producing a drying model that will accurately interpret the experimental results.

There are many questions to be addressed. One question is how do the components associate? This should influence the evolution during drying as shown schematically in Figure 77 where particles, particles and solvents interact through multiple component dynamics and component deposition processes to form the coating substrate. In concentrated dispersions of interest, some of the traditional concepts and language may be misleading. Two particles can be similar in size but may behave differently in the drying process. Does the polymer move around separately or is it mixed in with the carbon black? Are the particles uniformly coated and, if so, does the polymer float in the suspension or is it all absorbed? The LBNL experiments are focused on the dispersion structure dynamics and computer automated control. The first experiment is to study the effects of mixing.

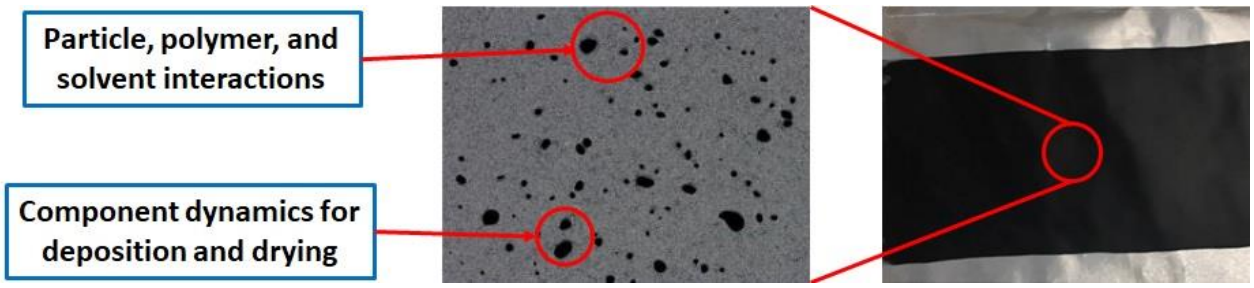

Figure 77. Modeling approach for multilayer coating drying. Sources: LBNL and ORNL

LBNL built an experimental setup for mixing to help address these questions. The preliminary setup is shown in Figure 78. Computer-automated control of dispersion preparation is a major goal; every sample or experiment is designed as a computer program. A portable mixing station was designed and fabricated to support reproducible sample production for instruments in different locations to investigate component interactions in dilute dispersions. The mixing station is connected to a high-speed particle size analyzer and is intended for use with additional instruments, such as a FTIR spectrometer. The current mixing experimental setup also includes a custom sample holder and temperature bath, a computer-controlled lab jack, a computer-controlled chiller, a computer-controlled disperser (Customized IKA T25 Easy Clean Control with a wide

range of rotational speeds), a computer-controlled peristaltic pump for dilute systems, a Malvern Mastersizer 3000 flow-through particle size analyzer with up to 5 Hz sampling rate for dilute systems, wetted materials (tubing, fittings, couplings) selected for compatibility with water/alcohol/N-methyl-2-pyrrolidone to support testing of dilute inks and battery slurries, a computer and control electronics, and a custom control software package.

Figure 78. Preliminary experimental setup for mixing experiments. Source: LBNL

The sample holders are constructed of clear material that allows direct observation of the dispersions during mixing. The beaker size is standardized and is isolated from the coolant to reduce risk of contamination and to streamline workflow. The objective is to have consistent positioning, so all devices are fixed. The lab jack base shown in Figure 79 is fixed relative to homogenizer, the bath is mounted to the lab jack, the beaker is mounted on the sample holder, and the inlet and outlet tubes are rigidly fixed to the apparatus. A beaker cover is used to limit evaporation, prevent premature drying, and protects researchers from solvent vapors. The cover also allows rapid, consistent addition of dispersion components during the mixing process without interrupting the automated operation.

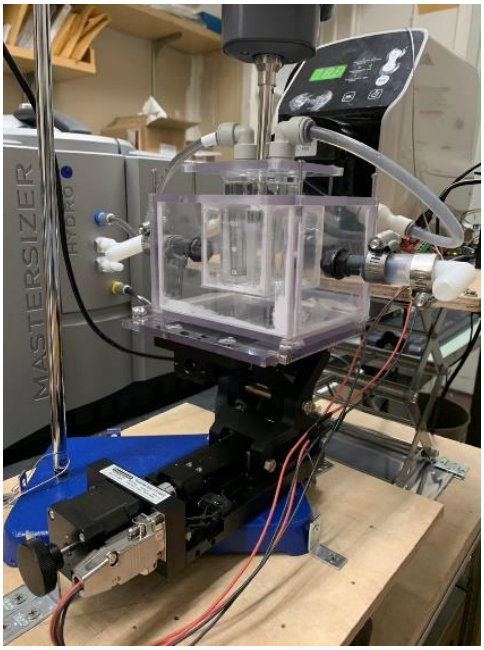

Figure 79. The lab jack base for positioning of the samples. Source: LBNL

The mixing equipment is vibration isolated from sensitive instruments. Again, there is consistent positioning of the mixing equipment components relative to each other using positioning brackets, and relative to different instruments using height adjustments. Effective positioning keeps tubing lengths, height changes, and flow velocities consistent and allows the entire mixing setup to be moved to different analytical instruments for consistent dispersion sample production.

Some preliminary experiments were performed using carbon black dispersed in mixtures of water and alcohol to gain intuition about the experimental system and the broad trends associated with the system. Figure 80 shows results from two experiments with varying percentages of IPA that suggest the solvent composition can have an enormous influence on the size distribution and in shear stress that appears to have opposite effects in the two cases. Results for these mixing experiments showed that with a 10 vol% IPA solution mixed at 4000, 6000, and 8000 rpm gave particle sizes ranging from 150 µm to 200 µm, however for a 70 vol% of alcohol, the particle size was 0.02 µm.

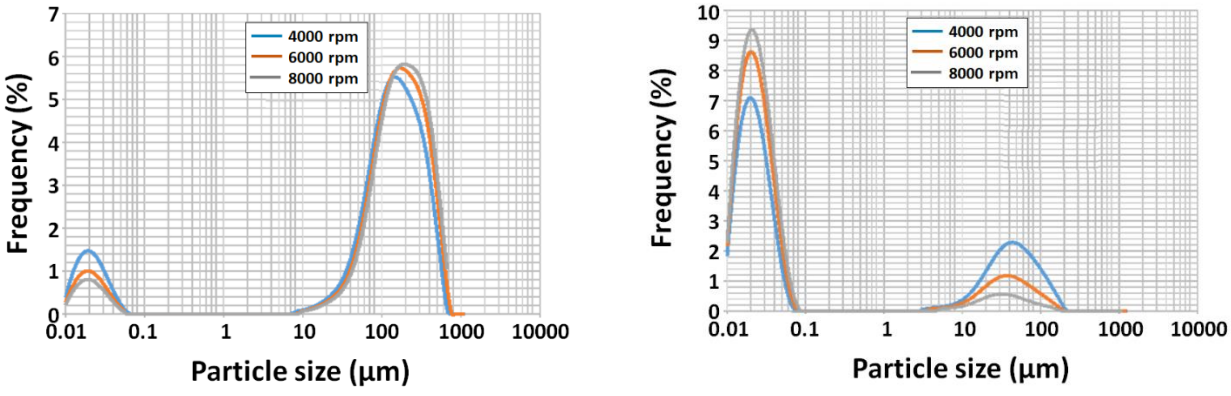

(a) (b)

Figure 80. (a) Carbon black nanoparticles (0.2 wt.%) in IPA/water (10 vol.% IPA) and (b) carbon black nanoparticles (0.2 wt.%) in IPA/water (70 vol.% IPA). Source: LBNL

To improve compatibility with the dispersion preparation techniques used by the other R2R Collaboration laboratories, the chiller was upgraded with a serial communication port and an additional code was added to the equipment control library to control and query the chiller. To aid in loading samples consistently and keeping them at a controlled temperature, custom temperature bath sample holders were designed that are compatible with the motorized sample stages. A portable custom cart with an adjustable platform was also designed to isolate the motorized components of the mixing experimental setup (mixer, stage, pump, and chiller) from vibration-sensitive instruments (particle size analyzer and confocal microscope) and to position the mixer and pump in a consistently reproducible position relative to different instruments.

The computer-controlled mixing setup was transformed into a portable mixing station to reliably recreate samples in the vicinities of instruments in different locations. This station includes the custom temperature bath along with a heat exchanger and coolant pump that allow the powerful chiller to be used to maintain an open bath.

Finally, LBNL released an update to their highly-flexible open-source simulation package that will be used to implement future models. A paper describing this software was submitted to the Journal of Open Source Software and the actual software is available for download from https://bitbucket.org/berkeleylab/esdr-pygdh.

Coating and drying

LBNL designed a coating and drying observation table to simulate the fabrication conditions used by the other R2R Collaboration laboratories but at a scale that is small enough to be easily combined with analytical tools such as Advanced Light Source beamlines. After many design iterations, the LBNL-supplied SolidWorks software was used to produce an initial design of the observation table shown in Figure 81. This design will be subject to modifications as new ideas and challenges arise during the fabrication process. Early experiments with the table in beamline hutches (as opposed to observation in a laboratory using visible light imaging) was planned for battery materials research because of the typical particle composition found in these materials.

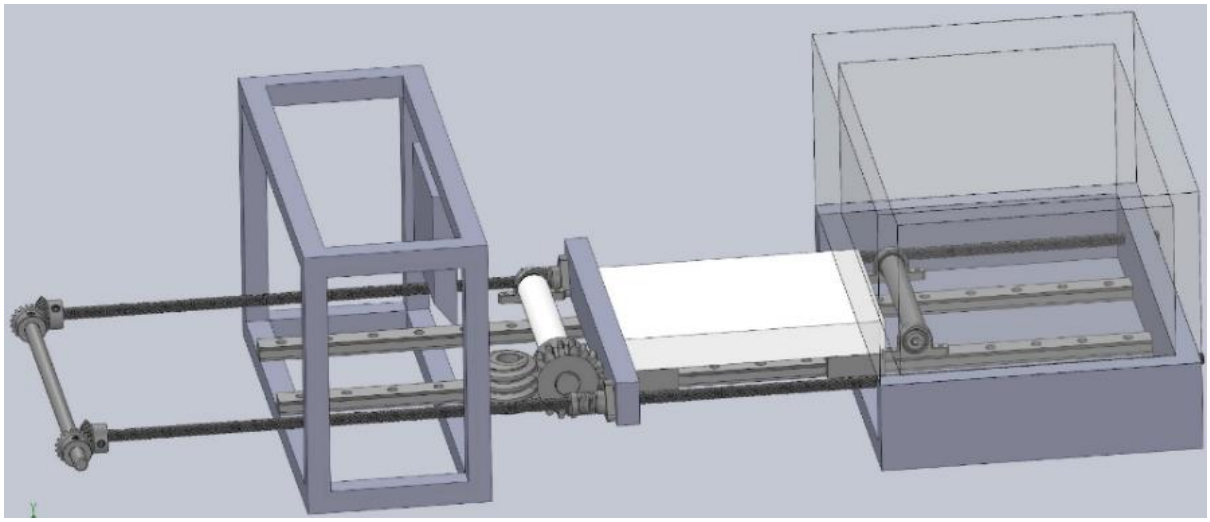

Figure 81. Schematic of the coating drying observation table initial design. Source: LBNL

LBNL began drying table design modifications to insure confocal microscope compatibility. Optical microscopes and radiography beamlines have very different physical configurations and sample mounting requirements, so the design was modified to be compatible with both. A modular design was selected to allow the sample to automatically move between the different locations for coating, observation, and drying. To prepare for the drying experiments, reviews of papers on dispersion drying models were performed by the

LBNL postdocs and graduate student during the stay-in-place order in California which limited laboratory access. Over 100 papers of dispersion drying models were surveyed which described techniques ranging from Monte Carlo and molecular dynamics approaches to continuum scale. The intent of the review was to look for trends and connections among different approaches and to summarize the knowledge base for the research community to serve as evaluation of possible approaches for planned modeling efforts.

Validated Continuum-Scale Models to Accelerate Design and Scale-up of Simultaneous Die Coating Process Technology (SNL Lead Laboratory)

Model Development and Validation for Multilayer R2R Applications

SNL joined the R2R collaboration in Phase 2 at an annual funding rate at one-half of the other partners. SNL's primary role was to advance modeling and simulation tools and commensurate validated models to accelerate design and scale-up of drying and coating technologies. SNL partnered with the UNM to assist in developing these tools. These tools that are based on the finite element method and the open-source software Goma 6.0 (www.gomafem.com) are constructed in a way that makes them agnostic to the coating system and product (single layer or multilayer) but can be easily adapted to specific applications (e.g., multilayer fuel cell or battery films) through thermophysical property inputs that characterize the coating formulations and inks.

The basic programming tool for the SNL model development is GOMA 6.0 which is being updated as GOMA 7.0. Basic features of GOMA 6.0 are presented in Figure 82. The tool was designed for manufacturing process modeling with a core element of capillary hydrodynamics which is underpins the physics of deposition modeling. The models are used to solve differential equations for capillary hydrodynamics which have a Navier-Stokes equation foundation.

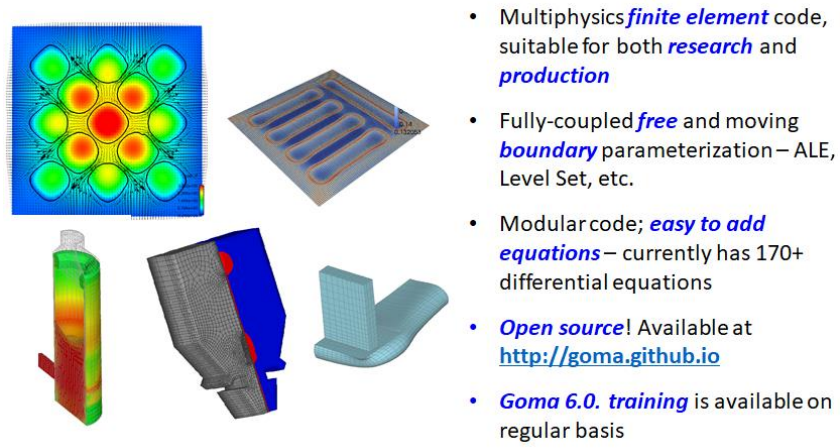

Figure 82. Basic features of GOMA 6.0. Source: SNL

Multilayer slot-die coating model

SNL and UNM completed the deposition models of single- and two-layer slot-die coating flow, together with a working user interface to improve usability by the partners and industry and achieved qualitative validation of the single-layer model against coating trial observations at ORNL. An example of the two-layer slot-die coating flow and the conditions occurring in the flow regime are illustrated in Figure 83. ORNL provided SNL with rheological data for a representative single- and two-layer-slot coating stack, and the data were fit with standard constitutive equations and implemented in the models.

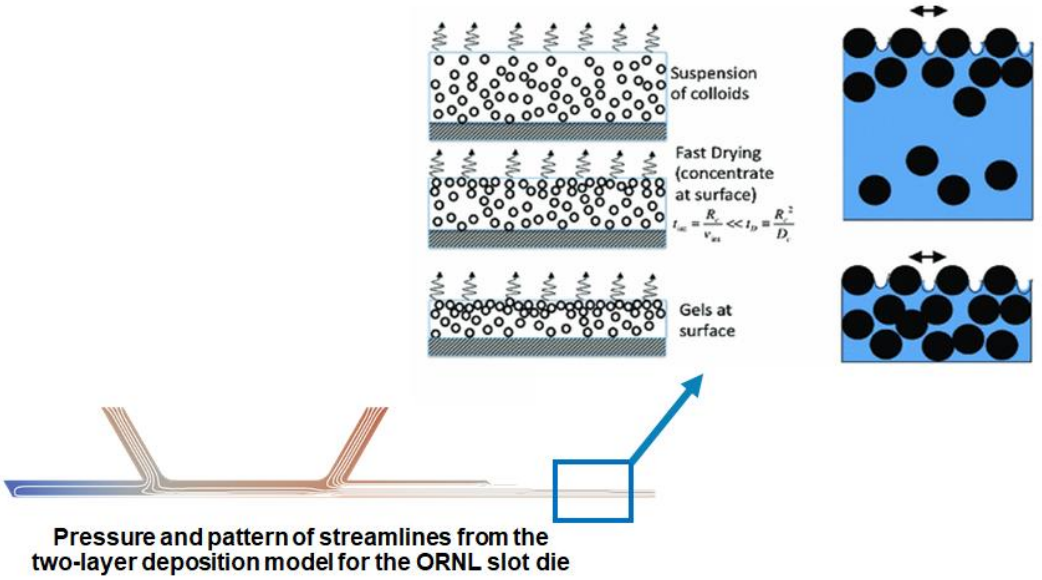

Figure 83. Pattern and flow model for a two-layer slot-die simulation. Source: SNL

For the multilayer slot-die coating model, SNL investigated the coated side and the uncoated side of GDLs to better understand the types of defects. Mapping was performed on the shear rate and coating bead for a dual layer slot-die flow with a 30-µm wet thickness for an 8 wt% platinum-carbon ink and a 20-µm overcoat of Nafion. Shear rates range from 2000/s to 0.2/s. Nafion is fairly Newtonian above 1 cm/sec or 0.1 Pa·s. The predicted coating operability window (vacuum vs coating speed) for the single-layer high-vacuum case and a 90-µm gap and 30-µm wet coating thickness showed a stable coating which was achieved in coating trials. In those coating trials at ORNL, the vacuum was reduced to zero and streaking occurred. The exact location of the boundary is unknown, but a qualitative validation of the model was accomplished. Figure 84 illustrates the results of the process models for the single-layer slot-die flow using a 90-µm gap and a 60-µm gap relative to a typical operability window. These efforts guided the experiments aimed at increasing the coating gap (slot-to-web) for better coating quality and informing coating configuration changes for high-solids loading catalyst inks.

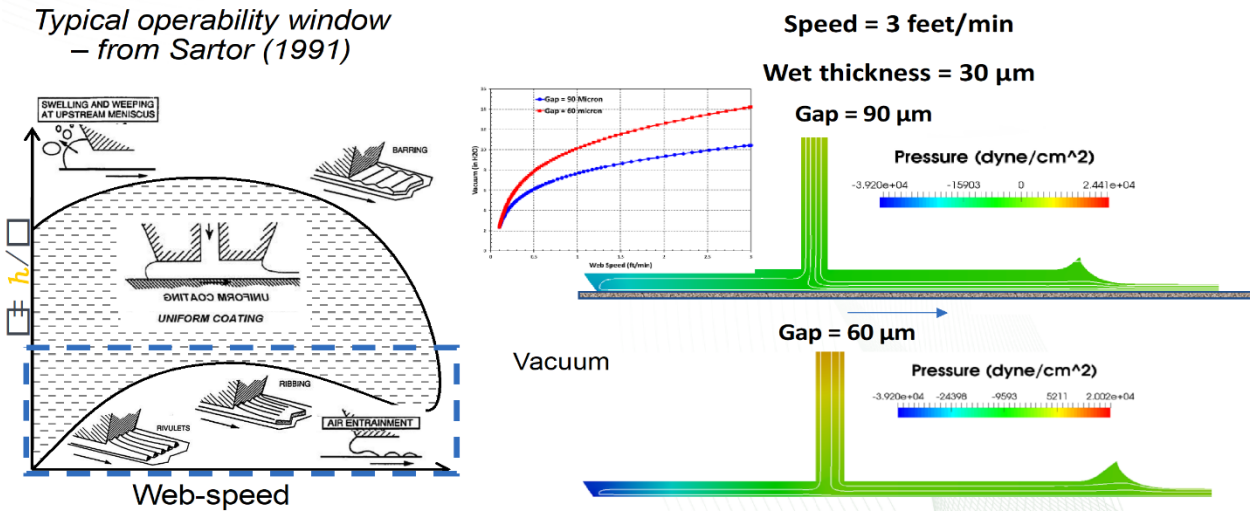

Figure 84. Process models of the single-layer slot-die flow that were used to inform coating configuration changes for high-solids loading catalyst inks at ORNL. Source: SNL

Analytical visco-capillary data from a model at Saint Gobain was complementary to the ORNL data for the single-layer case. For the two-layer case, SNL models have predicted the pattern of streamlines and viscosity throughout the bead. Compared to the single-layer case, a much higher vacuum bead was expected for a stable bead because of the longer region of lubrication. In the single-layer case, there is only two die lips and for two layers there are three die lips and a long run of flow in a confined gap. When coatings were processed using 60-µm and 90-µm die gaps at the high-vacuum limit, significant changes occur in the coating window as shown in Figure 85. The low-vacuum limit disappears so vacuum is not needed for a stable coating at a 60-µm gap, but vacuum is needed at the 90-µm die gap. Also, the time decreases for the vacuum needed to stabilize the coating at higher web speeds because of shear thinning. At much lower viscosity for the higher shear rates, the coating gap can be drastically closed to thin the liquid layer. SNL continued to work on a graphic user interface for the slot-die model to allow a wider range of users to operate the models. GOMA is a very specific tool that commercial software sources do not have because models for coating flows are not large enough market. SNL/UNM extended all the models to include the rheological behavior of fuel-cell inks, both active catalyst layer and ionomer layers given the data taken by ORNL and the constitutive equation fits.

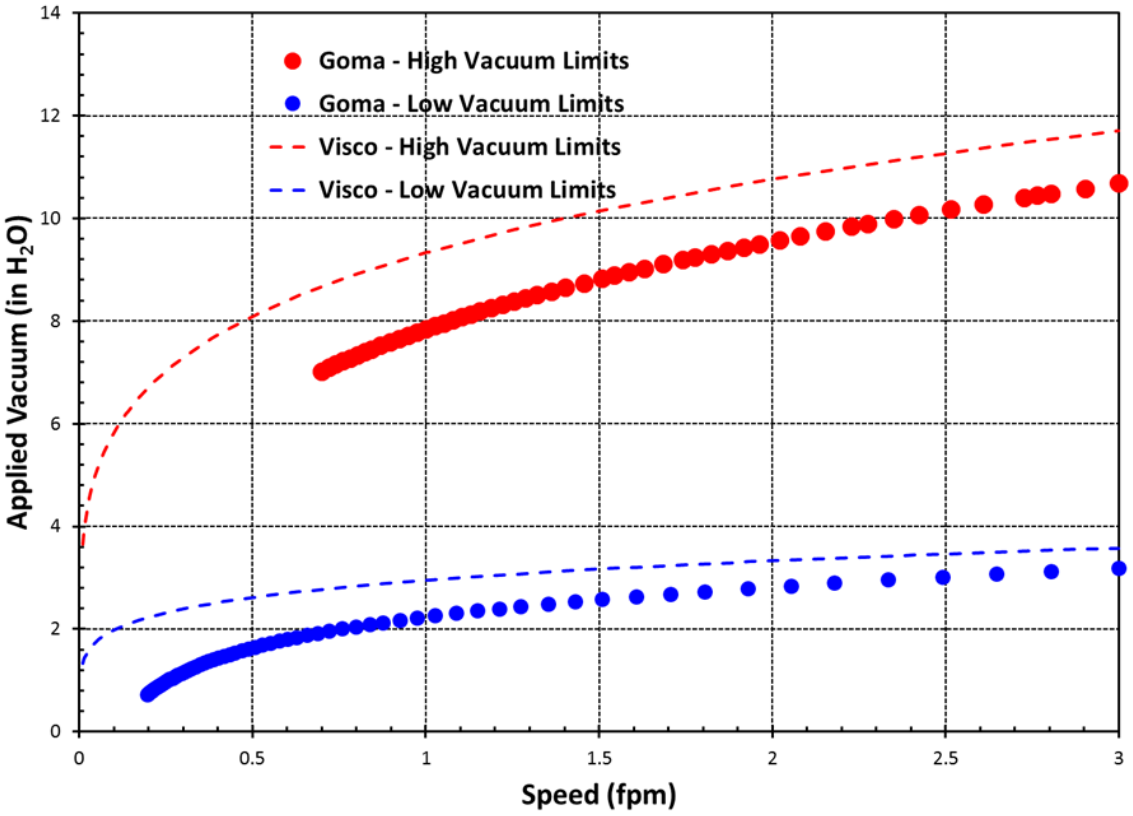

Figure 85. Effect of applied vacuum on the coating window predictions. Source: SNL

Slide die coating model

For the multilayer slide coating model, the liquids flow out of the feed slots and down the die face and then to a bridge that is moving by rapidly. The starting geometry was the NREL slide die made by Allied Die as shown schematically in Figure 86(a). A finite element mesh is generated for a two-layer coating using the Galerkin finite element method as shown in Figure 86(b). Typically, operating conditions for slide die modeling are a line speed of 1 to 10 m/min and a wet thickness of 100 to 200 µm.

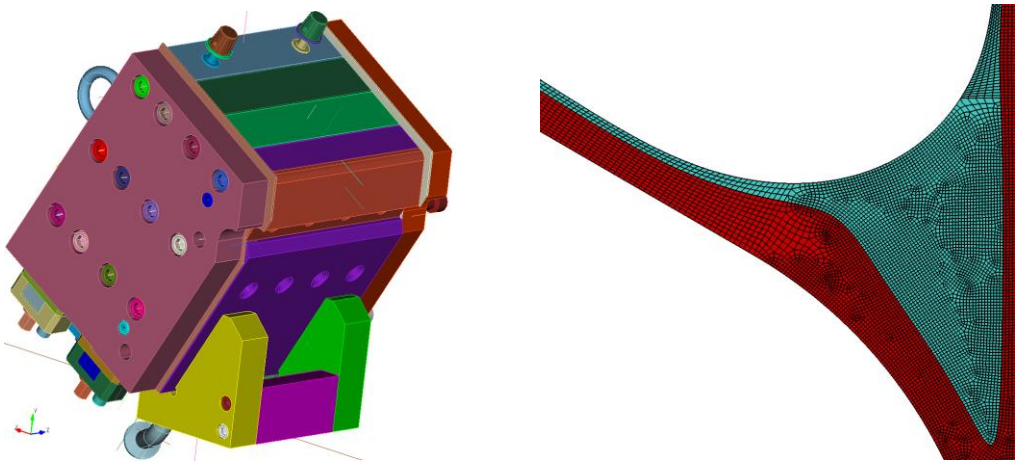

(a) (b)

Figure 86. (a) Geometry of the NREL slide die and (b) the finite element mesh for a two-layer slide die coating. Source: SNL

Fuel cell inks provided by NREL were modeled as the exemplar material because they have a wide range of rheology which provides options to achieve the largest operability window and are also shear thinning. The polymers at low dilutions exhibit a Newtonian behavior. The viscosity can be four orders of magnitude over a range of four orders or more of shear rates as shown in Figure 87(a) for Pt/Vulcan and Figure 87(b) for Pt/HSC. SNL continued modeling of the rheology with a viscosity that depends on shear rate with a power law functional form. A Carreau fit was used to provide upper and lower bounds of viscosity values. Viscoelastic and yield stress effects are not being considered at this point, which can be important at concentrated high solids loadings for the inks.

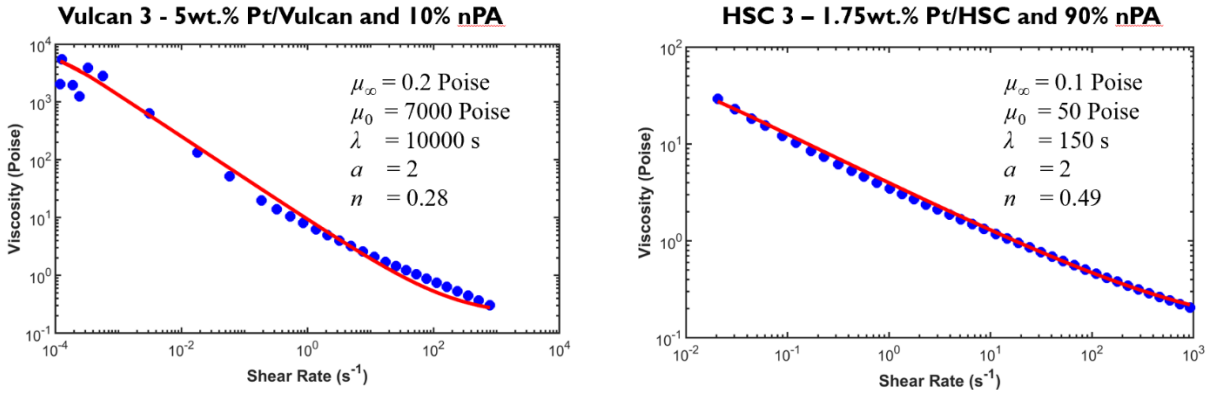

(a) (b)

Figure 87. (a) Rheology of a 5 wt.% of Pt/Vulcan and 10% n-propanol and (b) rheology of a 1.75 wt.% Pt/HSC and 90% n-propanol. Source: NREL

SNL models predicted the coating bead and transfers to the web for a single-layer case using a Nafion polymer with a wet thickness of 250 µm and line speeds up to 12 meters per minute. Predictions were also made for a two-layer case using Nafion polymer with the same wet thickness on a base layer of Pt/Vulcan with a thickness of 64 µm. By applying vacuum to the bottom layer with a given target film thickness, a process coating window can be established for a high-vacuum limit and a low-vacuum limit. Between these coating limits, there is a stable coating. Above the high-vacuum limit, weeping in the vacuum box can occur. Below the low-vacuum limit, air entrainment and streaking can occur. The NREL slide die does not use a vacuum box so the

coating windows do not address vacuum. Models have to address the die gap to be useful for slide die coatings.

SNL also continued to advance the three-layer slide die model which is a first-of-a-kind model ever produced and supported/advised NREL on multilayer constructions in advance of their first trials with the new slide die. A special slide-only model is being used to help NREL redesign the slide die lip geometry. Figure 88(a) shows modeling for a two-layer slot-die model compared to the three-layer slide die model shown in Figure 88(b). Fuel cell ink rheology data used for the modeling is shown in Figure 88(c).

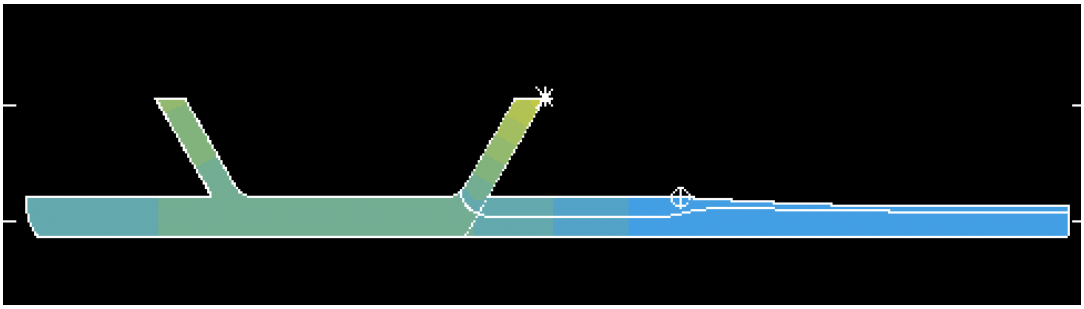

(a)

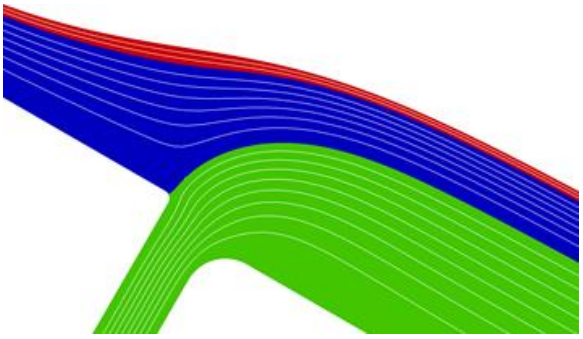

(b)

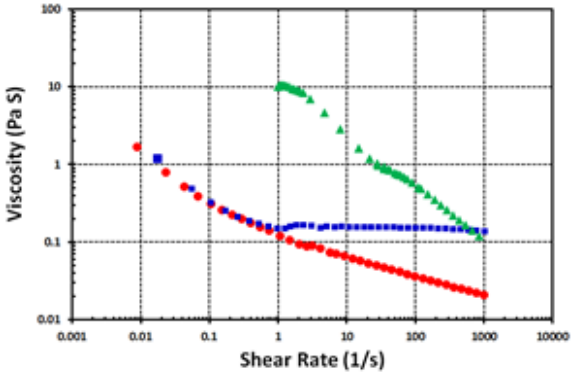

(c)

Figure 88. (a) Two-layer slot-die model, (b) three-layer slide die model for slide flow only with a thin top Nafion overlayer, and (c) the fuel cell ink rheology data used with the models. Sources: SNL and NREL

In addition to the slot-die coating studies, a special slide-only model was completed to assist redesign of the lip geometry for the NREL slide die. A stability analysis on the slide-only multilayer models revealed potential for interlayer defects

Continuum drying model

The approach was to develop a continuum scale model to evaluate drying in an oven. The boundary conditions can be changed to simulate the effects of a multi-load oven. These models do not distinguish the effects of drying at the particle level that LBNL is pursuing. Because the SNL models are at the continuum scale, they use very complex differential equations for heat transfer, solute transport, free volume, and uptake of polymer and particles. GOMA has been run with the model that uses these equations and results compared well with values found in the open literature for residual solvent versus time. Particle dynamics are being added to the model for a support such as an active ceramic, depending on the application, and active colloidal particles in a solvent to add to the diffusion equations used in the model. There was an experimental component to the modeling and equipment was ordered to conduct experiments to study skinning and drying effects. The experimental portion of the project was performed in collaboration with LBNL. SNL also has a Rheolaser

coating apparatus from Formulaction that is used to observe the Brownian motion of small particles. Observing Brownian motion versus time over various speckle rates will allow prediction of when the coating reaches its percolated state in particles and the coating generates residual stresses.

SNL completed the initial polymer-solvent drying model (single- and two-layer), with materials representing toluene solvent and PMA polymer, and validated the model against published literature data. The model was extended to include active particles and conductive particles and initial efforts were to regress the model using an optimization wrapper for diffusion coefficient parameter estimation.

SNL/UNM together with funding from National Science Foundation have advanced a machine-learning model to connect coating defects of particulate conductive films (pinholes, striations) to process parameters for gravure coating/printing. Data was captured with high-end optical microscopy coupled with open computer vision image recognition tools as exemplified in Figure 89.

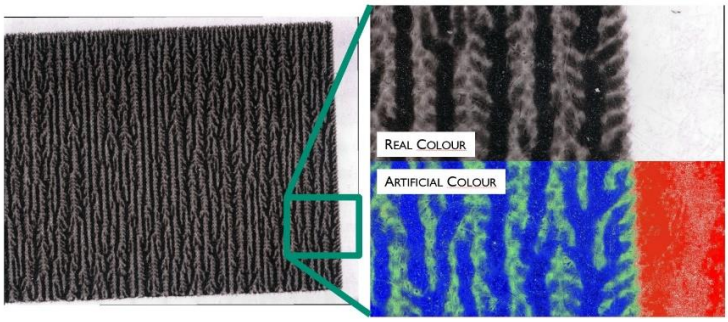

Figure 89. Example of high-end optical microscopy coupled with open computer vision image recognition. Source: SNL

One development for the hypothesis that a ribbing instability is the source of a class of defects known as striations was discovered with some fascinating flow visualization as shown in Figure 90.

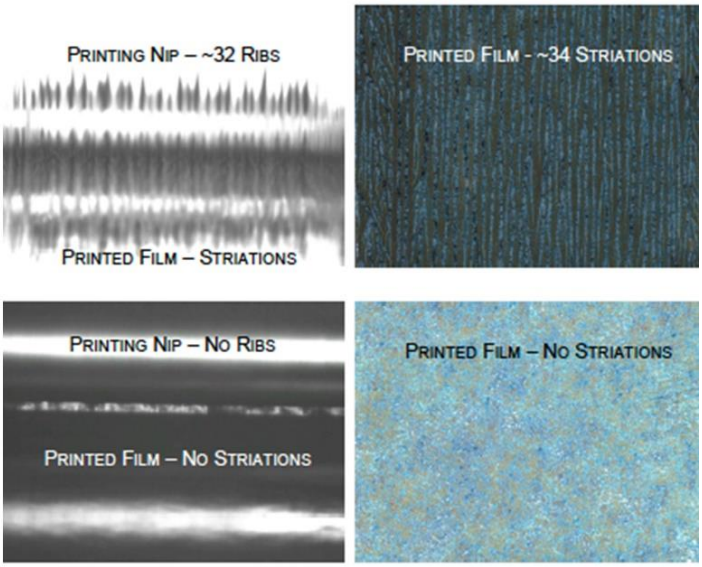

Figure 90. Flow visualization of striations caused by ribbing instabilities. Source: SNL

The visualizations coupled with the Machine Learning Defect Prediction model provided a connection between the complex capillary-hydrodynamics at play and the root causes of printing process defects. The count and positions of the ribbing instabilities match the count and positions of the striation patterns. Ribbing instability is a key mechanism in striation generation.

Collaboration/Coordination/Outreach/CRADA Projects

Core Program

The Collaboration laboratories collaborated and with each other on a weekly basis, either through visits or via telecommunications. Team meetings involving the laboratory leads and principal investigators occurred bi-weekly and included the DOE Technical Managers at one meeting every month. Outreach continued through the principal investigators and researchers presenting at conferences, symposia, peer reviews and during direct contact with industry and the commercial sector. Specific research was reported in technical journals and through patent applications.

CRADA Projects

USC Title 15, Chapter 63, Section 3710c, paragraph 7(A) allows for non-disclosure of trade secrets or commercial or financial information that is privileged or confidential, which is obtained in the conduct of research or as a result of activities from a non-Federal party participating in a CRADA. The government agency may provide appropriate protections against the dissemination of such information for a period of up to 5 years after development of information. As such, some technical information on the CRADA projects will not be included in this report. The following information for each CRADA project was approved or provided by the CRADA partner.

Navitas Systems, LLC

Navitas Systems, Inc. partnered with ORNL and NREL to demonstrate R2R production of advanced separator for lithium ion batteries. A R2R method was developed to fabricate the separator, which replaces the conventional discrete operations and enables superior safety, high throughput, and low manufacturing cost.

An initial gravure printing run was performed on the NREL coating line using excess inks and substrates to better understand the impact of the printing process parameters. Two platinum-carbon inks with water and n-propanol solvents, one n-propanol-rich and one water-rich, were printed and a pattern was achieved. However, several non-ideal situations were observed. First, based on the ink properties and the design of the wells in the machining of the patterned cylinder where a diamond pattern was printed, there was not a continuous coating at a micro-scale within the area of the diamond. Rather, there was a discontinuous sub-pattern as shown in Figure 91 at different magnifications. This is presumably due to a mismatch between ink properties and pattern design. Second, in addition to printing of the diamond pattern, transfer of ink in the "land" areas of the cylinder, i.e., the area in between the diamonds where no ink is supposed to transfer, was observed.

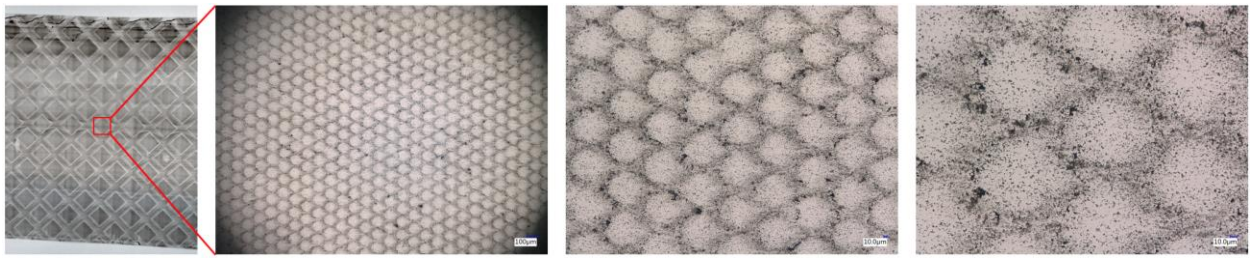

(a) (b) (c) (d)

Figure 91. Interior of coated diamond section: (a) macro image of the coating, (b) 100X magnification of the area in red in (a), (c) 300X magnification, and (d) 700X magnification. Source: NREL

Figure 92 shows this effect of ink streaking in the land areas. In all four of the images, the sub-pattern within the diamond is shown along with apparent "streaks" of ink in the land area between the diamonds. The exact

cause of this behavior is unknown, though it is presumed to be related to non-optimal orientation and pressure of the doctor blade.

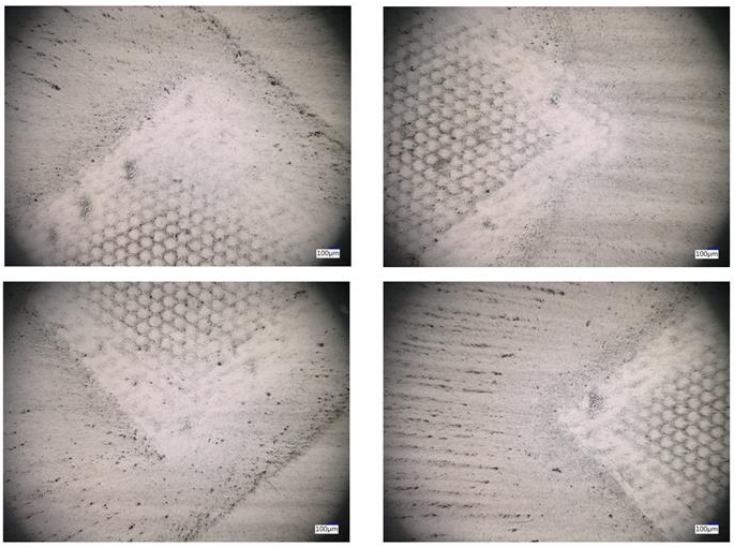

Figure 92. Streaking of ink in the land areas. NREL

The third non-deal condition was that the exact match of the web speed with the gravure roll speed is difficult with the current controls on NREL's coating line causing stretching or compression of the pattern. Figure 95 shows images of the printed pattern at three different relative speeds of the web and cylinder, where the image in Figure 93(a) shows slight stretching of the pattern, the image in Figure 93(b) shows large stretching as a result of ~2x mismatch in speeds, and the image in Figure 93(c) shows as good matching as could be achieved with the available speed controls on the coating line. Another observation was an effect of the solvent ratio which is likely due to differing drying rates and a non-optimal configuration of NREL's gravure printing head where the freshly printed web is turned vertical. This can potentially lead to gravity-induced streaking. Significant wear on the doctor blade may have also led to macro-scale streaking in the printed pattern (different than the micro streaking in the land areas). For overall capability development, installation of a rubber impression roller behind the web to nip (squeeze) the web when in contact with the printing cylinder may be beneficial. Many (though not all) gravure printing activities in the literature and industry are configured in this way. Alternately, there is an impression roller insert above the gravure cylinder that is not optimally configured for printing cylinders but, with modification, may provide this functionality. Overall, this work demonstrated gravure printing as a new R2R capability with wide applicability.

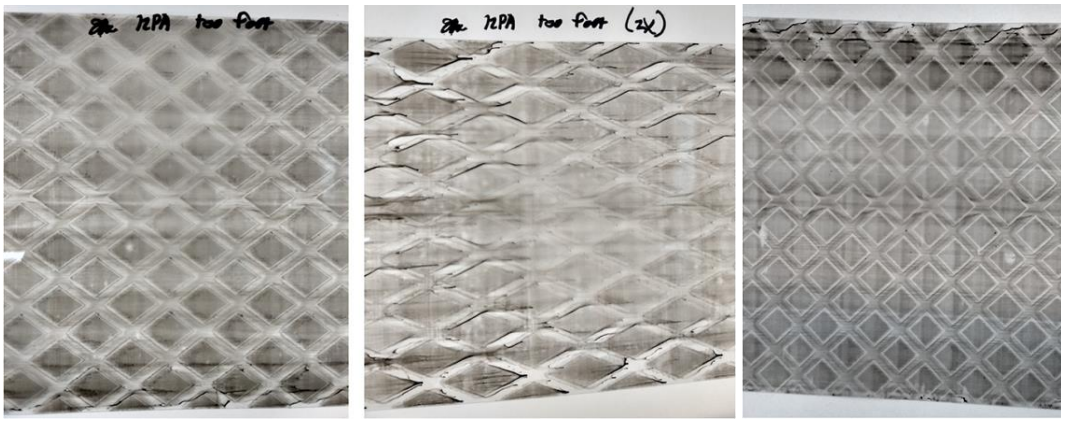

Figure 93. Patterning at different speed and matching conditions: (a) slight stretching, (b) 2x stretching, and (c) as close to 1:1 matching as possible. Source: NREL

Upon completion of this CRADA project, a method was developed to create a patten of alumina and titania in an interdigitated coating with a honey-combed structure. This would take advantage of the benefits of alumina as a heat-dissipating material used as a lithium-ion battery separator interface between the electrodes, and titania for its mechanical strengths. Two separators demonstrated a 2% to 3% improvement for thermal stability in terms of shrinkage over an uncoated separator. Self-discharge tests on coated separators showed that all separators had decay rates between 100 and 200 mV/hr which is very acceptable. The major accomplishments for this CRADA project, which completed in March 2020, were the development of a process to fabricate interdigitated pattern coating of ceramic on a polymer separator and the results for the design and patterning of the separators

SolarWindow Technologies, Inc. (SWT)

SWT partnered with NREL and ANL to demonstrate diffractive multiplexing for high-throughput R2R laser patterning of flexible organic PV modules. SWT is a developer of transparent LiquidElectricity™ coatings and processes which generate electricity on glass and plastics. The objective of the CRADA project is to greatly facilitate the processing steps needed to make a thin-film photovoltaic module that consists of multiple solar cells connected in series. To do this, interconnects are required between individual sub-cells. Typically, three sequential laser ablation scribes are made to create space for the interconnects between two sub-cells. The first is referred to as the P1 scribe that separates the bottom conductor or electrode. More layers are applied and the P2 scribe is made as a spacer to fill in the conduit that would connect the bottom of one cell to the top of the next cell. Finally, a P3 scribe is made for the top contacts. So, the P1 separates the bottom electrode, the P2 is the series connection, and the P3 isolates the top contacts. Typically, the scribing is performed with a single laser source to produce a series of P1, P2 and P3 scribes, one scribe at a time.

The project plan consisted of five stages. Stage 1 was to design and build the diffractive optic laser multiplexed scribing station and integrate it into the R2R webline. Part of Stage 1 was to use a sheet-to-sheet single-laser scribing unit as the baseline for comparison with the multiplex system. Data from the single laser scribes were used to design the multiplex scribing system. Stage 2 was to demonstrate feasibility of the multiplexed scribing. Stage 3 was to compare functionality of the multiplexed scribed samples to single beam scribed control samples. Stage 4 was to achieve entirely multiplexed scribed (P1, P2, and P3 steps) samples in a fully processed module. Stage 5 was to gradually increase the process speed to demonstrate suitability of the multiplexed scribing process for true high-throughput R2R manufacturing.

The concept for this project was to use a single laser source and multiplex the laser beam into multiple beams or lines so that all P1s, then all P2, and all P3 scribes could be made individually and simultaneously. The resulting multiplex system would be incorporated onto a R2R webline as shown in Figure 94. The P-scribes cannot cross one another. Each set of scribes needs to be parallel to the previous set. A web camera is mounted to view the scribe area and the laser is in a safety enclosure. NREL has successfully multiplexed the laser into 13 individual laser spots so as the web advances, the scribe lines are created. Initially, much effort was spent characterizing the resulting scribes and optimizing their size and shape. ANL performed SEM imaging and chemical mapping with EDS to evaluate the different scribe conditions and the data was used for NREL's optimization of the scribing process. The system also incorporated a "smart" camera to do real-time analysis of the scribe as the web is moving. The camera is directly connected to a translation station controller that moves all the laser optics to ensure that the P2 scribes remain parallel to the P1 scribes and eliminates drift of the laser beams.

Figure 94. Multi-spot diffractive optical element scribing integrated onto the NREL R2R webline. Source: NREL

The smart vision camera and improved programming software is used to control the laser optics position to maintain a constant spacing between subsequent scribing. The smart vision camera system is shown in Figure 95. Tests were successful for maintaining a laser scribe parallel to an existing scribe for a few meters of sample running through the R2R laser scribing tool.

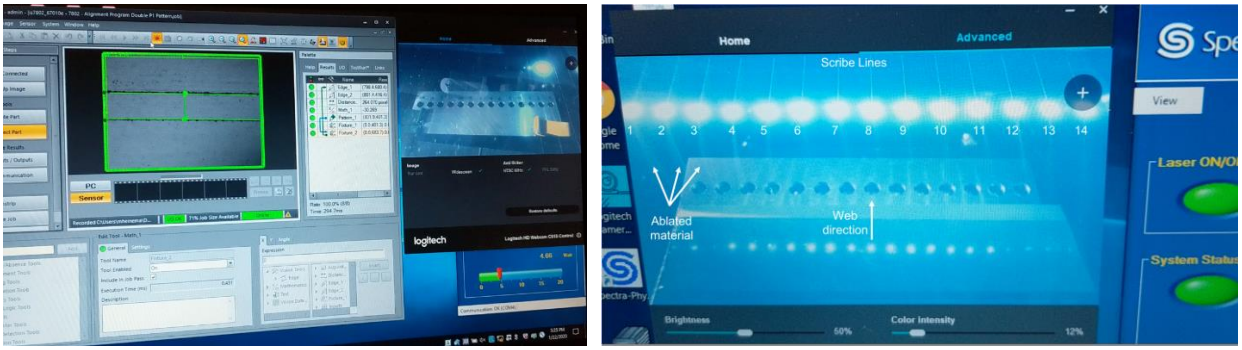

Figure 95: The smart vision camera calculates distance between previous scribe (e.g., P1) and active scribe (e.g., P2) then controls alignment of optics to maintain a constant distance. Source: NREL

There were some challenges initially to assemble a system that was environmentally and operationally safe to use. The system employees a high-power ultraviolet laser which typically requires an enclosure that prevents laser energy from escaping but this is not practical for an open R2R process where the web enters at one point and leaves at another. Also, the ablated material must be contained. The laser power also needed to be attenuated without opening the enclosure. The diffractive optic is custom made for this application and tailored to the NREL laser for the distance needed for appropriate separation of the scribe lines. As the laser beam is split by the diffractive optics, it goes through a very large collimating lens to make the beams parallel to each other. Individual focusing lenses are used to focus the individual collimated beams perpendicular onto the sample surface. Initial runs showed that if the power is too high then the scribe will be too deep and if the power is too low, the sample will swell, and no scribing will occur. Several runs are needed to determine the best processing window for optimized scribes.

NREL scribed several meters of P1 scribes on zinc oxide/ indium tin oxide/polyethylene terephthalate (ZnO/ITO/PET) on their R2R system. Comparable samples were made with single-laser P1 scribes.

Approximately 5-in x 4-in sections were cut and coated with photoactive ink and finished with hole-collection and top contact layers. Figure 96 shows an example of completed mini-modules. Using the un-scribed portions of our ZnO/ITO/PET roll, small-area solar cells were fabricated with various combinations of different photoactive inks (blade-coated) and evaporated the top contacts which were molybdenum oxide/silver.

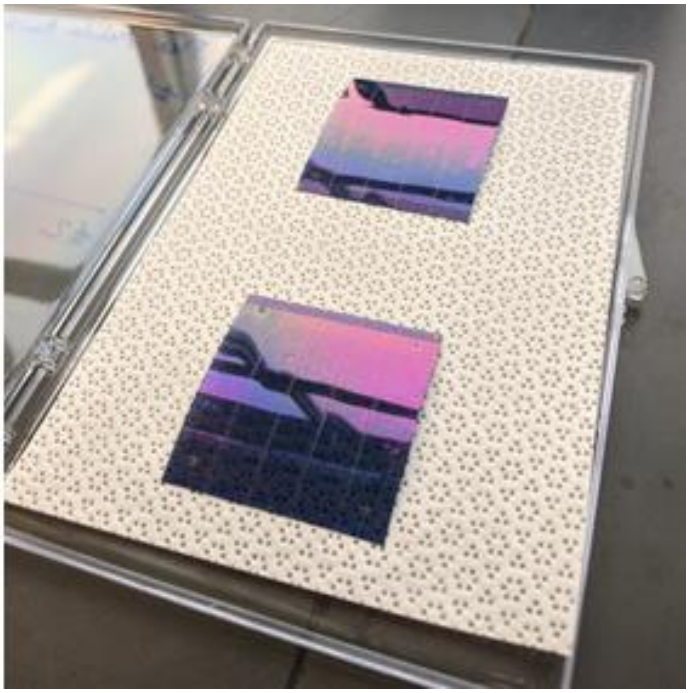

Figure 96: Example of PV mini-modules consisting of three cells. Source: NREL

Due to low module performance from shunting, efforts were concentrated on improving the ZnO coating layer. The ZnO is formed via a sol-gel method utilizing a zinc-organic precursor, e.g., zinc acetate ($Zn(Ac)_2$), in an alcohol solvent such as methanol. After coating, the ZnO must be thermally annealed to remove residual unreacted precursor and moisture, however, the required use of a plastic PET substrate in this application limits the ZnO annealing temperature to less than 150°C. The problems with failed devices were due to (1) a very rough substrate surface (all layers deposited on top of the substrate were probably too thin, so short circuiting was experienced through the layer stack, and (2) a lack of adequate annealing of the ZnO coating. Annealing and UV-ozone surface treatment are critical to enabling the ZnO to perform properly. Reasonable performance was achieved with small-area cells using an extended annealing time of 20 mins at 140°C and UV-ozone surface treatment. The photo-absorber layer was also upgraded. A new material provided by SWT gave a more consistent coating and much better power conversion efficiency. Blade coating was used to fabricate small-area test PV device to optimize the coating conditions for gap height, blade speed, solution volume, etc. With the new absorber, the organic hole-transport layer that is deposited on top of the absorber was optimized and resulted in improved module performance.

SEM images in Figure 97 showed jagged edges on some of the P1 scribes which indicates violent ablation and possibly too much thermal load on the sample. This can also cause tearing of the material near the edge. NREL fabricated some small two-inch by two-inch PV mini-modules of three cells and two interconnects which provided suitable test samples for evaluating both the coatings and scribes. Some undesirable P1 scribes were obtained with protruding edges. ITO, the bottom transparent conductor, will sometimes lift off and redeposit onto the substrate which produces a larger sidewall. This can create penetration into the top conductor and cause an electrical short. The ITO lift-off occurs because the adhesion between the ITO and PET is not strong enough to withstand the laser ablation process. As such, alternative substrates were investigated.

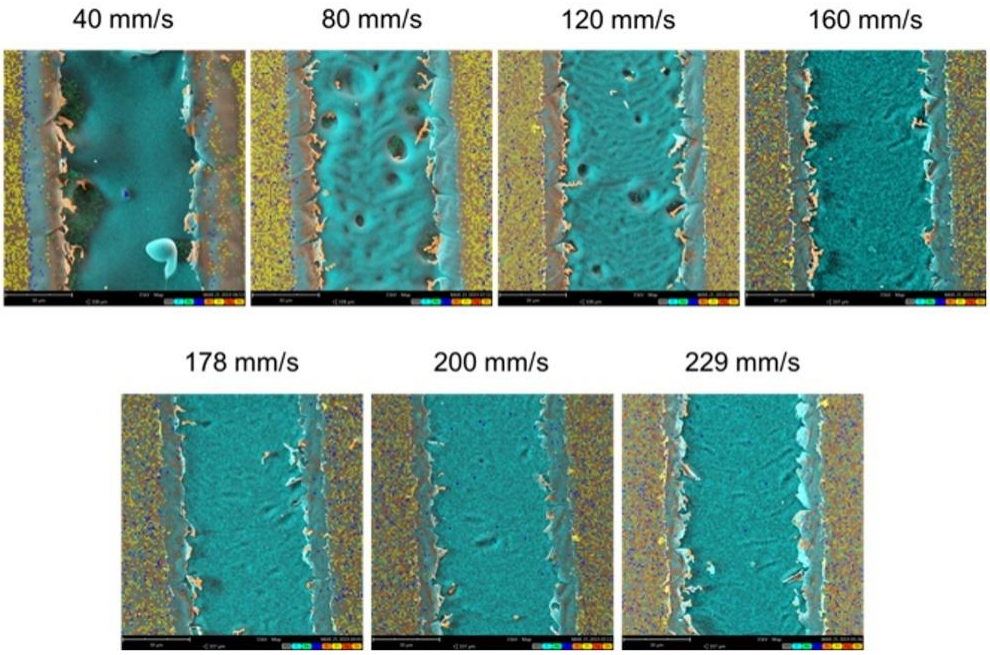

Figure 97. Elemental mapping of the P1 scribes showing various distortions at the scribe edge a different scribe rates.
Source: NREL

Many of the initial PV mini-modules fabricated on a flexible ITO/PET substrate suffered from low photocurrent collection (high current loss) and exhibited poor power conversion efficiency. Dark lock-in thermography (DLIT) was used to investigate the quality of the module interconnects. Figure 100 shows DLIT images of the flexible organic PV min-modules with three different ZnO electron transport layers and two different P1 laser scribing settings. However, Figure 98(a) shows many "pinholes" remain in the film leading to a high number of current loss pathways. In Figure 98(b), most of the pinholes are gone when the sol-gel solvent was switched. In this case, the P1 was revealed as the source of most current loss. From surface profile measurements using a Dektak profilometer, the ITO sidewalls of the P1 were observed to peel up from the PET, extending up to a couple of microns, which is taller than the total PV stack thickness. Therefore, the bottom and top electrodes contacted each other causing the cell to short circuit at the P1 edges as shown by the bright current spots seen in the Figure 98(b) for a high laser pulse density and less in Figure 98(c) for a low laser pulse density.

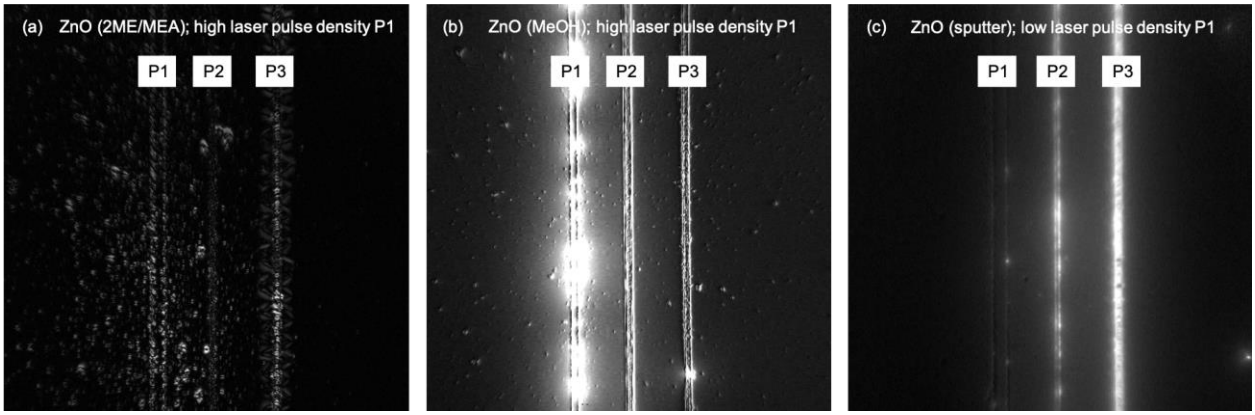

Figure 98: DLIT images of flexible organic PV min-modules with three different ZnO electron transport layers and two different P1 laser scribing settings. Also shown are the bright current spots caused by the electrodes short circuiting.
Source: NREL

Efforts were refocused on improving the quality of the P1 scribe. P1 laser scribing was done on the ITO prior to ZnO electron transport layer deposition which resulted in less ITO delamination. In addition, the laser pulse frequency was adjusted to reduce the density of pulses striking the sample during ablation. This subjected the PET to less thermal load from the laser and less damage to the substrate. Figure 99(a) shows the initial P1 scribe with damage and debris in the middle of the scribe. In Figure 99(b), the P1 scribe at lower pulse densities has a much cleaner looking trench. Surface profile measurements showed that these new P1 scribes have much reduced side wall heights down to 100-150 nm. DLIT measurements confirmed that the P1 scribe is no longer the primary source of current loss as seen in Figure 98(c) above. While scribe edges are improved, some sharp edge features were observed, particularly at laser spot overlaps, that can lead to short circuiting in the PV modules. Transforming the laser beam profile from Gaussian to square shaped has been shown to greatly improved the scribes, especially at the side walls. To this end, a beam expander and "top-hat" beam shaper was used to improve the scribes. Figure 99(c) shows results of P1 scribing of ITO on PET using the "top hat" beam shaper. This approach was further optimized by adjusting the beam input size (via beam expander) and the x-y position of the beam shaping optical element.

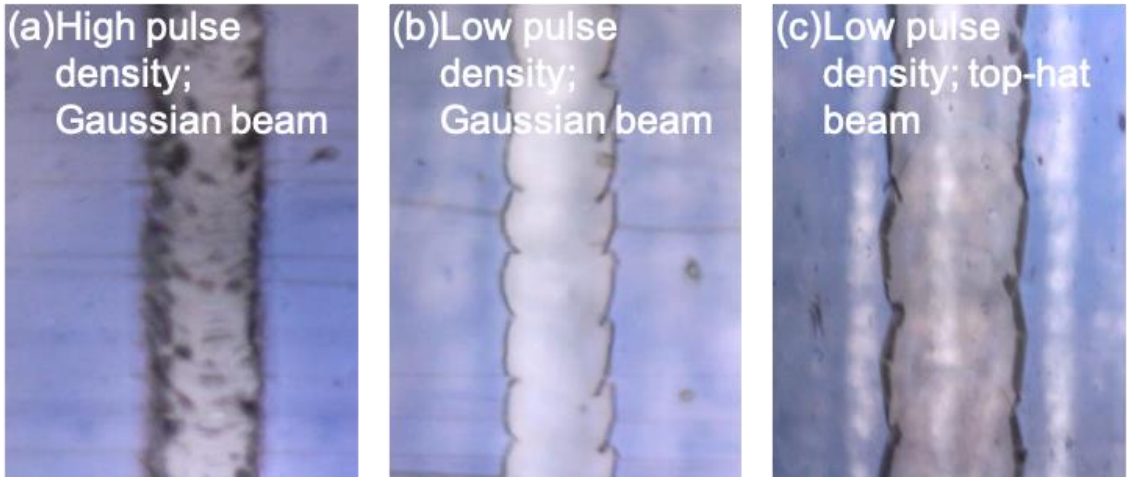

Figure 99: Optical images showing optimization of P1 laser scribes. Source: NREL

Sputtered ITO will have a stronger adhesion to another oxide than to an organic polymer (i.e., PET), so improvements for adhesion were attempted by adding a thin layer of SiOx between the PET and ITO. Approximately 20 nm of SiOx was thermally evaporated onto bare PET. Then, 250 nm of ITO was sputtered onto the SiOx. Also, the laser pulse frequency (used for the P1 scribing) was varied to explore its effects on the P1 scribe quality.

Although the scribing processes with the PET substrates continues to improve, a decision was made to use flexible glass as an alternative to the PET. The glass has many advantages, specifically better optical uniformity, much smoother surfaces, and most critically, better adhesion with the ITO deposited on top of it. Integration of the flexible glass onto the R2R multiplexed laser scribing tool was achieved. Figure 100 shows the surface profiles of initial laser P1 scribes using the R2R multiplexed laser. P1 scribes with minimal sidewalls were fabricated by tuning the repetition rate of the laser pulses striking the ITO/glass, for example the blue curve shows sidewalls less than 60 nm.

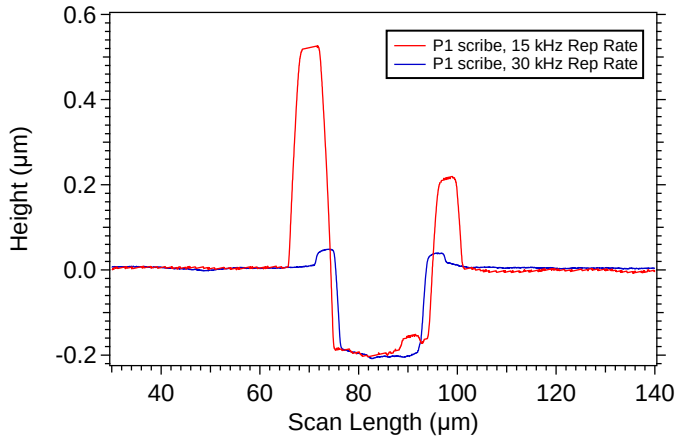

Figure 100: Surface profile scans across laser P1 scribes showing that doubling the laser pulse repetition rate resulted in significantly improved edge features. Source: NREL

Having overcome the major problems with P1 scribes, the R2R multiplexed laser tool was successfully used to scribe P2 lines, and eventually to finish a working PV module comprising 12 individual sub-cells connected in series through the P1/P2/P3 interconnects. Figure 101(a) shows the results of an increase in voltage that results from increasing the module size from 1 to 12 cells (black curve). However, each cell does not contribute an equal amount of voltage (grey curve), suggesting that some of the cells are suffering performance losses. Initially, PET was used as a plastic substate which has a rougher surface than the normal solid glass substrate. The PET also had poor adhesion with the ITO button contact when it was sputtered onto the ITO. As a suitable alternative, a thin, flexible glass substrate was demonstrated for an organic PV using a sheet-to-sheet single laser scribing for the interconnects on the NREL R2R system. Working full modules were fabricated on flexible glass shown in Figure 101(b) using the single line laser scriber as a comparison to R2R-processed modules. The fraction of the open circuit voltage (Voc) contributed by each individual cell is included in the module, for example, cell #1 contributed ~13% whereas cell #3 only contributed ~4% to the module's Voc. Module performance was similar between the two scribing processes and demonstrated the success of the multiplexed laser scribing on the R2R. The fastest R2R scribing obtained was 14 simultaneous scribe lines at a rate of 2 ft/min. It is possible to increase this speed by at least 2x.

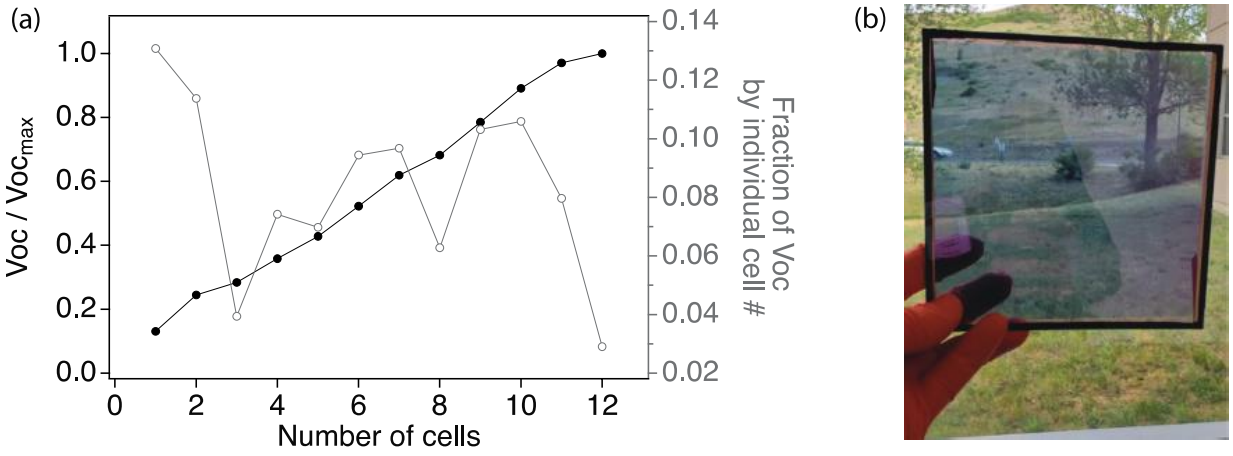

Figure 101: (a) Increase in the PV module size from 1 cell to 12 cells produced an increase of the module's Voc increasing the number of cells in module. (b) A photo of a completed semitransparent PV module on flexible glass. Source: NREL

Characterizing of the scribes will continue after the project to analyze scribe quality, uniformity, and stability. This includes advanced spectroscopic analysis (SEM/EDS and micro-Raman mapping) in collaboration with

ANL. NREL will continue to fabricate flexible organic photovoltaic modules with R2R processing using diffractive optic multiplexed laser scribing to make sub-cell interconnects and evaluate module performance as a function of R2R processing speed to determine the feasibility of multiplexed laser scribing for scalable, high throughput thin film photovoltaic module production. SWT also plans on continuing with the multiplex scribing development after the CRADA project ends. SWT has renewed a CRADA with NREL and part of the scope of work is to continue to use the NREL R2R capabilities.

Nel Hydrogen

Nel Hydrogen has partnered with NREL, ORNL, and ANL to conduct research on R2R manufacturing of advanced (low loading, direct coated onto membrane) electrolysis electrodes for low-cost hydrogen production. Ink characterization and optimization, R2R coating, advanced electrode characterization, and metrology development capabilities at the labs will be used to support the overall goals of reducing the manufacturing labor for the MEA by a factor of 15-20 and the overall cost of the MEA by over 60%. Work began for this project in January 2020.

The current procedure for making MEAs is a slow, inefficient batch process. A Nel Hydrogen techno-economic analysis showed that R2R can provide a method that would significantly reduce the cost of their system. The overall goal is to develop a R2R coating process for direct coating of anode catalyst layer to a PFSA membrane. This is not a straightforward process because the membrane tends to swell in the water/alcohol dispersion media of the catalyst ink. The ink and the process must be designed to minimize or negate the effects of the swelling and produce a uniform and defect-free coating with the desired performance.

The project team consisted of Nel for the in-situ testing and characterization; NREL for the catalyst ink development, solvent-membrane interactions, and R2R gravure catalyst layer coating; ORNL for catalyst ink development, R2R slot-die catalyst layer coatings, and electron microscopy to investigate catalyst structures; and ANL for the X-ray scattering and tomography experiments at the Argonne APS beamline to investigate the agglomerate size of the catalyst in the inks as well as the structure of the catalyst layers after coating. The goal of this project was to determine the appropriate ink formulation and coating process for achieving the target loading.

One effort was to understand the interplay between membrane swelling and tensioning and the impact on web handling and stretching of the membrane. The approach was to investigate adjusting the ratio of water to 1-propanol in the ink (which affects the absorption rate and swelling), the drying rate, and tension on permanent elongation of the membrane once the membrane was dried. NREL devised the fixture shown in Figure 102 where the membrane is clipped to a weight that goes over a pulley which simulates the web tension. The coating of a mixture of water and alcohol can be applied with a Mayer rod to simulate a R2R coating. The weight was selected to match the actual tensioning on the R2R coating system. The weight was selected to match the actual tensioning on the R2R coating system. The goal was to understand interplay between membrane swelling and tensioning and the impact on web handling.

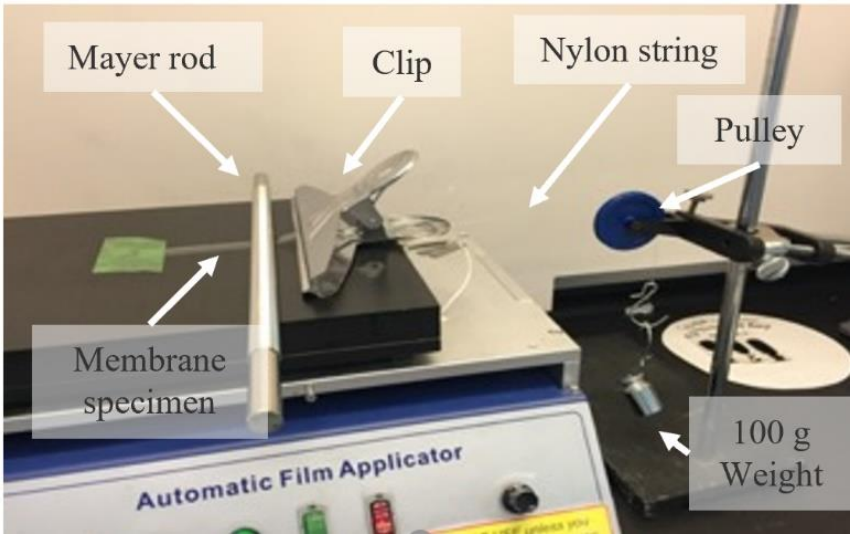

Figure 102. NREL setup for determining the impact of the solvents in the dispersion media on the stretching of the membrane. Source: NREL

NREL investigated the effect of water, 1-propanol, and no solvent on the percent elongation of the membrane after the process at different tension loads, i.e., tension per linear centimeter of membrane width. Very little tension produced very little elongation. At the higher tension loads, which are typical of what is observed in actual coating processes, 1-propanol produced significantly more elongation than water. At even higher tension loads, the water starts to produce elongation as seen in Figure 103. This is consistent with the absorption rate studies. Water has a very low adsorption rate, whereas 1 propanol has a high two-phase adsorption rate which results in greater elongation. As the solvents are absorbed into the membrane, they plasticize the membrane leading to plastic deformation under tension.

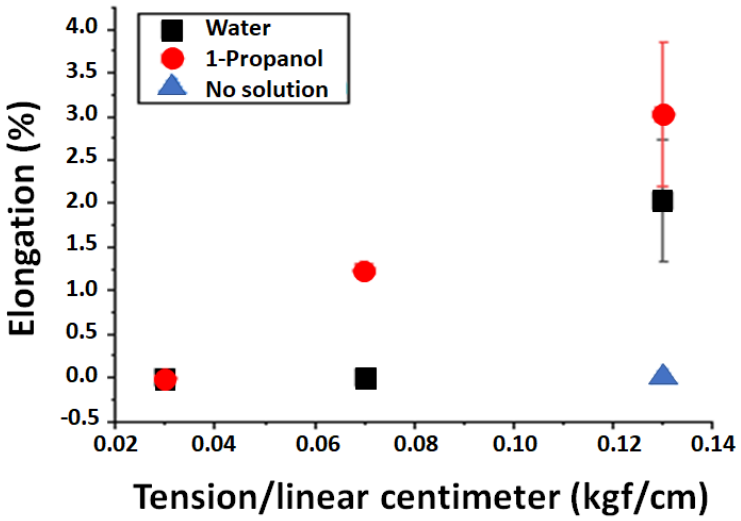

Figure 103. Effect of water and 1-propanol on the membrane at different tension loads. Source: NREL

NREL investigated the effect of drying processes in air at room temperature for three conditions: (1) no drying, (2) one minute of wetting and two minutes of drying, and (3) three seconds of wetting and two minutes of drying. This simulates reducing the distance between the coating zone and the drying zone. As the wetting time

increases for the same drying time, there is an increase in the percent of elongation, as shown in Figure 104. Solvent media with low adsorption rates and minimizing the wetting time of the membrane or increasing the drying rate is needed to reduce membrane elongation

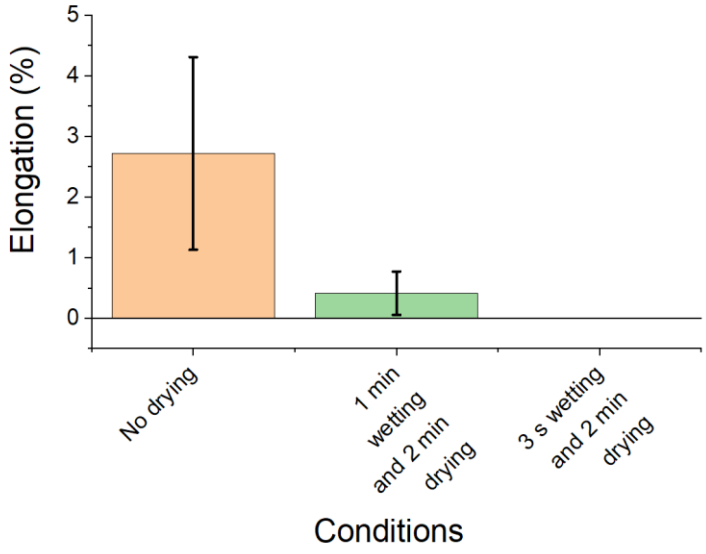

Figure 104. Effects of wetting and drying times on membrane elongation. Source: NREL

NREL also studied the uptake of water/alcohol mixtures by the PFSA membrane. Using a force tensiometer, pure water and alcohols were found to absorb more slowly than mixtures. Figure 105(a) shows the weight adsorbed over time for six mixtures of water and n-propanol and pure water and pure alcohol. The uptake rate for the Nafion and Aquivion membranes for different percentages of n-propanol is shown in Figure 105(b) and the distortion time for each membrane is shown in Figure 105(c).

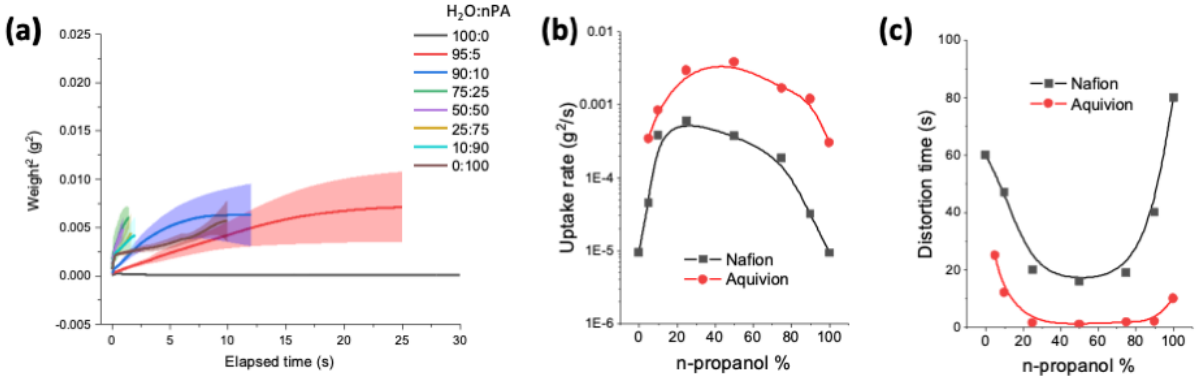

Figure 105. (a) Weight gain of solvent mixture over time, (b) uptake rates for n-propanol by Nafion and Aquivion membranes, and (c) distortion times for Nafion and Aquivion membranes at n-propanol concentrations. Source: NREL

Another task was to perform electrode ink development and characterization. The goal of the study was to understand how the catalyst ink solvent ratio affects agglomeration in the inks and resulting catalyst layers. The properties of the membrane need to be balanced with how the catalyst ink affects the structure and performance of the catalyst layers. NREL prepared catalyst inks and catalyst layers with IrO_2 catalyst and Aquivion ionomer. The inks were prepared with water/alcohol dispersion media mixtures using 1-propanol and ethanol with varying ratios of water/alcohol. These inks were sent to ANL for USAXS/SAXS analysis. Figure

106 shows the raw data for these experiments. Final results for the USAXS/SAXS will be provided in FY 2021.

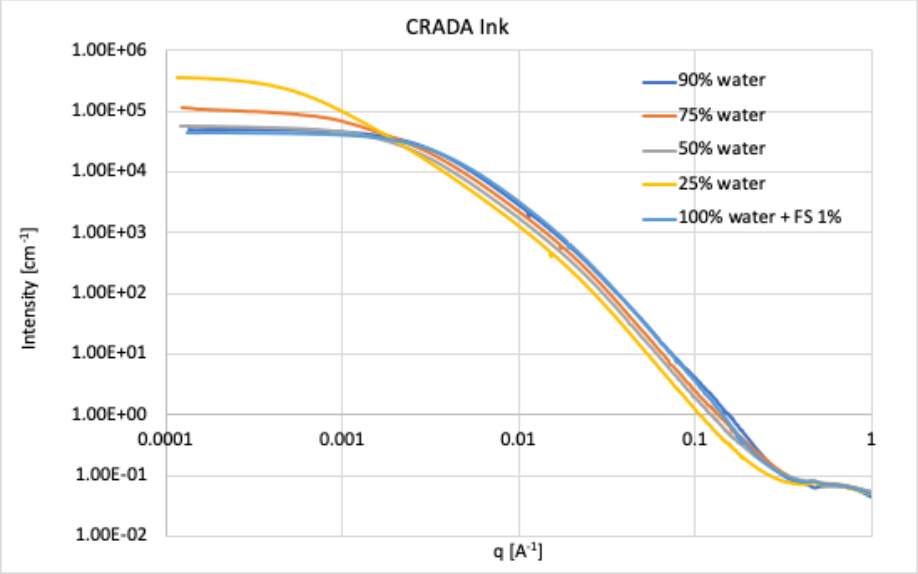

Figure 106. Preliminary USAXS/SAXS results for catalyst inks and catalyst layers with IrO_2 catalyst and Aquivion ionomer. Source: ANL

NREL continued to improve the gravure coating parameters to get to the target loadings. A trial coating was made on polytetrafluoroethylene to determine how the selection of the gravure roller and the rotational rate of the gravure cylinder affected the loading. The ink formulation consisted of 20 wt.% Alfa Aesar IrO_2, Aquivion D79-25B ionomer (790 EW, 25% in water), a 50/50 H2O/nPA mixture, and an ionomer-to-catalyst ratio of 0.2. The coating conditions were a web speed of 1 m/min, a MG USA roller size of an R80 (tri-helical patterns, 80 lines per inch), oven #1 (one meter in length) temperature of 80˚C, an oven #2 (one meter in length) temperature of 100˚C, and a coating length of ~7 m. The operating parameters are listed in Table VIII.

Table VIII. Operating Parameters for the Gravure Coating Trial

No.	Gravure roll speed	Speed ratio
1	16 rpm (1 m/min)	1
2	24 rpm (1.5 m/min)	1.5
3	32 rpm (2 m/min)	2
4	40 rpm (2.5 m/min)	2.5
5	16 rpm (1 m/min)	1
6	24 rpm (1.5 m/min)	1.5
7	32 rpm (2 m/min)	2

There was not much impact of the rotational speed of the gravure roller on the as shown in Figure 107. The grey boxes are indicative of the different speed ratios tested (as labeled at the top of each box). A speed ratio of SR1 means that the speed of the gravure roller matches the webline speed and a higher speed ratio means that the roller is going faster than the webline speed. The loading appeared to be independent of speed ratio.

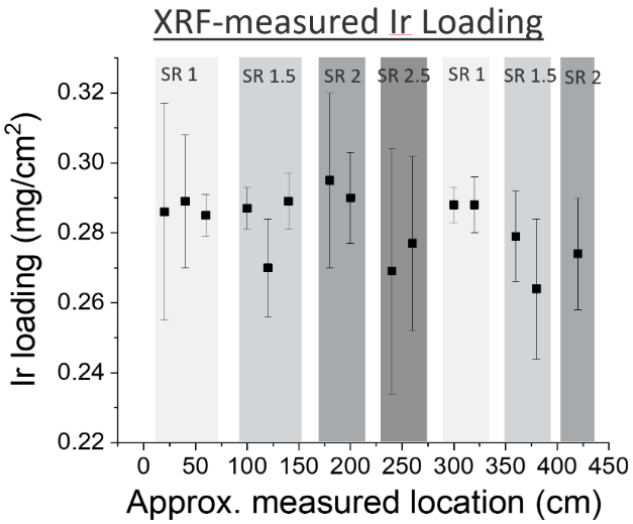

Figure 107. Effect of gravure roller speed on IrO_2 loading. Source: NREL

NREL prepared R2R gravure coatings to create IrO_2 catalyst layers using polytetrafluoroethylene substrate and the baseline catalyst material to tune the loading. With this particular ink and gravure roll, the average loading was around 0.3 mg/cm^2 compared to the target of 0.5 mg/cm^2. The target loading can likely be achieved by changing the ink concentration or gravure pattern volume factor. Two different IrO_2 catalysts were successfully coated on the perfluoro sulfonic acid membrane to make catalyst-coated membranes. The target loading was achieved with the baseline material. The second catalyst resulted in a lower loading, which is likely due to the catalyst ink having different properties. Overall, the coatings were very uniform, as shown in Figure 108, and that the membrane is no longer deformed after drying. Samples from these runs were sent to Nel Hydrogen for in-situ electrochemical testing.

(a) (b) (c)

Figure 108. Photographs of IrO_2 catalyst layer coatings performed at NREL. (a) Gravure coating station showing slight wrinkling of membrane due to solvent absorption. (b) The coated membrane entering drying oven. (c) A sample of the dried catalyst coated membrane. Source: NREL

Workforce Development/Educational Outreach

The Collaboration laboratories integrated students and postdocs into all aspects of the program and ensured proper education and dissemination of information from the program thereby promoting a workforce with skill sets that support research, development and modeling for manufacturing technologies and processes. The R2R AMM DOE Laboratory Collaboration expanded its workforce development and educational outreach efforts in FY 2020 for the laboratories and universities listed in Table IX.

Table IX. Educational Development at the R2R Collaboration Laboratories

Collaboration Lab	Post Doc/Student/Intern	University
LBNL	Zhi Huang, Post Doc Bei Fan, Post Doc Buyi Zhang, Graduate Researcher	Purdue University University of California San Diego University of California Berkeley
ANL	Devon Powers, Post Doc Appointee Ashley Simmons, Undergraduate Intern	Vanderbilt University Kettering University
ORNL	Erin Creel, Post Doc Alexander Kukay, PhD Student	University of California Berkeley University of Tennessee
NREL	Sunil Khandavalli, Post Doc Brian Green, Post Doc Sadia Kabir, Post Doc Janghoon Park, Post Doc Min Wang, Post Doc Derek Jacobsen, Graduate Researcher Mason Liu, Graduate Researcher Radhika Iyer, Graduate Researcher	University of Massachusetts Amherst University of Denver University of New Mexico University of Massachusetts, Amherst Case Western University Colorado School of Mines University of Colorado Illinois Institute of Technology
SNL	Chris Wall, Graduate Student Ben Wall, Graduate Student Robert Malakhov, Graduate Student Andrew Cochrane, Post Doc	New Mexico Tech (Albuquerque, NM) New Mexico Tech (Socorro, NM) University of New Mexico University of New Mexico
Total	**19**	**15 different universities**

Results of the research will be published and where applicable intellectual property be filed in collaboration with all contributing laboratories. The collaboration continued to reach out to industry to ensure technology transfer.

Challenges/Contingencies

In FY 2020, the R2R AMM DOE Laboratory Collaboration built upon successes from the previous Phase 1 R2R Consortium efforts in battery and fuel cell materials R&D and expanded to include ES, multilayer coating, ion-exchange membrane materials, air filtration media, continuum coating flow modeling, and printed electronics inks in Phase 2. The biggest programmatic challenge was to meet established and approved milestones after schedules were impacted by the COVID-19 pandemic. Task schedules and milestone dates were adjusted contingent on access for approved personnel to laboratory facilities. Typical challenges occur

when additional time is needed to get test equipment operational (downtime) or to receive new equipment and materials from vendors as well as negotiating contractual agreements which creates delays. This challenge was exacerbated by the closure of all laboratory facilities including procurement offices and machine shops that prevented parts and equipment from being ordered or fabricated in a timely manner.

Risks and Risk Handling

Early stage research usually has higher risks for the outcome of successful technologies compared to advanced development because of the nature of the basic science and phenomenology being investigated. Other risks occur when funding or materials/equipment are not readily available to begin experimentation, but FY 2020 had an additional risk that was not anticipated nor effectively mitigated without a timeframe for the laboratories to return to a normal full-time operation.

Beginning mid-March 2020, all National Laboratories were closed, and no in-house laboratory work was allowed due to COVID-19 restrictions. In accordance with the respective State's guidance, the R2R Collaboration teams worked from home and continued with data analysis, literature research, writing manuscripts, performing design activities, and leveraging manufacturers who still have ongoing operations to have parts fabricated. Once restrictions started to relax, a staged reopening of the laboratories was initiated. Some minimum amount of research was conducted in limited blocks of time and on a special case basis and with limitations on the number of people occupying each laboratory at a given time to ensure distancing. This significantly impacted the research tasks and milestone schedules.

FY 2020 introduced significant risks that could only be mitigated by reprogramming many tasks to FY 2021, the last year of Phase 2 for the R2R Collaboration, with the expectation that all the National Laboratories would return to full operations, and lost time could be made up by focusing on the major tasks and accelerating efforts on those tasks.

Project Ratings

Project performance assessments are determined through quantitative and qualitative methods in accordance with DOE Program and Project Management for the Acquisition of Capital Assets. [13] Programs are assessed by the following definitions: green – project is expected to meet its current performance baseline; yellow – project is potentially at risk of not meeting an element of the current performance baseline; red – project is highly at risk of requiring a change to the performance baseline by the Acquisition Executive or is not being executed within the acquisition strategy and Project Execution Plan.

Because of the COVID-19 pandemic, the R2R Collaboration Labs redefined project milestones to maintain an achievable schedule and meet those milestones that did not require extensive laboratory experimentation. Efficient use of personnel with limited access to the facilities was invoked to conduct necessary experiments and collect the needed data to remain within the scopes for each project as access was permitted. Budgets were managed to allow some carryover of funds into FY 2021 that will be used to accelerate those tasks that were not completed in FY 2020 and rescheduled for FY 2021 execution. As such, and within the constraints of each State's guidance to relax requirements that will allow researchers to return to the laboratories, all projects were considered green for scope, schedule, and budget for FY 2020.

Conclusions

FY 2020 was the second year of a three-year Phase 2 project for early stage R&D on R2R advanced technologies in a national multi-laboratory collaboration. Efforts will deliver advances in the fundamental

understanding of R2R processing on moving webs, carriers, or other substrates and develop tools, metrology approaches, processes, and new materials to improve yields, overall quality, processing rates and reduce cost. Technologies under development will overcome the lack of scalability and understanding of fundamental chemistry and materials properties demonstrated on selected key technology applications with cross-cutting impacts.

Beginning mid-March 2020, all National Laboratories were closed, and no in-house laboratory work was allowed due to COVID-19 restrictions which created unusual challenges for completing FY 2020 program requirements. Once restrictions started to relax, a staged reopening of the laboratories was initiated, and some minimum amount of research was conducted in limited blocks of time and on a special case basis.

At ANL, ES recipes for the precursor fibers of the pristine and Al-LLZO were successfully developed and optimized on ANL's R2R ES system. ANL also tested and validated R2R ES for a similar Al-LLZO ES recipe that was developed on ORNL's laboratory-scale ES tool. These experiments demonstrated the scale-up capability of the R2R ES for recipes developed in lab-scale. In-situ simultaneous SAXS, WAXS, and CO2 characterization was performed during LLZO precursor annealing at the Argonne APS which revealed the phase transformation kinetics of LLZO from amorphous precursors. Cubic crystal structure was obtained after 600 °C annealing even for un-doped LLZO nanofibers that was attributed to nanocrystalline grain size by molecular dynamic modeling. Experimental protocols for surface lithium carbonate removal was developed and validated by XPS characterization. EIS measurements for Li/LLZO/Li symmetric cell showed 10-5 S/cm conductivity at 100 C. The relatively low ionic conductivity was due to low nanofiber packing density of the LLZO pellet prepared by cold pressing. Future work will focus on preparing high density LLZO electrolyte membranes by slot-die coating and improving electrolyte-electrode interface.

ANL also fabricated Nafion (cationic) and Sustainion (anionic) fibers as an electrospun ion-exchange membrane demonstration. Both fibers showed ~0.3 mS/cm ionic conductivity. A multi-nozzle co-ES system was built for scalable synthesis of dual-fiber ion-exchange membranes with well-intermixed Nafion and Sustainion fibers. In addition, antiviral electrospun nanofiber filter media with >95% filtration efficiency was developed to support DOE Basic Energy Sciences Office National Virtual Biotechnology Laboratory program. No filtration efficiency degradation was observed for the filter media after the filters were disinfected by autoclaving for ten cycles. Antiviral test showed a complete destruction of bacteriophage Phi6 (i.e., a SARS-CoV-2 surrogate virus) after the phage was in contact with the electrospun filter media for 15 minutes, indicating an acute virus kill effect. These results indicated a great potential for the electrospun media to be used as reusable N95 filter media. Finally, copper-based high-viscosity nanoparticle inks were prepared and characterized for rheological properties as an exploratory ink formulation study for printed electronics, an emerging electronics fabrication technology for cost, size, and power sensitive device applications. The goal is to develop ink and printing-curing process for R2R manufacturing of printed electronic devices.

ORNL conducted annealing studies on the Al-LLZO crystal structure determined the annealing time that is required to achieve cubic phase with no significant change in the fiber morphology. The fibers must be annealed in argon to remove the carbonates and increase their conductivity. The thickness and Pt loading of a coating prepared by different mixing techniques was determined to have a larger variability than is typical for slot-die coating. A gas diffusion catalyst layer loading of 0.1 mgPt/cm^2 was achieved across multiple electrodes with 8 wt.% Pt/C slurries processed with a R2R slot-die. Static sessile drop contact angle measurements showed that addition of Nafion ionomer did not decrease the contact angle for 1-propanol and ethanol solutions; however, the high viscosity of the ink due to the presence of Pt/C decreased the apparent contact angle. Catalyst ink rheology measurements showed that the shear viscosity of lower solids-loading 6 wt.% Pt/C ink is lower than that of the higher solids-loading 8 wt.% Pt/C ink. Coatings trials were performed with coating gaps smaller and larger than the wet coating thickness. Larger gaps gave smaller Pt loading variations (4-7%) than the smaller gaps (Pt loading variation is typically 10-40%) due to vacuum and ink pump limitations. Composite Al-LLZO/PAN nanofibers were synthesized that had diameters from approximately 800 nm to 1.4 µm. Spectroscopic analyses showed that the Al-LLZO is uniformly distributed on carbon fiber structures. Deposition of an ionomer overlayer on a PEMFC cathode at the same time as the cathode

electrocatalyst layer was achieved and trials were completed that eliminated the need for it altogether. Composite cathodes were tested and exhibit more noticeable power law contributions, in the low frequency regime, which is indicative of a more pronounced ion diffusion mechanism. At higher C-rates, a marked improvement in the specific capacity is evident for the cells based on composite cathodes (due to their enhanced Li conductivity) and especially for the cathode filled with porous Al-LLZO fibers.

NREL coordinated with ORNL on colloids, coating, and drying focus areas as well as cell fabrication and in-situ testing using the ORNL-coated GDEs. NREL coordinated with ANL on ES efforts for scaling an initial NREL-developed ES formulation on the ANL R2R ES system. A three-layer slide die was received at NREL and multiple high-resolution cameras were identified for use in flow imaging, and bracketry was obtained to mount the cameras in different configurations. The slide die was installed in a hood for initial flow testing and newly machined flow inlets were installed to make the die operational. Slurry particle size data was collected during USAXS experiments that confirmed the reduction of agglomerates in a slurry by the addition of PAA and XRF measurements were performed to validate catalyst loading. MEAs were fabricated and in-situ testing was performed using R2R slot-die-coated GDEs from ORNL. Electrochemical performance evaluation determined that catalyst layers without ionomer overlayers (spray or dual slot-die coated) performed better than catalyst layers with ionomer overlayers. A two-layer GDE with the least amount (thickness) of overlayer provided the best performance of the two-layer GDEs. NREL developed spectroscopic methods to be used for heterogeneous particle-polymer inks and explored scattering and index-of-refraction matching the spectroscopic behaviors that may be affecting measurements for NDE. Mid- to far-IR measurements of common porous carbon substrates were made to understand the transmission (penetration of dissimilar layers) characteristics of these materials and elucidate possible modes of measurement for observing active layers adjacent to and “through” the porous substrate.

LBNL designed a coating and drying observation table to simulate the fabrication conditions for materials being investigated at the other Labs, but at a scale that is small enough to be easily combined with analytical tools such as the Advanced Light Source beamlines. The base automated mixing experimental setup comprised of custom electronics and computer-controlled disperser, pump and motorized lab jack that is needed for the experiments was constructed and includes a flow-through particle size analyzer operating up to a 5 Hz sampling rate. Preliminary experiments were performed on carbon black dispersed in mixtures of 70% alcohol in water and 10% alcohol in water and results show significant effects of solvent composition on particle size distribution. Custom temperature bath sample holders were designed that are compatible with the motorized sample stages to load samples consistently and keep them at a controlled temperature. A portable custom cart with adjustable platforms was designed to isolate the motorized components of the mixing experiment setup (mixer, stage, pump, and chiller) from vibration-sensitive instruments (particle size analyzer and soon, confocal microscope) and to position the mixer and pump in a consistently reproducible position relative to different instruments. The LBNL computer-controlled mixing setup was transformed into a portable mixing station, allowing reliable recreation of samples in the vicinities of instruments in different locations. LBNL also released an update to their highly flexible open-source simulation package that will be used to implement upcoming models.

SNL completed the deposition models of single- and two-layer slot-die coating flow along with a working user interface to improve usability. Rheological data for a representative single- and two-layer-slot coating stack were fit with standard constitutive equations and implemented in the models. Development continued for the first-of-a-kind, 3-layer slide die model. Configurations were planned for the slide die coating trials. A special slide-only model is being used to help NREL redesign the lip geometry. The single-layer model operating space was validated using process inputs from ORNL. SNL models predicted the coating window (11 in. H_20 for 60 µm gap and 14 in. H_20 for 60 µm vacuum at 3 ft/min coating speed) for ORNL single-layer slot-die coating trials with a complex 8 wt % Pt/C catalyst ink that guided the experiments aimed at increasing the coating gap (slot-to-web) from 60 µm to 90 µm for better coating quality at a 30 µm coating wet thickness. The initial PMA polymer and toluene solvent single- and two-layer drying model was completed with

comparable values found in the literature. A new mesh/solid-model design for the slot-die model was developed to ease in gap-based parameter studies. A significant finding that needs to be experimentally verified is that the models predict that the low-vacuum limit disappears at all web speeds for smaller gaps and concentrated Pt/C inks. Stability analysis on the slide-only multilayer models has revealed potential for interlayer defects. SNL and UNM continued to advance a machine-learning model to connect coating defects of particulate conductive films (pinholes, striations) to process parameters for gravure coating/printing. Data was captured with high-end optical microscopy coupled with open computer vision image recognition tools.

Efforts will continue for the projects that continued in FY 2020 with the goal of advancing our understanding of R2R processing for high-throughput advanced manufacturing to enable new devices and lower the cost of existing processing routes for competitive U.S. manufacturing. The projects directly support the AMO's Multi-Year Program Plan challenges for the use of multilayer coating technologies applicable to flexible and integrated electronics, separation membranes, PVs, and selective barrier materials addressing the AMO identified targets of technologies with a 10x production capacity increase and in-line instrumentation tools to evaluate the performance and functionality.

Key Publications

Doeff, Marca M., Eongyu Yi, Hao Shen, Guoying Chen, Stephen W. Sofie, "Towards Scalable Manufacturing of Solid State Batteries", Presentation at the 236th meeting of the Electrochemical Society, Atlanta, GA, Oct. 13-17th, 2019.

Kabir S., Khandavalli S., Van Cleve T., Medina S., Pylypenko S., Kariuki N.N., Myers D.J., More K.L., Mauger S.A., Ulsh M., Neyerlin K.C. "Electrochemical and rheological investigation of catalyst-solvent-polymer ink formulations for electrospun fuel cell electrode structures." Oral presentation I01A-1445 at the Fall ECS Meeting, Atlanta, GA; October 2019.

Khandavalli S., Kabir S., Sur S., Rothstein J.P., Neyerlin K.C., Ulsh M., Mauger S.A. "The influence of carrier polymer on the microstructure and rheology of catalyst inks for electrospun proton exchange membrane fuel cell electrodes." Oral presentation 513e at the AIChE Annual Meeting, Orlando, FL; November 2019.

Khandavalli, Sunilkumar S., Sadia Kabir, Samrat Sur, Johnathan P. Rothstein, Kenneth C. Neyerlin, Michael Ulsh, Scott A. Mauger, "The Influence of Carrier Polymer on the Microstructure and Rheology of Catalyst Inks for Electrospun Proton Exchange Membrane Fuel Cell Electrodes." American Institute of Chemical Engineers Annual Meeting, Orlando, FL, November 10-15, 2019: 513e

Khandavalli, Sunilkumar S., Jae Hyung Park, Nancy N. Kariuki, Sarah F. Zaccarine, Svitlana Pylypenko, Deborah J. Myers, Michael Ulsh, and Scott A. Mauger "Investigation of the Microstructure and Rheology of Iridium Oxide Catalyst Inks for Low-Temperature Proton Exchange Membrane Water Electrolyzers." ACS Appl. Mater. Interfaces 2019, 11, 48, 45068–45079, November 7, 2019, https://doi.org/10.1021/acsami.9b14415

Khandavalli, Sunilkumar S., Radhika Iyer, Jae Hyung Park, Deborah J. Myers, Kenneth C. Neyerlin, Michael Ulsh, Scott A. Mauger, "The Effect of Dispersion-Medium Composition and Ionomer Concentration on the Microstructure and Rheology of Fe-N-C Platinum Group Metal-Free Catalyst Inks for Polymer Electrolyte Membrane Fuel Cells", American Chemical Society Publications, Langmuir 36 (2020), 12247-12260. https://doi.org/10.1021/acs.langmuir.0c02015

Mauger S.A., Wang M., Medina S., Pylypenko S., Ulsh M. "Influence of Coating Method on Performance of Roll-to-roll Coated PEM Fuel Cell Catalyst Layers." Oral presentation I01B-1491 at the Fall ECS Meeting, Atlanta, GA; October 2019.

Mauger S.A., Wang M., Medina S., Pylypenko S., Ulsh M. "Influence of coating method on performance of roll-to-roll coated PEM fuel cell catalyst layers." Oral presentation at the International Symposium of Coating Science and Technology (virtual); September 2020.

Medina S., Wang M., VanCleve T., Mauger S.A., Ulsh M., Neyerlin K.C., Pylypenko S. "Membrane electrode assembly fabrication method effects on catalyst layer structure, interfaces, and performance." Poster presentation I01A-1394 at the Fall ECS Meeting, Atlanta, GA; October 2019.

Osmieri, Luigi, Guanxiong Wang, Firat C Cetinbas, Sunilkumar Khandavalli, Jae Hyung Park, Samantha Medina, Scott A Mauger, Michael Ulsh, Svitlana Pylypenko, Deborah J Myers, Kenneth C Neyerlin, "Utilizing ink composition to tune bulk-electrode gas transport, performance, and operational robustness for a Fe–N–C catalyst in polymer electrolyte fuel cell", Nano Energy 75 (2020), 104943.

Park J., Kang Z., Bender G., Ulsh M., Mauger S.A. "Roll-to-roll direct coating of catalyst inks on membrane films: progress and challenges." Oral presentation at the International Symposium of Coating Science and Technology (virtual); September 2020.

Park J., Pfeilsticker J., Tjiptowidjojo K., Schunk P.R., Mauger S.A., Ulsh M., "An experimental investigation of multilayer flow in a slide die coating process." Poster presentation at the International Symposium of Coating Science and Technology (virtual); September 2020.

Park J., Kang Z., Bender G., Ulsh M., Mauger S.A. "Roll-to-roll Production of Catalyst Coated Membranes for Low-temperature Electrolyzers." *J Power Sources*, 479, 2020.

Sharma, N. "Studying the impact of ink and process parameters on electrospun fibers for electrocatalytic applications." Oral presentation at the MRS Fall Meeting & Exhibit, Boston, MA; December 2019.

Tjiptowidjojo K., Park J., Mauger S.A., Ulsh M., Schunk P.R. "Multilayer slide coating modeling for manufacturing of PEMFC." Oral presentation at the International Symposium of Coating Science and Technology (virtual); September 2020.

Wang M., Park J.H., Kabir S., Neyerlin K.C., Kariuki N.N., Lv H., Stamenkovic V.R., Myers D.J., Ulsh M., Mauger S.A. "Impact of Catalyst Ink Dispersing Methodology on Fuel Cell Performance Using In-situ X-ray Scattering." *ACS Applied Energy Materials*, 2 6417-6427 (2019).

Zhang, Yuepeng, "Scalable synthesis of nanofibers for energy storage and filtration applications", Center for Compact and Efficient Fluid Power Summit, Invited talk, September 2020.

References

1. Advanced Manufacturing Office (AMO) Multi-Year Program Plan for Fiscal Years 2017 Through 2021 (DRAFT). December 2016. https://www.energy.gov/eere/amo/downloads/advanced-manufacturing-office-amo-multi-year-program-plan-fiscal-years-2017
2. Howell, D., "An Overview of Advanced Batteries R&D at the U.S. Department of Energy – Plenary Presentation". 236th Electrochemical Society 2019 Meeting, Atlanta, GA, October 13-17, 2019. Abstract MA2019-03 1. https://iopscience.iop.org/article/10.1149/MA2019-03/1/1/meta
3. Boyd, S. "Batteries and Electrification R&D – Plenary Presentation". Vehicle Technologies Office 2020 Annual Merit Review (virtual), June 1-4, 2020. https://www.energy.gov/eere/vehicles/downloads/plenary-presentation-batteries-electrification-electric-drive-systems
4. Energy Storage Research, University of Louisville Conn Center for Renewable Energy Research. https://www.conncenter.org/energy-storage-research

5. Satyapal, S. “U.S. Department of Energy Hydrogen and Fuel Cell Technologies Office and Global Perspectives)”. Presentation at the Innovation for Cool Earth Forum (ICEF) 7th Annual Meeting (virtual), September 28, 2020. https://www.energy.gov/sites/prod/files/2020/10/f79/hfto-satyapal-ICEF-sept28_0.pdf
6. Macknick, J.; Newmark, R.; Heath, G.; Hallett, KC. “A Review of Operational Water Consumption and Withdrawal Factors for Electricity Generating Technologies”. (2011) Technical Report NREL/TP-6A20-50900, March 2011. https://www.nrel.gov/docs/fy11osti/50900.pdf
7. Pasupathi, S and Maiyalagan, T., “Components for PEM Fuel cells An Overview”. (2012). Materials Science Forum 657, DOI: 10.4028/www.scientific.net/MSF.657.143
8. Kutz, R.B., Chen, Q., Yang, H., Sajjad, S.D., Liu, Z., Masel, I.R. “Sustainion Imidazolium-Functionalized Polymers for Carbon Dioxide Electrolysis”. (2016), Wiley Online Library, https://doi.org/10.1002/ente.201600636
9. “DOE Seeking Input and Collaboration on Science and Technology Response to COVID-19”. EERE Bulletin, March 17, 2020. https://content.govdelivery.com/accounts/USEERE/bulletins/2819de3
10. https://bioaid.us
11. C.K. Chan, T. Yang, J.M. Weller, Nanostructured garnet-type Li7La3Zr2O12: synthesis, properties, and opportunities as electrolytes for Li-ion batteries, Electrochim. Acta 253 (2017) 268–280.
12. K. Fu, Y. Gong, J. Dai, A. Gong, X. Han, Y. Yao, C. Wang, Y. Wang, Y. Chen, C. Yan, Y. Li, E.D. Wachsman, L. Hu, Flexible, solid-state, ion-conducting membrane with 3D garnet nanofiber networks for lithium batteries, Proc. Natl. Acad. Sci. (2016), 113, 7094–7099.
13. DOE Program and Project Management for the Acquisition of Capital Assets, DOE 413.3B updated April 12, 2018. https://www.energy.gov/projectmanagement/directives

ORNL/SPR-2021/1892 April 2021

For more information, contact: R2RAMM.ornl.gov